DASA-13.018

Technical Report **R 474**

STATIC AND DYNAMIC BEHAVIOR OF ANTISYMMETRICALLY LOADED ARCHES

September 1966

NAVAL FACILITIES ENGINEERING COMMAND

U. S. NAVAL CIVIL ENGINEERING LABORATORY

Port Hueneme, California

STATIC AND DYNAMIC BEHAVIOR OF ANTISYMMETRICALLY LOADED ARCHES

Y-F008-08-02-102, DASA-13.018

by

R. H. Chiu and S. K. Takahashi

ABSTRACT

Four pinned-base steel arches with a 96-inch radius, 143.8-inch span, and uniform cross section were cold-rolled from 4M13 sections and tested under various static and dynamic loads uniformly distributed over one-half the arc length. A maximum static load of 72,000 pounds was applied by the NCEL blast simulator using compressed air. A dynamic peak load of 64,000 pounds was attained by detonating Primacord in the blast simulator. The blast loading had a rise time of about 3 milliseconds and a decay time of about 1.6 seconds. An equivalent triangular load-time function was used for the dynamic analysis. The applied loads and the resulting deflections, strains, and reactions were measured. The reduced data are presented in graphical and tabular form.

The theoretical analyses for statically and dynamically loaded arches were based on the discrete framework which represented the continuous arches tested. A 16-bar system was used for both static and dynamic response calculations, and a 40-bar system was used for natural mode and frequency calculations.

In the static analysis, the effects of stress amplification, misalignment, and elastic supports on the response of the arch were considered. Due to the strain-hardening characteristics of the arch material, the idealized stress-strain curve was represented by a trilinear curve rather than by the usual bilinear stress-strain curve.

A simplified dynamic analysis gave results reasonably close to those from more rigorous methods; the values were on the conservative side. Nearly complete correlation between the theoretical and experimental results was obtained.

This work was sponsored by the Defense Atomic Support Agency.

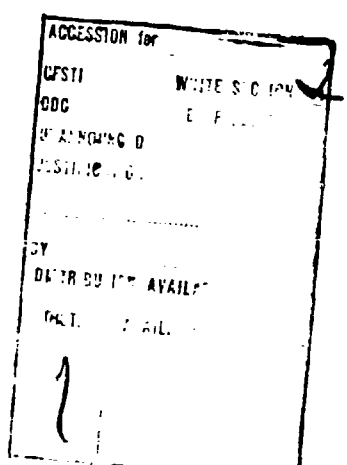

TABLE OF CONTENTS

LIST OF ILLUSTRATIONS

LIST OF TABLES

INTRODUCTION

The purpose of this report is to provide information on the theoretical and experimental behavior of two-hinged steel circular arches subjected to uniformly distributed static and dynamic loads on one-half the arch. Many theories and procedures have been advanced in recent years for determining the elastic and elastoplastic response of structures to uniformly distributed dynamic loads. However, due to the lack of large dynamic testing facilities, there have been few direct comparisons of the theoretical and experimental behavior of large-scale models.

The blast simulator at the U.S. Naval Civil Engineering Laboratory can test nearly full-sized structural members under transient loads up to 185 psi.

This report covers the third and last phase of tests on structural steel members; the first dealt with the static and dynamic behavior of portal-frame knee connections[1] and the second with static and dynamic behavior of pinned- and fixed-base portal frames.[2,3] For the third phase, four steel arches of 96-inch radius and 143.8-inch span were designed, fabricated, and tested. The primary objectives of the test series were to obtain information on the behavior of members subjected to static and dynamic loads and to examine the behavior and failure mode of the members under static and dynamic loads. The information obtained will be used to recommend changes in the present design criteria of structures subjected to blast loads.

The work was accomplished under Work Unit Y-F008-08-02-102, Blast Resistance of Structural Shapes, and was sponsored by the Defense Atomic Support Agency through the Naval Facilities Engineering Command.

Wherever possible, symbols used in this report are those recommended by the Defense Atomic Support Agency. A complete list of symbols appearing in this report precedes the appendixes.

EXPERIMENTAL TECHNIQUES AND PROCEDURES

Design Procedure and Description of Arch

Two criteria in determining the size and strength of the antisymmetrically loaded arches to be tested were that they should fit in the blast simulator and that the maximum load should be limited to approximately 50 percent of the capacity of the simulator. It was determined that the central angle of the arch would be 97 degrees and the radius to the neutral axis would be 96 inches. The width between the skirts of the simulator is 8 inches. In previous tests, it was determined that the most efficient width of the test member should be between 7-3/4 and 7-7/8 inches.

With these dimensions and loading conditions, the mechanism method of plastic design was used.[4,5] It should be noted that the load produces sidesway and that plastic hinges develop in the vicinity of the quarter points, b and d, as shown in Figure 1. The instantaneous center of rotation then lies at the intersection, c, of straight lines drawn through the hinge points, a and b, and d and e; the central angle is designated ϕ_o. For simplicity, the load, w, has been replaced by two resultant forces, F_1 and F_2, acting normal to chords ed and dk. From Figure 1, the following geometrical relations can be obtained:

$$ed = 2R \sin \frac{\phi_o}{8}$$

$$dq = 2R(\tan \psi) \left(\sin \frac{\phi_o}{8}\right) = 2R\, \psi \sin \frac{\phi_o}{8}$$

$$en = R \sin \frac{\phi_o}{2}$$

$$rn = df = R \sin \frac{\phi_o}{4}$$

$$of = R \cos \frac{\phi_o}{4}, \quad on = R \cos \frac{\phi_o}{2}$$

$$dr = of - on = R \left(\cos \frac{\phi_o}{4} - \cos \frac{\phi_o}{2}\right)$$

$$er = en - rn = R \left(\sin \frac{\phi_o}{2} - \sin \frac{\phi_o}{4}\right)$$

$$ec = \frac{(en)(ed)}{(er)} = \frac{2R \left(\sin \frac{\phi_o}{2}\right) \left(\sin \frac{\phi_o}{8}\right)}{\sin \frac{\phi_o}{2} - \sin \frac{\phi_o}{4}}$$

$$dc = ec - ed = \frac{2R \left(\sin \frac{\phi_o}{8}\right) \left(\sin \frac{\phi_o}{4}\right)}{\sin \frac{\phi_o}{2} - \sin \frac{\phi_o}{4}}$$

$$\psi' = \frac{dq}{dc} = \left(2 \cos \frac{\phi_o}{4} - 1\right) \psi \tag{1}$$

External work for very small deflections is determined as follows:

$$W_E = F_1 \frac{\Delta}{2} + F_2 \bar{x} \psi' \tag{2}$$

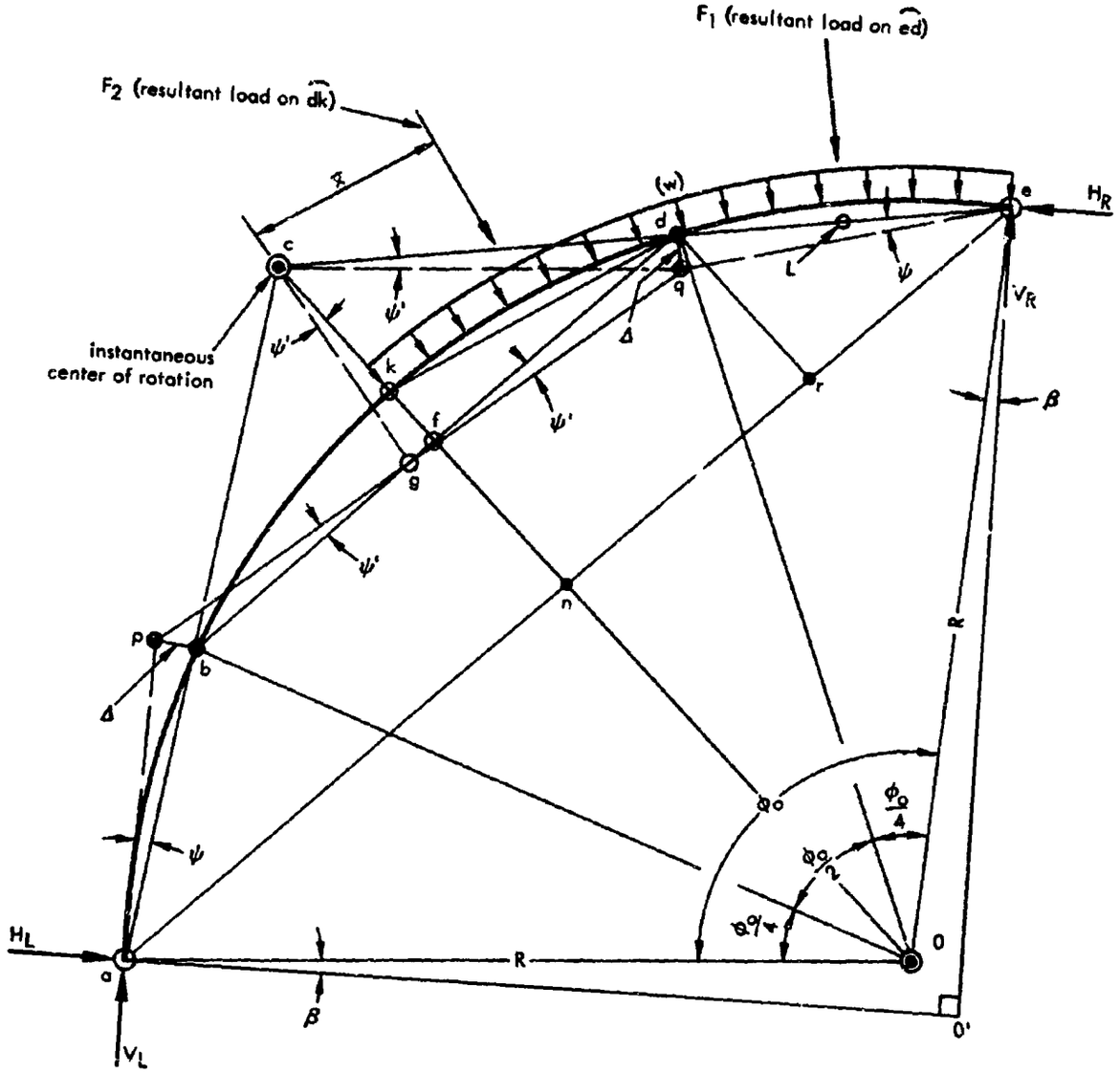

Figure 1. Schematic representation of the antisymmetrically loaded arch.

since

$$F = F_1 = F_2 = 2Rw\left(\sin\frac{\phi_o}{8}\right)$$

$$\Delta = 2R\psi\left(\sin\frac{\phi_o}{8}\right)$$

$$\bar{x} = oc\left(\sin\frac{\phi_o}{8}\right) = \frac{R\cos\frac{\phi_o}{8}}{\cos\frac{3\phi_o}{8}}\sin\frac{\phi_o}{8} = \frac{R\sin\frac{\phi_o}{4}}{2\cos\frac{3\phi_o}{8}}$$

$$W_E = FR\psi\left(\sin\frac{\phi_o}{8} + \frac{\psi'\sin\frac{\phi_o}{4}}{2\cos\frac{3\phi_o}{8}}\right)$$

or by using Equation 1, and employing identities

$$W_E = 2FR\psi\sin\frac{\phi_o}{8} \tag{3}$$

Internal work is determined as follows:

From Figure 1, it can be shown that

$$W_I = 2M_p\left(\psi + \psi'\right) = 4M_p\psi\cos\frac{\phi_o}{4} \tag{4}$$

Equating (3) and (4) and solving

$$M_p = \frac{1}{2}R^2 w\left(\frac{1 - \cos\frac{1}{4}\phi_o}{\cos\frac{1}{4}\phi_o}\right) \tag{5}$$

Since ϕ_o is equal to 97 degrees

$$M_p = 0.0484\,R^2 w \tag{6}$$

Using a radius of 96 inches and a design yield load of 75 x 8 or 600 lb/in., the plastic moment is calculated as

$$M_p = 267,384 \text{ in.-lb}$$

The plastic modulus, Z, is then

$$Z = \frac{M_p}{f_y} = \frac{267,384}{40,000} = 6.68 \text{ in.}^3$$

By referring to a plastic modulus table, a reasonable section was chosen as

4M13 lb

$$Z = 6.1 \text{ in.}^3$$

A section with a smaller plastic modulus was selected for testing in the blast simulator because the width of the top flange would have to be increased to about 7-3/4 inches. After the arch was rolled into shape, two steel strips 1-7/8 inches by 5/8 inch were welded to the top flange of the arches as shown in section B-B of Figure 2. The total area of the cross section was 6.16 in.^{2}. For this cross section, the elastic neutral axis was computed to be 2.64 inches above the base of the lower flange and the moment of inertia was computed to be 14.84 in.^{4}. The plastic neutral axis was found to be 3.58 inches above the base of the lower flange and the plastic modulus was 7.15 in.^{3}. Needle roller bearings were fastened to the transverse web stiffener (as shown in Figure F-1) to reduce friction as the arch deflected.

Loading System

The blast simulator (Figure 3) was used to test the antisymmetrically loaded arches. The load applied simulated a blast wave from an air burst initially striking the surface of the arch at one of the quarter points and also perpendicular to the longitudinal axis. The response of the arch, as the blast wave engulfed the entire arch, was not taken into account in this test program. For testing these arches, special extension plates, 6 feet in height and 8 feet in length, were bolted to the bottom of the blast simulator and tied together by three sets of massive collar beams to prevent separation. Figure 4 shows one side of the extension plates removed, exposing the arch to be tested. Static loads were applied by pumping air into the simulator from a compressor. Dynamic loads were produced by detonating Primacord within the firing tube in the simulator.[6] A blast loading was produced which had a rise time of approximately 2 to 3 milliseconds followed by an experimental decay of controlled duration (Figure 5). Leakage of the static or dynamic pressure was minimized by a neoprene seal placed on top of the flange (Figure 4).

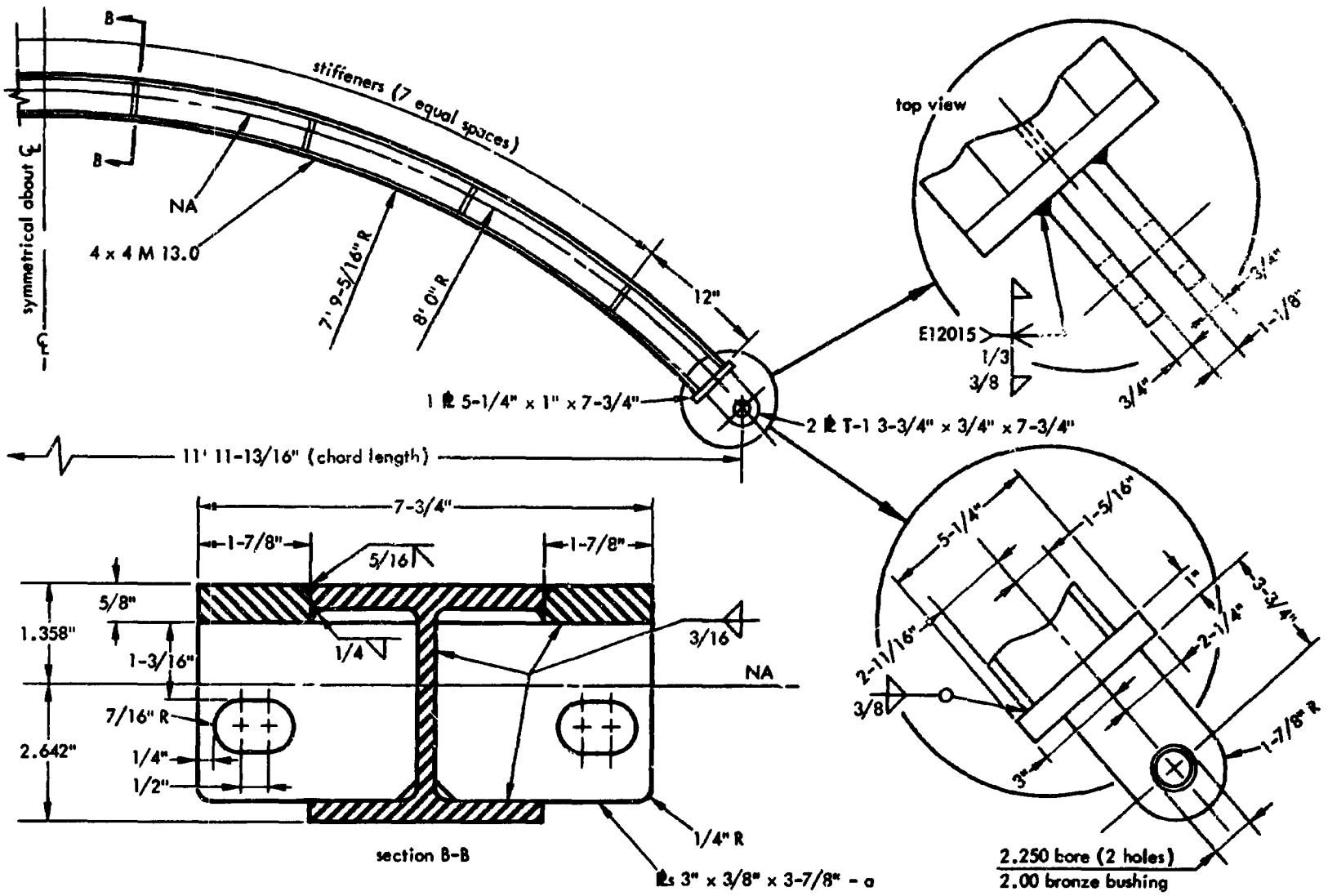

Figure 2. Dimensions of the antisymmetrically loaded arch.

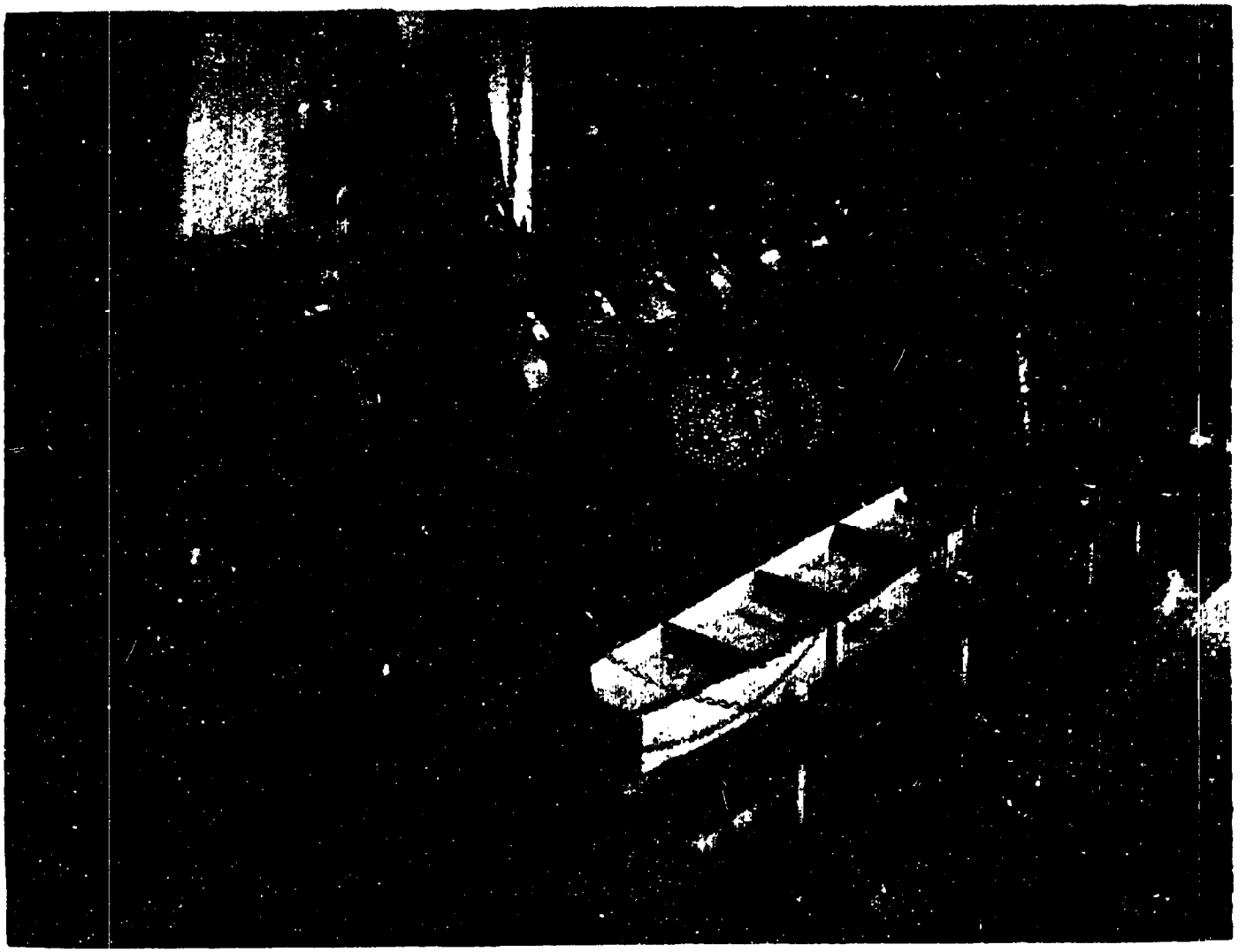

Figure 3. View of the blast simulator.

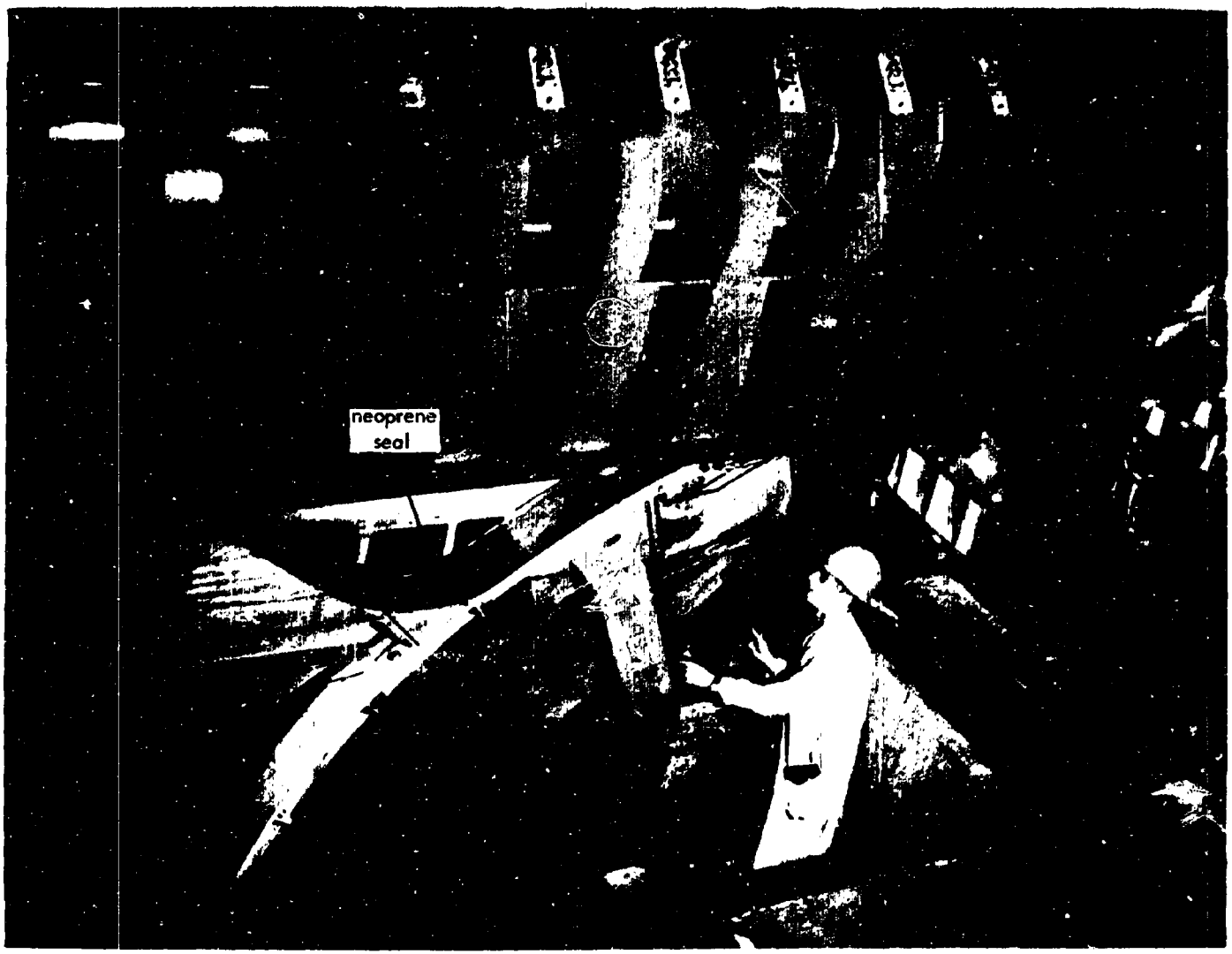

Figure 4. Setting up the arch in the blast simulator.

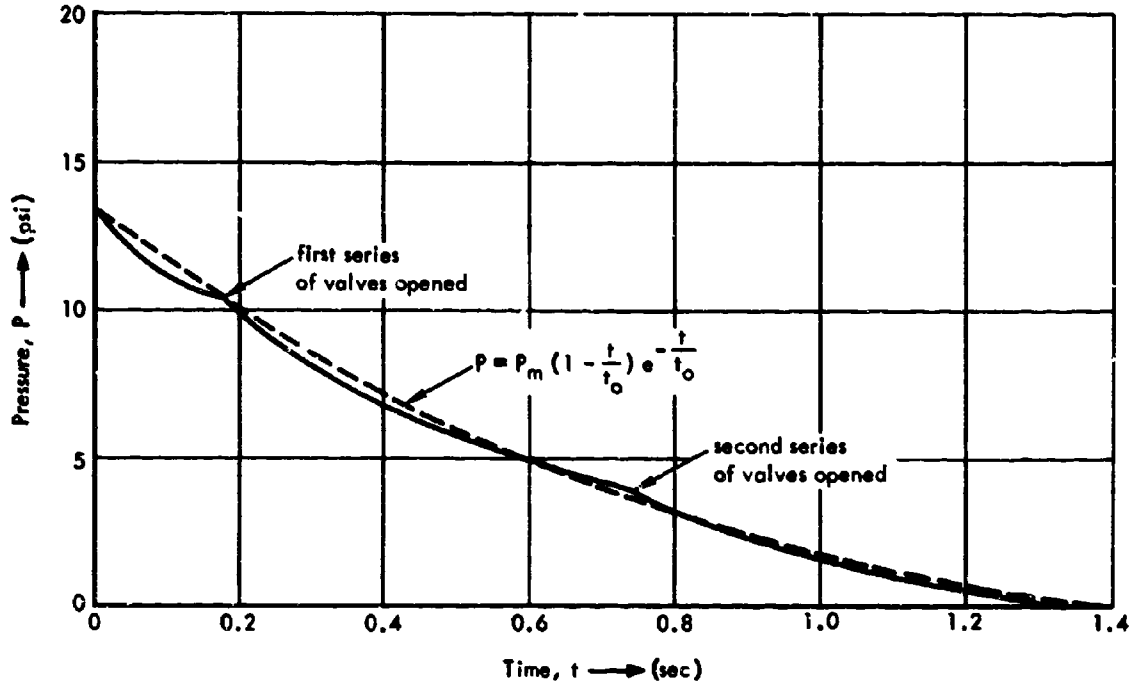

Figure 5. Typical load-time curve.

Instrumentation

Instrumentation of the test specimens consisted of strain gages, pressure cells, deflection gages, and an accelerometer located as shown in Figure 6. Information on the measuring instruments is presented in Table 1. The recording equipment is shown in Figure 7. In addition to the transducers listed in Table 1, deflection measurements were also obtained by the use of a rotating drum gage, and the reactions were measured with a pair of dynamometers (Figure 8) at each end of the arch. The rotating drum deflection gage revolved at a constant speed, recording deflection and as the arch deflected, a pencil attached to the end of a taut piano wire inscribed a deflection-time trace on the graph paper.

Test Procedure

The general test procedure for the arches was as follows: the arch was vibrated, a static load was applied (to failure for one arch and to approximately 60 percent of yield for the other arches), and a series of dynamic loads was applied to the arches that were not statically loaded to failure.

Two types of vibrational mode tests were conducted. The first was to excite the lowest natural frequency of the two-hinged arch in the deflection mode and the second was to excite the arch in the compression mode. For both types of tests, the arch was wedged upward by using a piece of timber at the desired location (at the quarter point for the deflection mode and at the crown for the compression mode). The timber was suddenly knocked out with a sledge hammer. The subsequent vibrations were recorded on the oscillograph; a typical oscillogram is shown in Figure 9. A smooth, continuous trace indicated that the specimen was vibrating freely in the blast simulator; the natural period of vibration was obtained from these records.

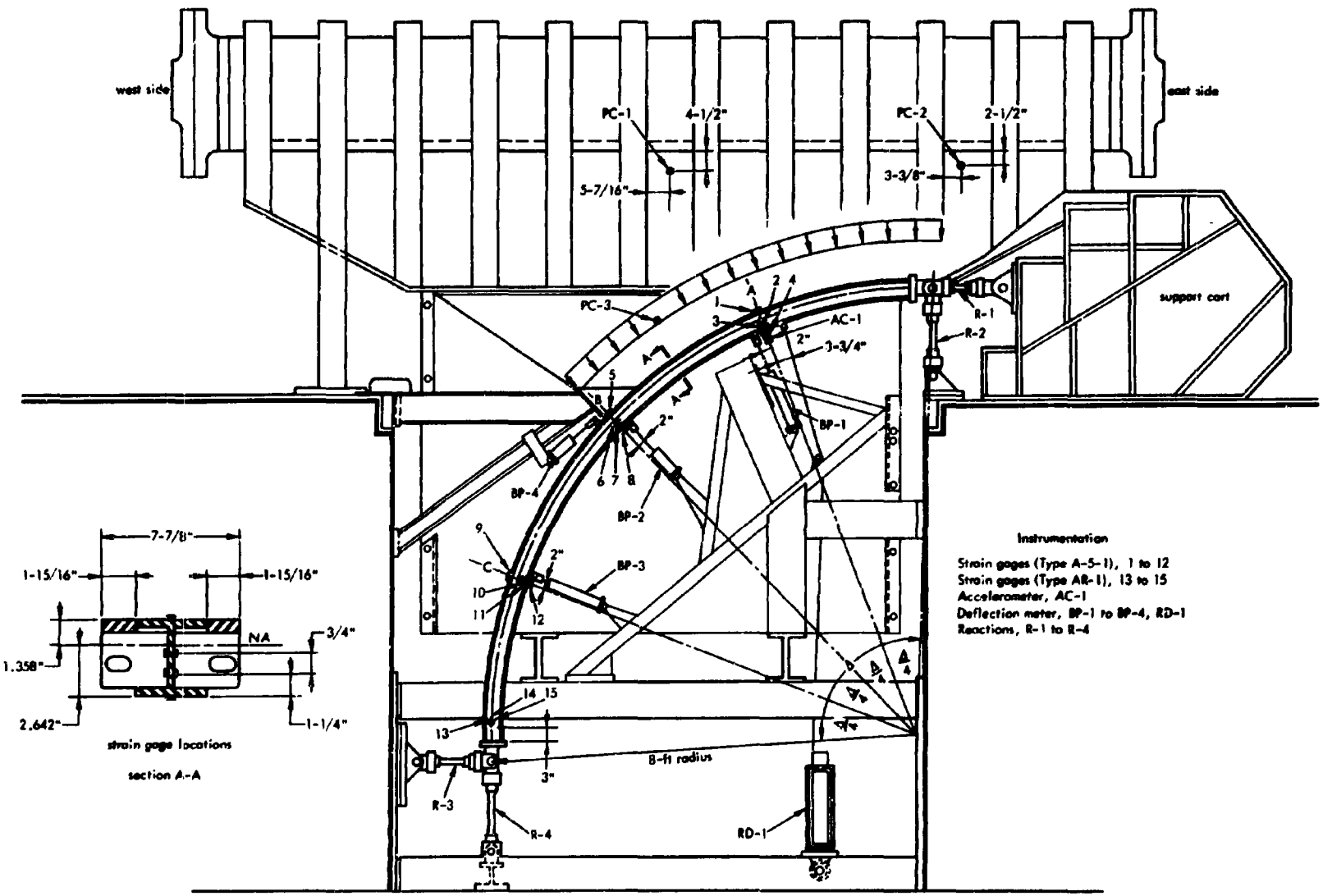

Figure 6. Test setup for 8-foot radius half-loaded arches AH-3 and AH-4.

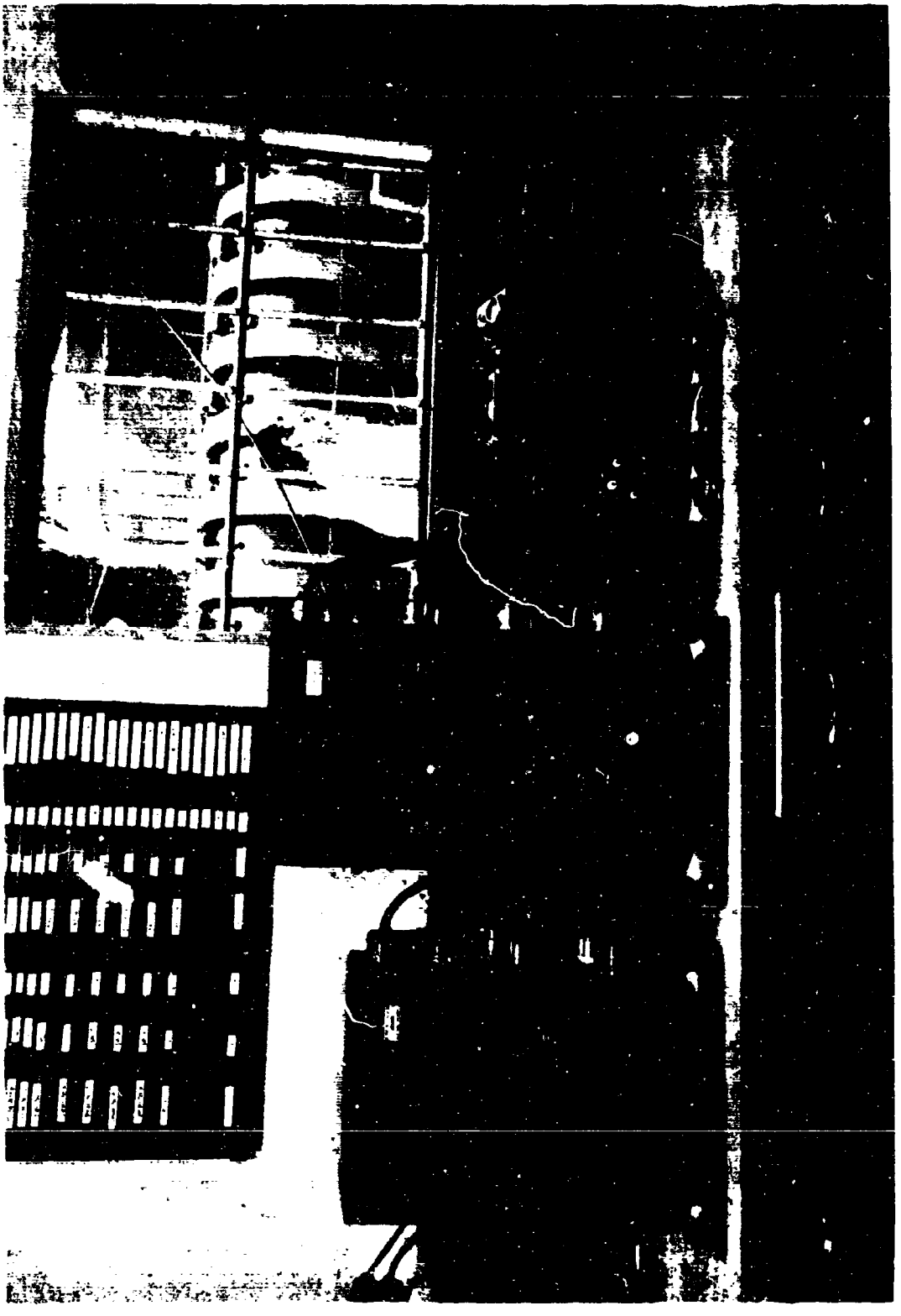

Figure 7. Electronic amplifier and recording oscillograph.

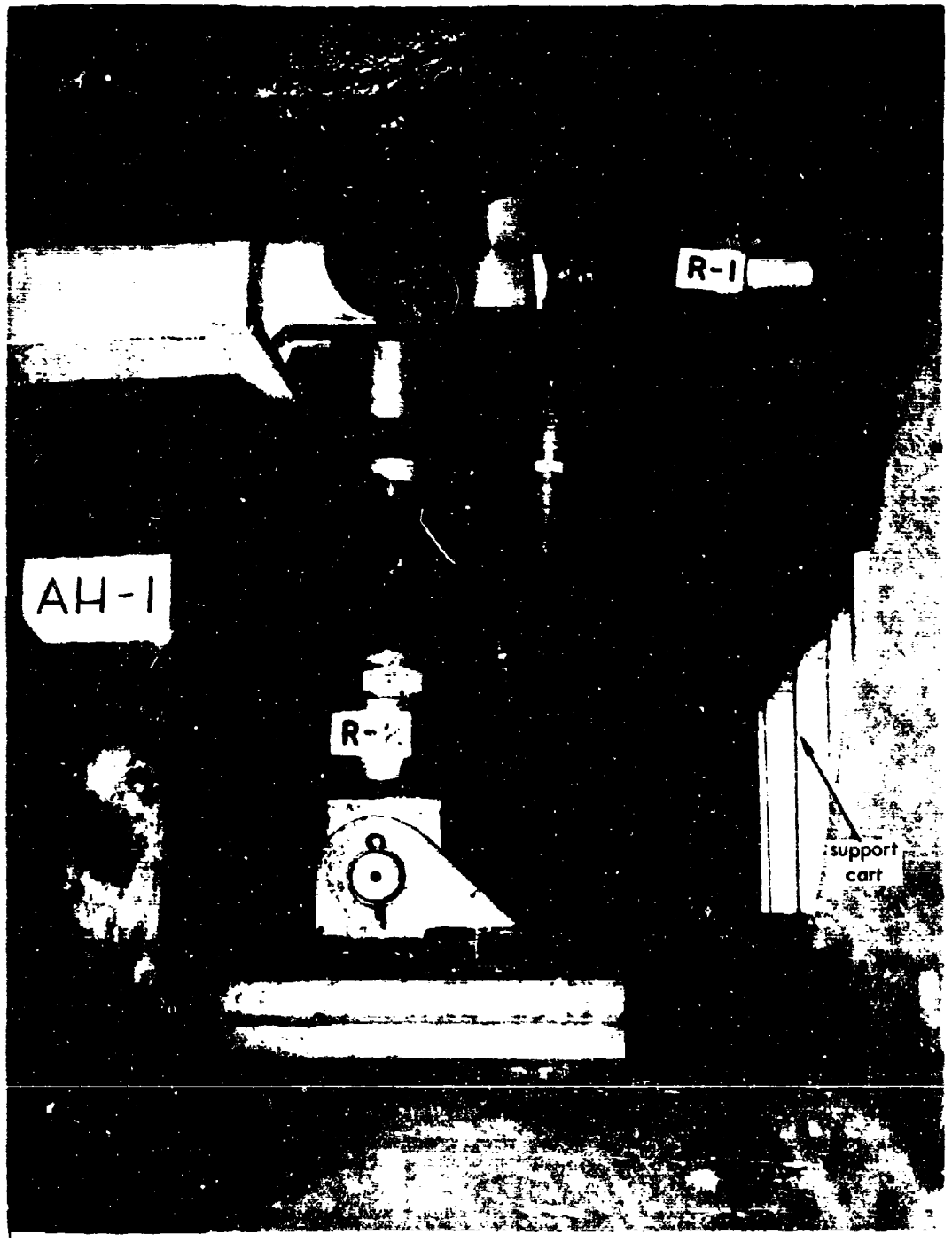

Figure 8. Horizontal and vertical reactions at the loaded end of the arch.

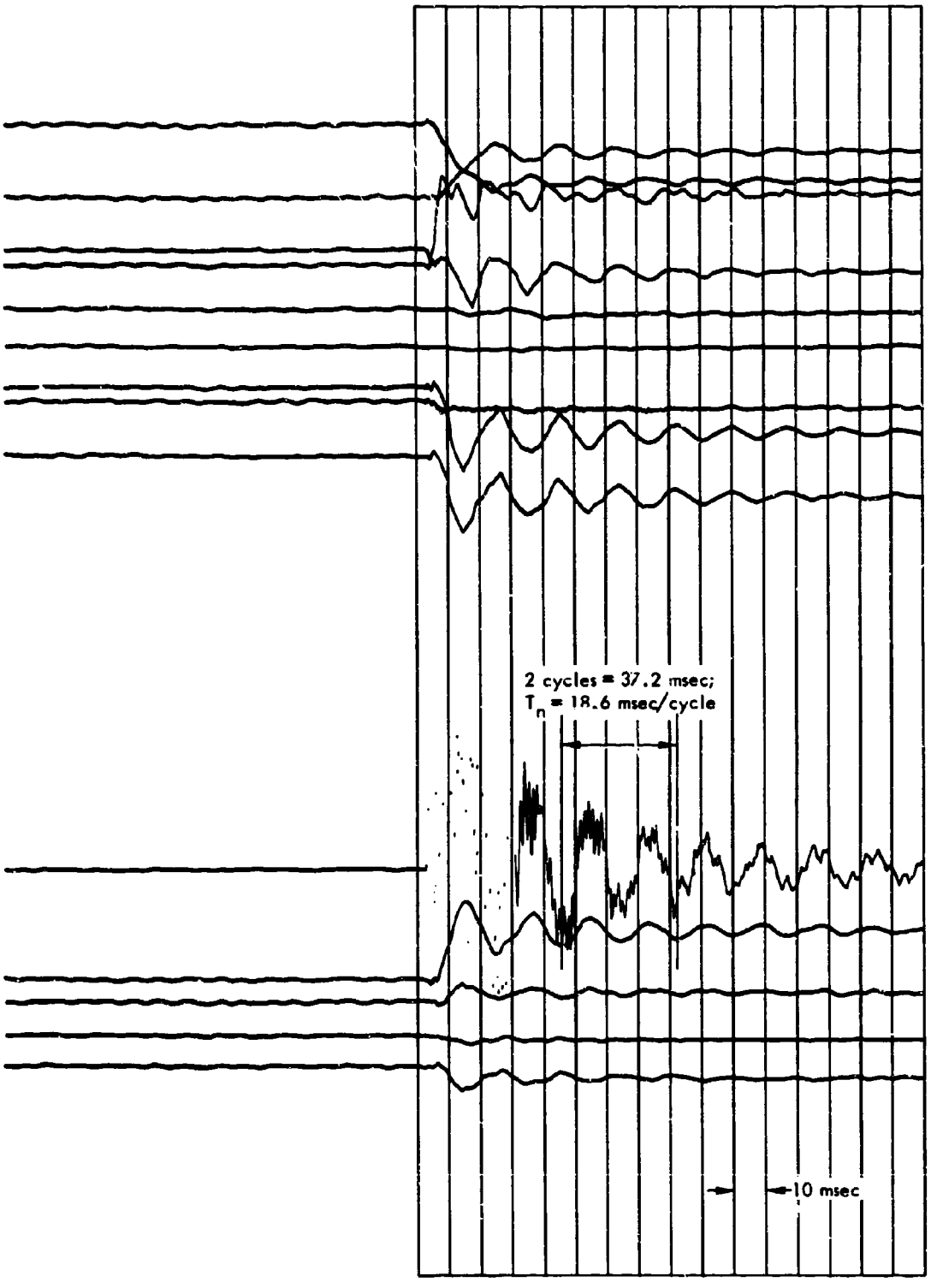

Figure 9. Free-vibration test of arch AH-2.

Table 1. Instrumentation Used in Tests

Measurement	Description	Type or Model	Manufacturer
Load	200-psi pressure cells	PA208TCA-200-350	Statham Instruments, Incorporated
Acceleration	200-g accelerometer	A5A-200-350	Statham Instruments, Incorporated
Deflection	6-, 10-, and 15-inch linear potentiometer	108	Bourns, Incorporated
Strains	SR-4 electrical resistance strain gages	A-5-1, A-R-1	Baldwin-Lima-Hamilton Corporation
	Whittemore strain gages	2-inch type	Baldwin-Lima-Hamilton Corporation
Other	Recorder with 36-channel oscillograph amplifiers	5-119P4-36 1-113B	Consolidated Electrodynamics Corporation

The first arch was tested statically to failure; the remaining arches were loaded statically to approximately 60 percent of the yield load and then tested dynamically in the elastic range. This was done so that the elastic static response of the arch could be compared with the elastic dynamic response. Typical dynamic test data recorded on the oscillograph are shown in Figures 10 and 11. The final dynamic load on each arch was in the inelastic range so that information on the dynamic response over a wider range of pressure could be obtained.

After a specimen had been tested completely, photographs of the overall arch, including closeups of the entire specimen, were taken (Appendix F).

COMPARISON OF EXPERIMENTAL AND THEORETICAL RESULTS

Tensile Coupon Tests

Static Tests. Standard tensile test coupons, 2-inch gage length, were fabricated from the flange strip, the web, and the upper and lower flanges. Figure 12 identifies the locations and symbols of static test specimens. It should be noted that the specimens were cut from the mid-spans of the arches where very little bending moment took place during the tests. It was assumed that the specimens were representative of the arch material before tests. Typical stress-strain curves for each location are shown in Figures 13 through 18.

Table 2 summarizes the results of static coupon tests. The average values of yield stress at 0.2 percent offset were 56,200, 41,700, 55,100 and 60,500 psi for the web, flange strips, and upper and lower flanges, respectively; the average values of ultimate strength were 70,000, 64,400, 70,700 and 72,800 psi, respectively; the average values of the elastic modulus were 30.0×10^6, 30.9×10^6, 27.9×10^6, and 26.7×10^6 psi, respectively. It should be noted that the 4M13 section was less ductile than the flange strips. This fact was reflected in the 2-inch elongation values of 34.3, 22.0, and 25.8 percent for the flange strips, the web, and flanges, respectively; this was due to the fact that the 4M13 section had been strained beyond the strain-hardening point during the cold-roll process (Figure 17). Further evidence is shown in the stress-strain curves of various specimens of the arch. No characteristics of a definite yield plateau are evident in the stress-strain curves of Figures 13, 15, and 16 for the web and upper and lower flanges of the 4M13 section.

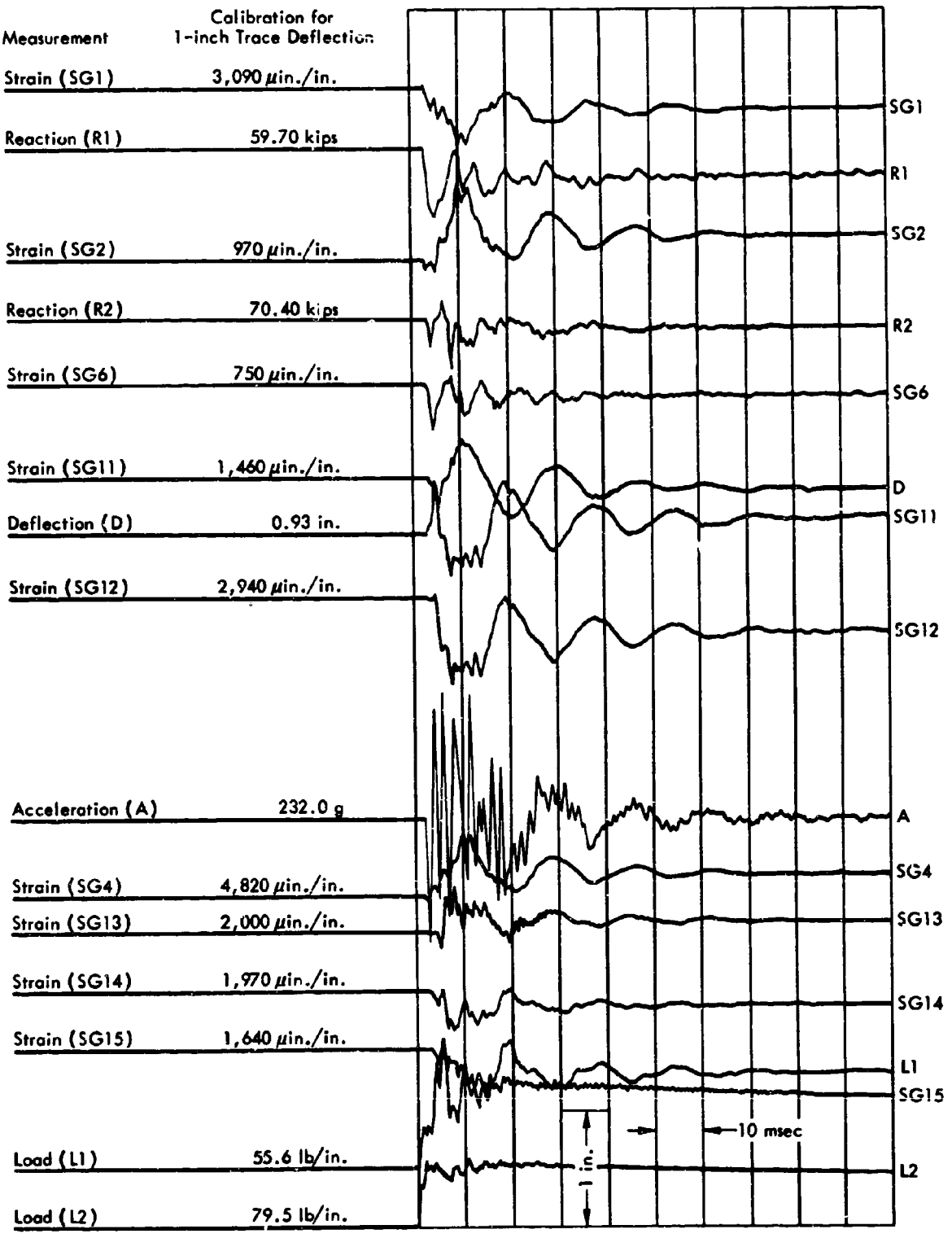

Figure 10. Oscillogram 1 for arch AH-2, test 11.

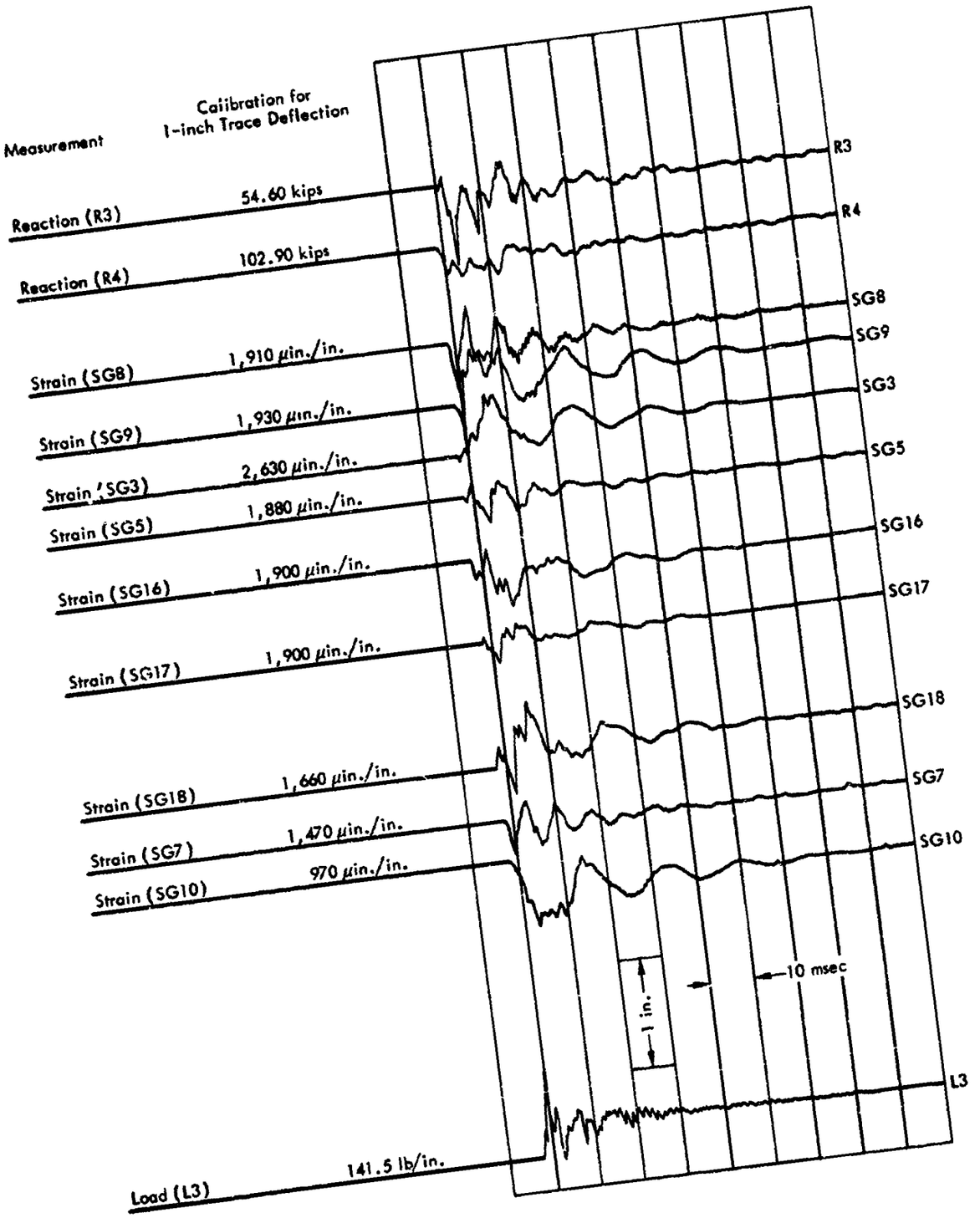

Figure 11. Oscillogram 2 for arch AH-2, test 11.

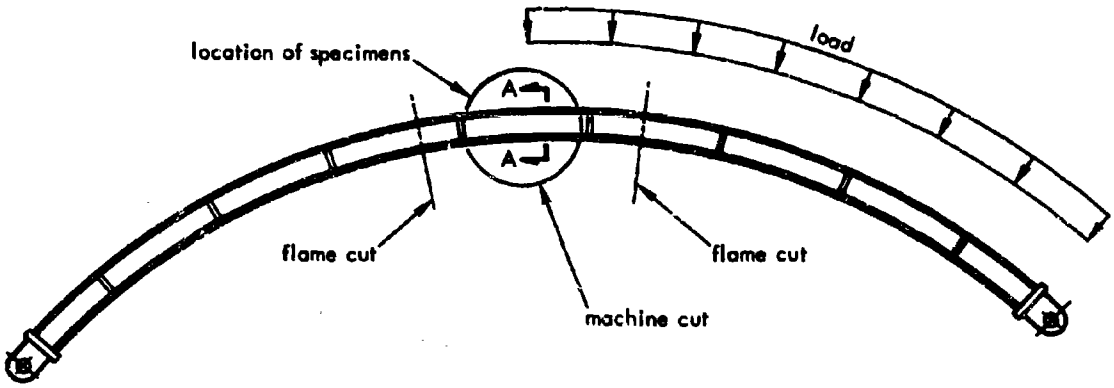

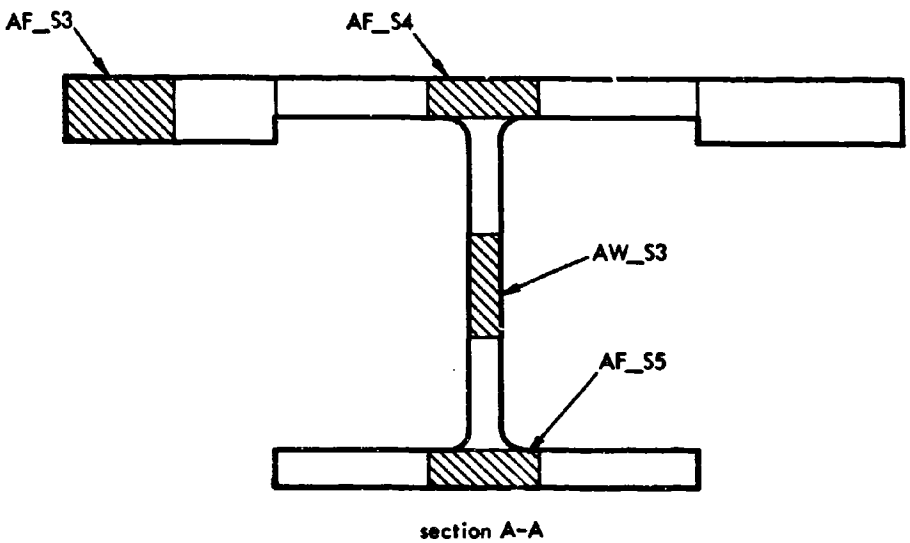

AH-1	AH-3
AF1S3	AF3S3
AF1S4	AF3S4
AF1S5	AF3S5
AW1S3	AW3S3
AH-2	**AH-4**
AF2S3	AF4S3
AF2S4	AF4S4
AF2S5	AF4S5
AW2S3	AW4S3

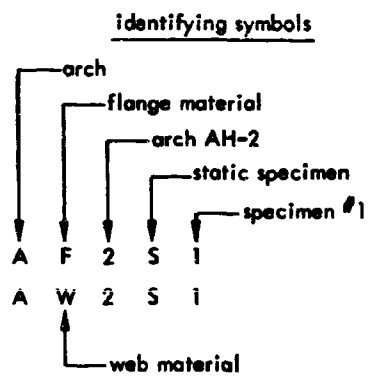

Figure 12. Locations of tensile test specimens for the antisymmetrically loaded arch.

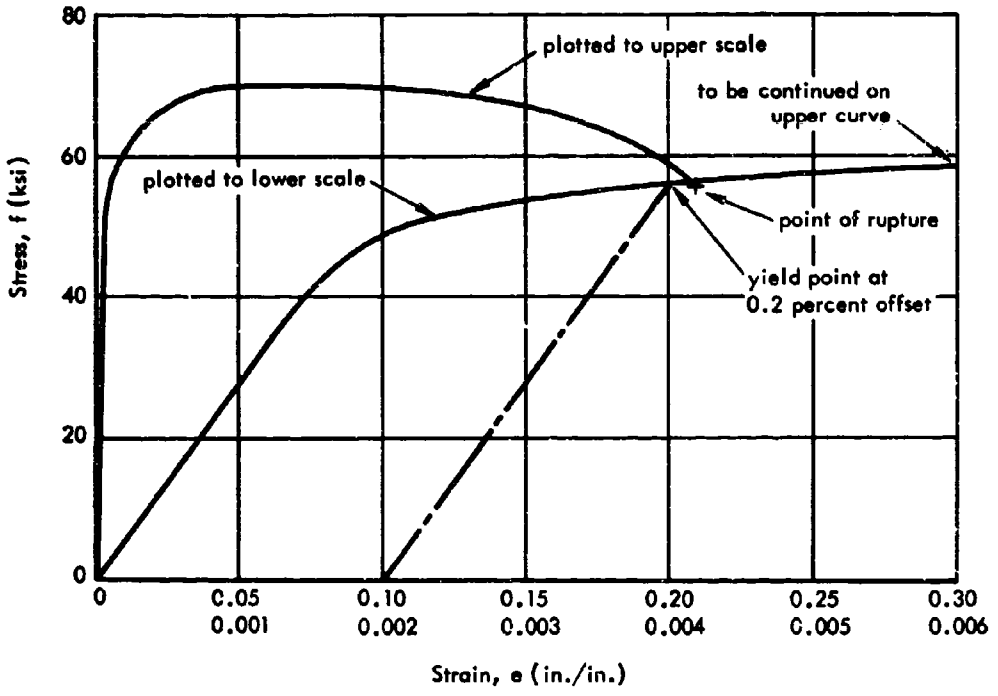

Figure 13. Static stress-strain curves of the web of the antisymmetrically loaded arch.

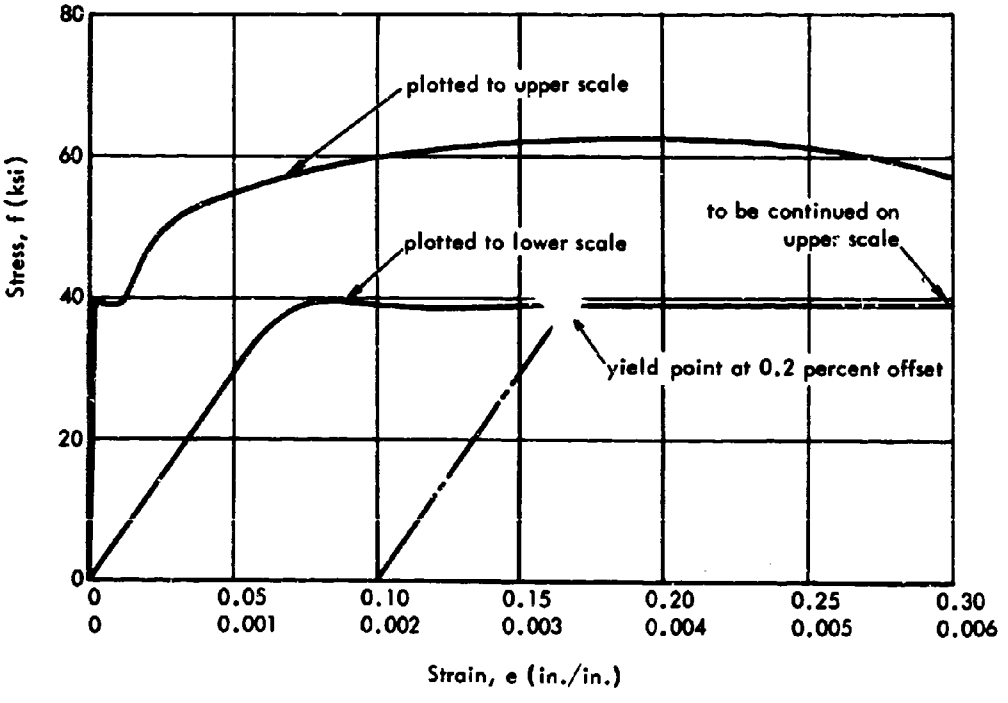

Figure 14. Static stress-strain curves of the flange strip of the antisymmetrically loaded arch.

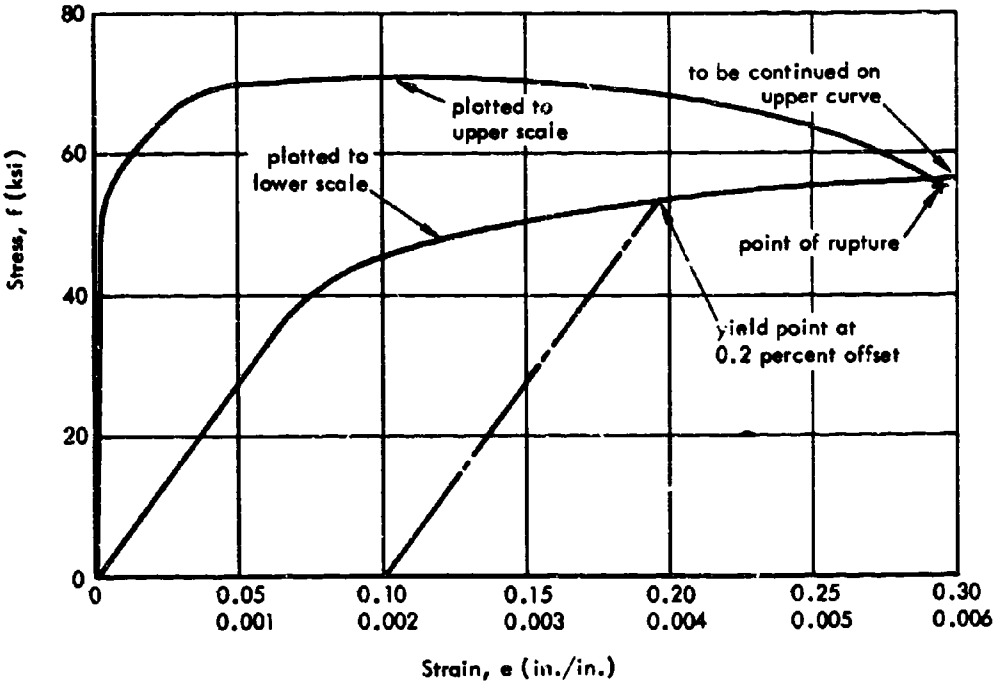

Figure 15. Static stress-strain curves of the upper flange of the antisymmetrically loaded arch.

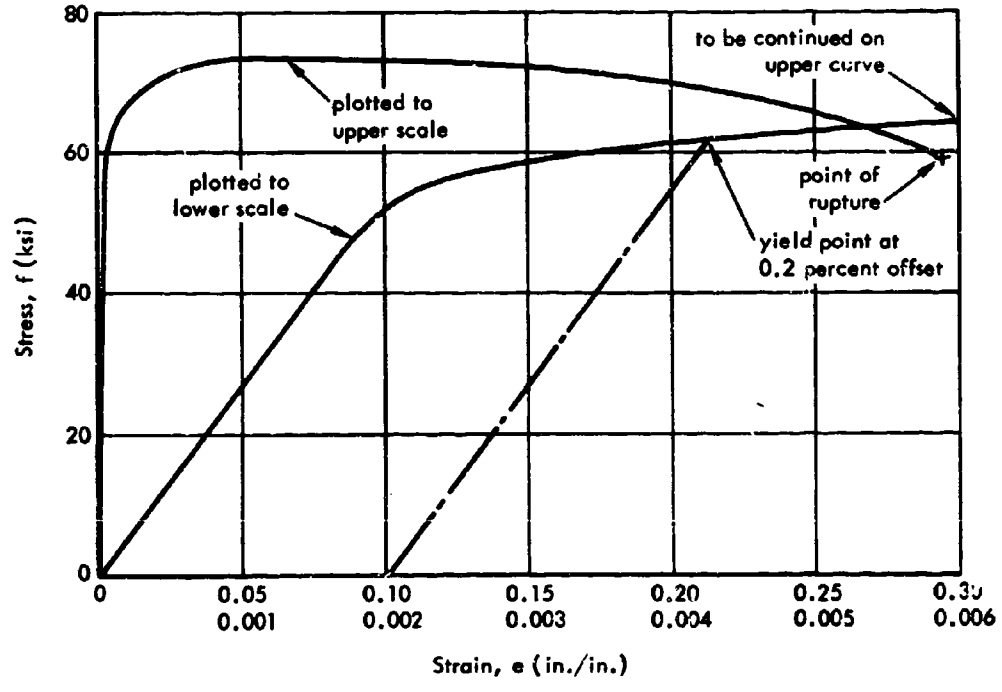

Figure 16. Static stress-strain curves of the lower flange of the antisymmetrically loaded arch.

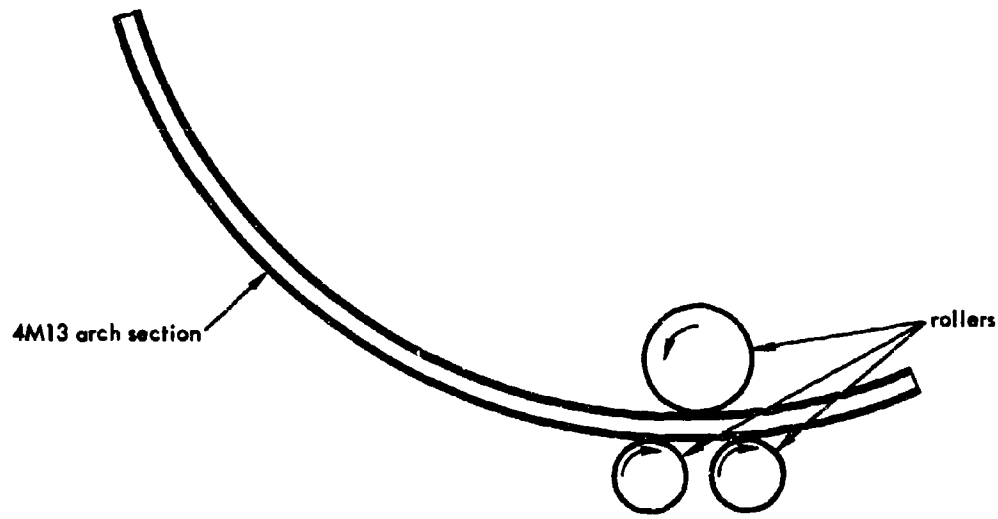

Figure 17. Cold-roll process of the arch.

Table 2. Static Properties of Steel for Antisymmetrically Loaded Arches

Location of Specimen	Arch No.	Yield Stress 0.2% Offset (psi)	Elastic Modulus (psi)	Inelastic Modulus (psi)	Ultimate Strength (psi)	Elongation in 2 Inches (%)
Web*	AH-2	57,100	31.0×10^6	---	70,000	21.0
	AH-3	56,500	28.9	---	70,000	24.0
	AH-4	55,000	30.1	---	70,000	21.0
	Average	56,200	30.0		70,000	22.0
Flange Strip	AH-2	43,200	30.4	7.29×10^5	64,600	36.0
	AH-3	41,800	31.6	5.84	65,900	32.0
	AH-4	40,200	30.7	8.60	62,700	35.0
	Average	41,700	30.9	7.24	64,400	34.3
Top Flange*	AH-2	57,700	27.3	---	71,000	23.0
	AH-3	53,900	29.0	---	70,400	25.0
	AH-4	53,800	27.4	---	70,600	29.5
	Average	55,100	27.9		70,700	25.8
Bottom Flange*	AH-2	58,500	26.3	---	72,100	---
	AH-3	62,600	26.6	---	73,600	---
	AH-4	60,500	27.2	---	72,600	---
	Average	60,500	26.7		72,800	

*The material was deformed beyond the strain-hardening point by the cold-roll process during fabrication of the arches.

Dynamic Tests. To determine the increase in the yield point of the steel under dynamic load, tensile specimens were fabricated and then tested with the Laboratory's 50,000-pound dynamic materials testing machine.[7] The machine has a maximum static capacity of 50,000 pounds and head velocities up to 15 in./sec. With a booster facility, the static load capacity can be increased to 80,000 pounds and the head velocity can be increased to 30 in./sec. Statically, the piston stroke is 4 inches; at higher velocities it is 0.75 inch. For standard tensile specimens (0.2 $in.^2$ area), strain rates of 1.5 in./in./sec can be obtained.

As shown in Figure 18, the specimens were taken from both ends of the arch, where bending moments were small due to hinged supports. The specimens were assumed to be representative of the arch material before tests.

A total of nine tensile specimens, six from the web and three from the flange, were fabricated and tested. Dimensions of the test specimens are shown in Figure 19. To determine the value of the strain rate to be used for the dynamic tensile tests, the strain rates from SG-12 (Figure 6) were obtained from several dynamic tests; the average strain rate was 0.9 in./in./sec. The strain rate was maximum at this point because the flexural and compressive strains were of the same sign. Typical stress-strain curves are given in Figures 20 and 21 for the web and lower flange, respectively. It should be noted that the stress-strain curve of the lower flange does not show a definite yield plateau.

Table 3 summarizes the results of the dynamic tests. The average values of upper yield stress were 70,500 psi and 69,700 psi for the web and lower flange, respectively; the average values of lower yield stress were 69,100 psi and 66,500 psi, respectively; the average ultimate strengths were 80,600 psi and 82,500 psi, respectively. The average increase in the lower yield point was 23.0 percent for the web and 9.8 percent for the lower flange. The marked difference between the two sections was due to the fact that the flanges had been stressed closer to ultimate stress than the web.

When structural steels are stressed above 60 percent of the ultimate strength, structural properties of the material are changed. To illustrate the effect of strain hardening, consider a typical stress-strain curve as shown in Figure 22. If the material were stressed to A and unloaded, the stress-strain diagram would return to the strain axis in practically a straight line, AB, parallel to the initial straight-line portion of the diagram. If the stress were again applied, the yield point would be raised to A, the diagram following the dashed line BAC. The ultimate strength would be practically unchanged but the ultimate elongation would be reduced. The effect of the single loading to A is to increase the elastic strength and to decrease the ratio of dynamic to static yield points. The higher the point A, the smaller the percent increase in dynamic yield point.[8]

Static Tests

Static tests of four circular arches were performed in the blast simulator as described earlier; the arches were loaded along one-half their arc length. For the majority of the tests, radial deflections and strains were measured at the quarter points and the crown; horizontal and vertical reactions were measured as shown in Figure 8. Only arch AH-1 was tested to failure; the other three arches were loaded to a maximum load of 243 lb/in. During the tests it was observed that the support cart (Figure 8) moved a fraction of an inch to the right; the exact distance was undetermined. This was partially due to the elastic strain of the reaction dynamometers and partially due to the movement of the tiedown bolts for the support cart. By proportioning the assumed total horizontal movement at the maximum load, the cart movement was introduced in the theoretical analysis as a boundary condition by assuming that the deformation was proportional to the horizontal reaction load at R_1; this factor was taken to be 6.25×10^{-6} in./lb.

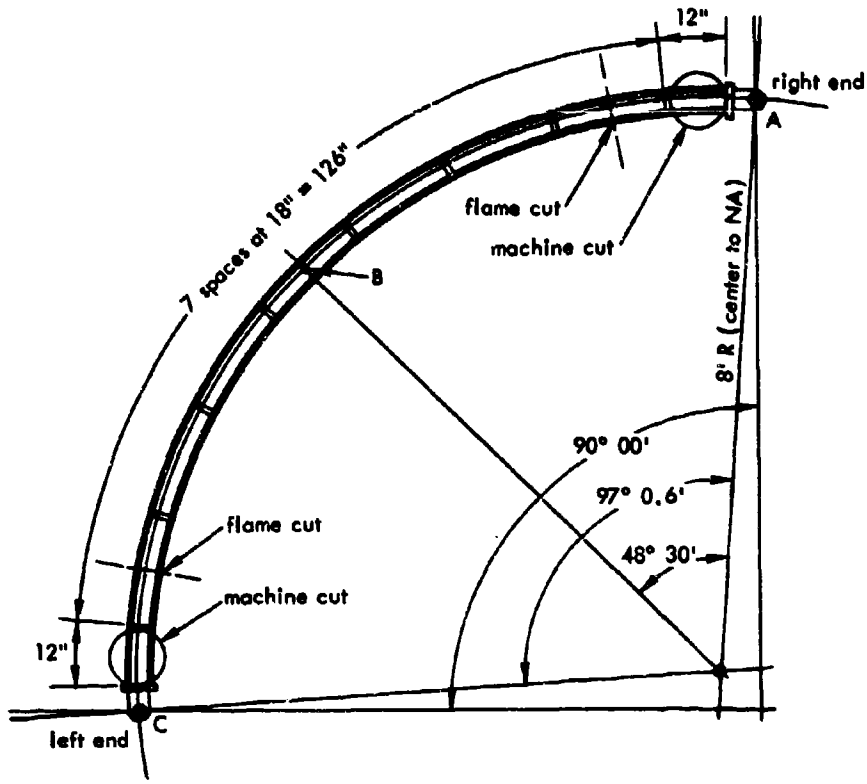

(a) two-hinged arch

AH-2
AW2D1
AW2D2
AF2D1
AF2D2
AH-3
AW3D1
AW3D2
AF3D1
AF3D2
AH-4
AW4D1
AW4D2
AF4D1
AF4D2

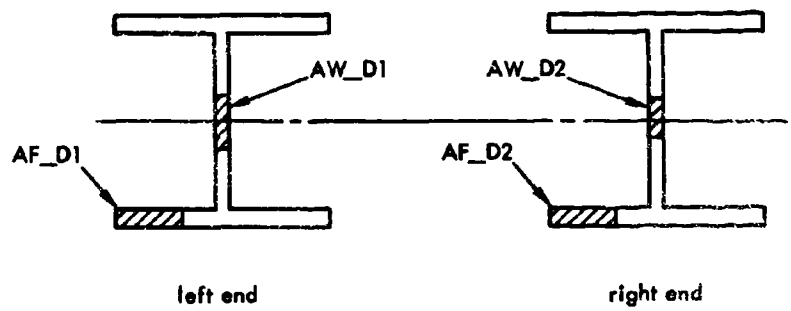

(b) AH-2, AH-3, AH-4

Figure 18. Location of specimens for the pinned-end arch.

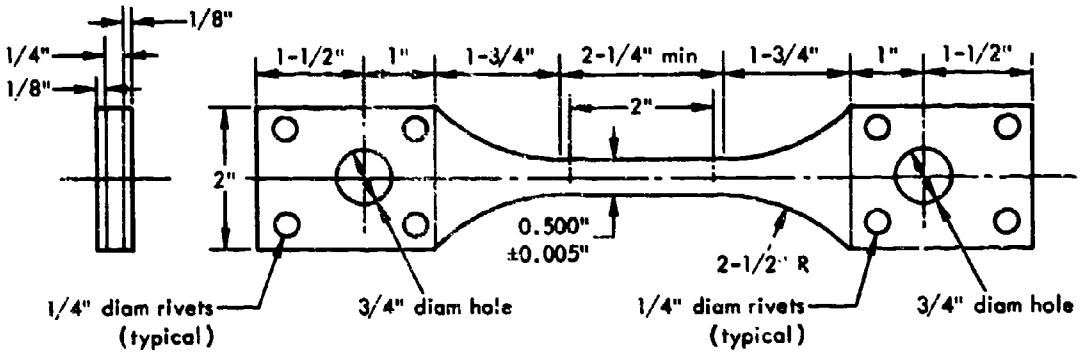

Figure 19. Dynamic tensile specimen.

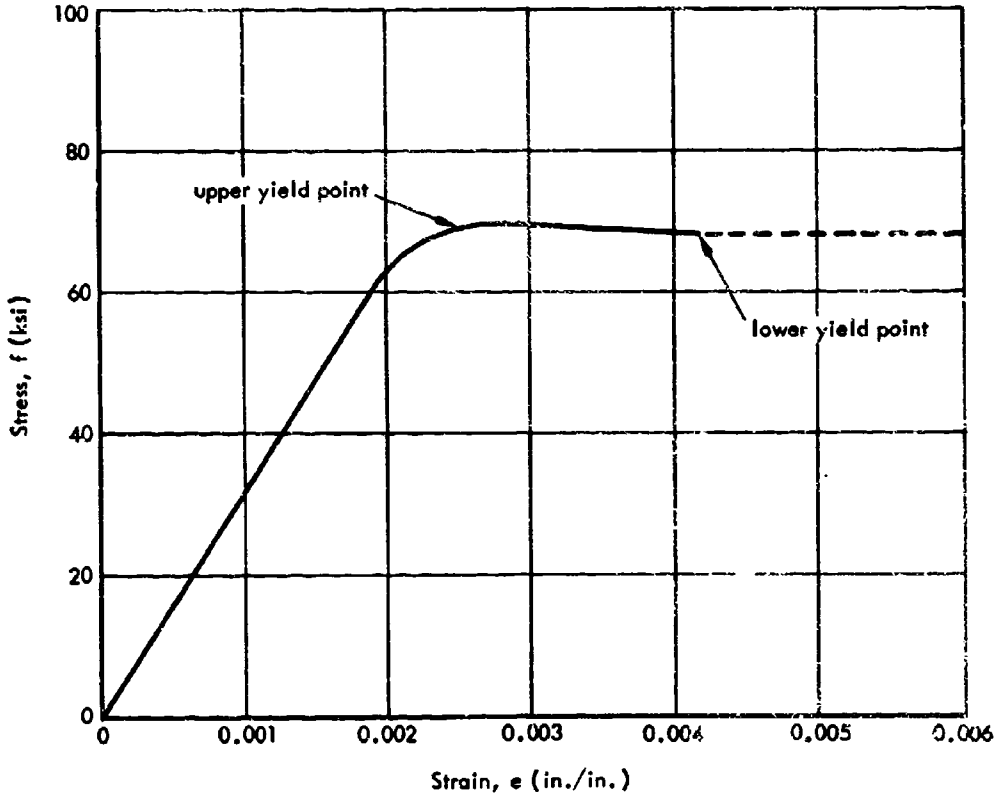

Figure 20. Dynamic stress-strain curve of the web at a strain rate of 0.825 in./in./sec.

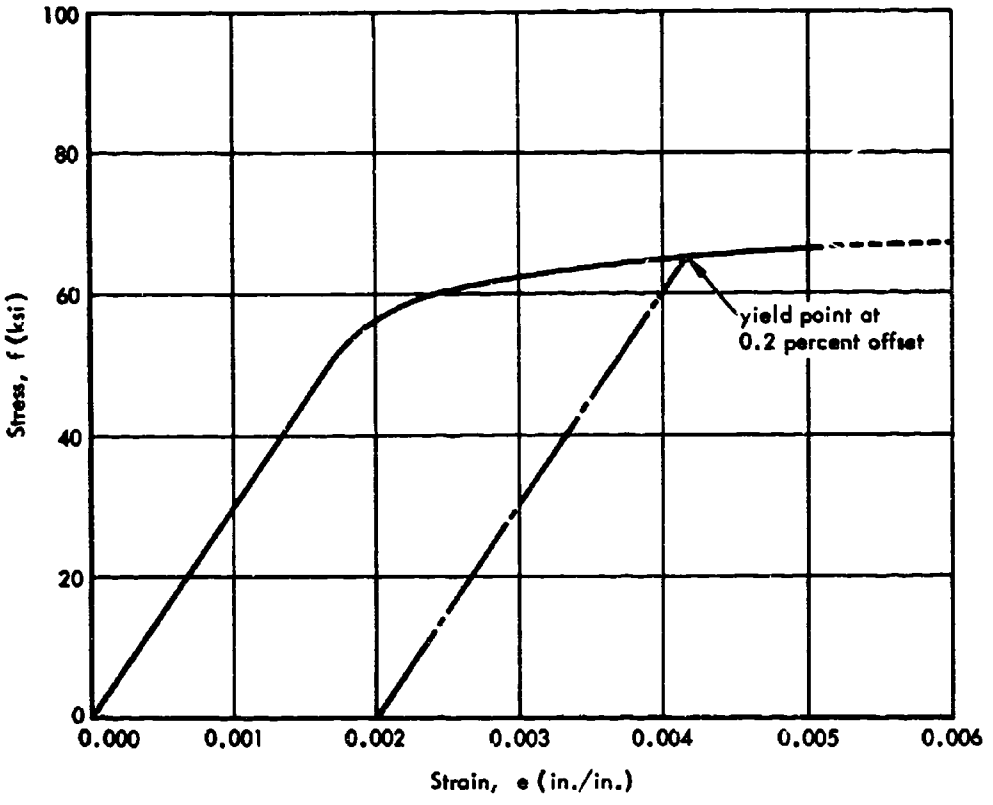

Figure 21. Dynamic stress-strain curve of the lower flange at a strain rate of 0.517 in./in./sec.

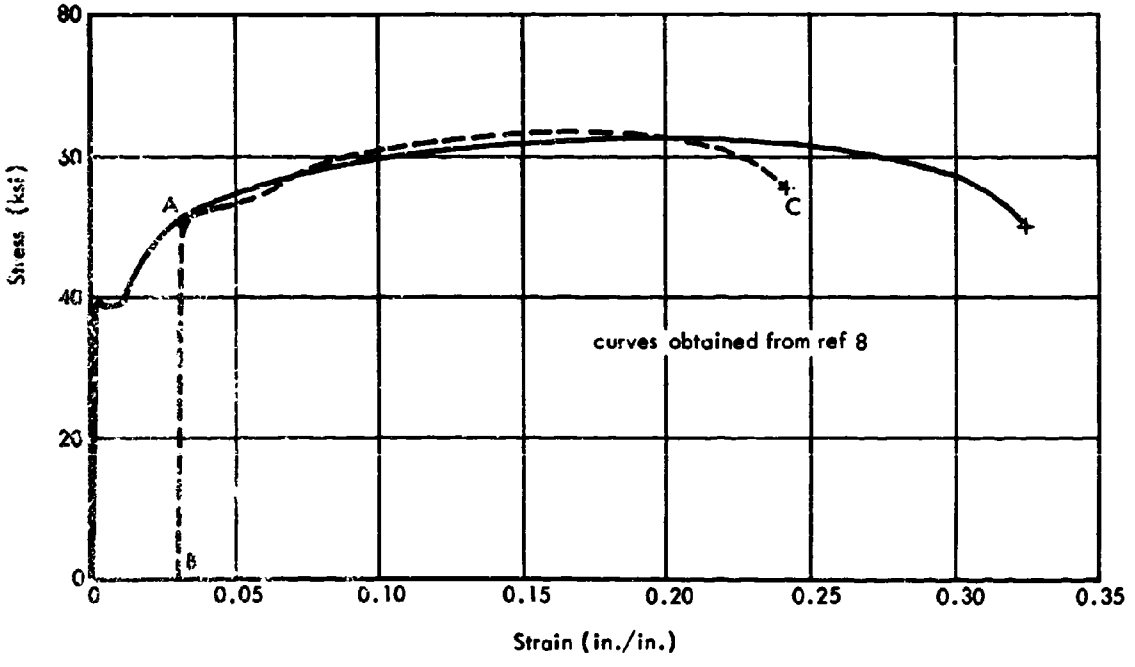

Figure 22. Strain-hardening effect in structural steel.

Table 3. Dynamic Properties of Steel for Antisymmetrically Loaded Arches

Location of Specimen	Arch No.	Upper Yield Stress (psi)	Lower Yield Stress (psi)	Ultimate Strength (psi)	Elongation in 2 Inches (%)	Strain Rate (in./in./sec)	Increase in Lower Yield Point (%)
Web*	AH-2	74,200	72,100	83,100	24.0	0.771	26.3
	AH-2	69,700	66,900	79,000	20.0	0.652	17.2
	AH-3	69,000	68,250	80,500	25.0	0.825	20.8
	AH-3	73,600	72,900	83,500	27.0	1.130	29.0
	AH-4	67,500	66,750	78,100	25.0	0.746	21.4
	AH-4	69,100	67,800	79,600	27.0	0.652	23.3
	Average	70,500	69,100	80,600	24.7	---	23.0
Lower* Flange	AH-2	---	64,200**	81,000	22.5	0.517	9.7
	AH-3	72,500	69,100	84,300	---	0.574	10.4
	AH-4	66,900	66,200	82,100	---	0.700	9.4
	Average	69,700	66,500	82,500	22.5	---	9.8

*The material was deformed beyond the strain-hardening point by the cold-roll process.
**Yield point stress at 0.2% offset.

Arch AH-1 was first preloaded to 487 lb/in. in increments of 162 lb/in. There were no appreciable permanent strains, deformation, or residual reactions observed after this test. Data from this test are not given in this report. Arch AH-1 was then reloaded to 568 lb/in. At this point, it was expected that certain sections of the arch would yield. The pressure was then increased in small increments to ensure that yield conditions would be recorded. At a load of 791 lb/in., air leakage at the neoprene seal exceeded the compressor capacity and a further increase in pressure was not possible. The reduced test data are presented in Table A-1. The maximum deflection obtained was 1.39 inches; the permanent deflection was 0.40 inch after unloading. The stiffness of the arch in the elastic range was 902 lb/in./in. and was close to the theoretical value of 937 lb/in./in. The strain data of Table A-1 were transformed into moments, direct forces, principal stresses, and shears; they are given in Table A-2.

After repair of the neoprene seal and retesting, the load-deflection curve rose slightly higher than the point of unloading before flattening out (Figure 23). This was the result of strain aging of the steel.[9] When strain aging is permitted, the sharp yield and yield elongation properties of mild steel return and increase the entire stress-strain curve. The arch collapsed at a load of 876 lb/in. with a corresponding deflection of 2.57 inches at the 3/4-point. No deflection was recorded at the 1/4-point. Figure F-1 shows the collapsed arch. There was evidence of buckling at the lower flange of the 1/4-point as a result of compressive strain. At the 3/4-point the lower flange and the web were ruptured.

The theoretical load-deflection values (calculated in Appendix B) are plotted in Figure 23 for comparison. Data for this test are given in Table A-3. Comparisons of experimental and theoretical load-strain curves at the quarter points of the arch are presented in Figures 24 and 25. Excellent correlation with strain gage 4 was obtained. Other theoretical strain curves were very close to their respective experimental curves in the elastic range but deviated somewhat in the inelastic range. A comparison of theoretical and experimental direct forces in the arch is shown in Figure 26. The experimental values showed that the direct forces at the 1/4-point and at the crown were very close to each other but were quite different from the direct force at the 3/4-point. Theoretically, the direct forces in the arch did not vary much at these points, as can be seen in Figure 26. Close correlation between the theoretical and experimental moment at the quarter points and at the crown of the arch is evident in Figure 27. Similarly, the shearing force at the location of strain rosette SG-13-14-15 is shown in Figure 28. The theoretical and experimental load-reaction curves are compared in Figure 29. Close correlations are evident in all four reactions.

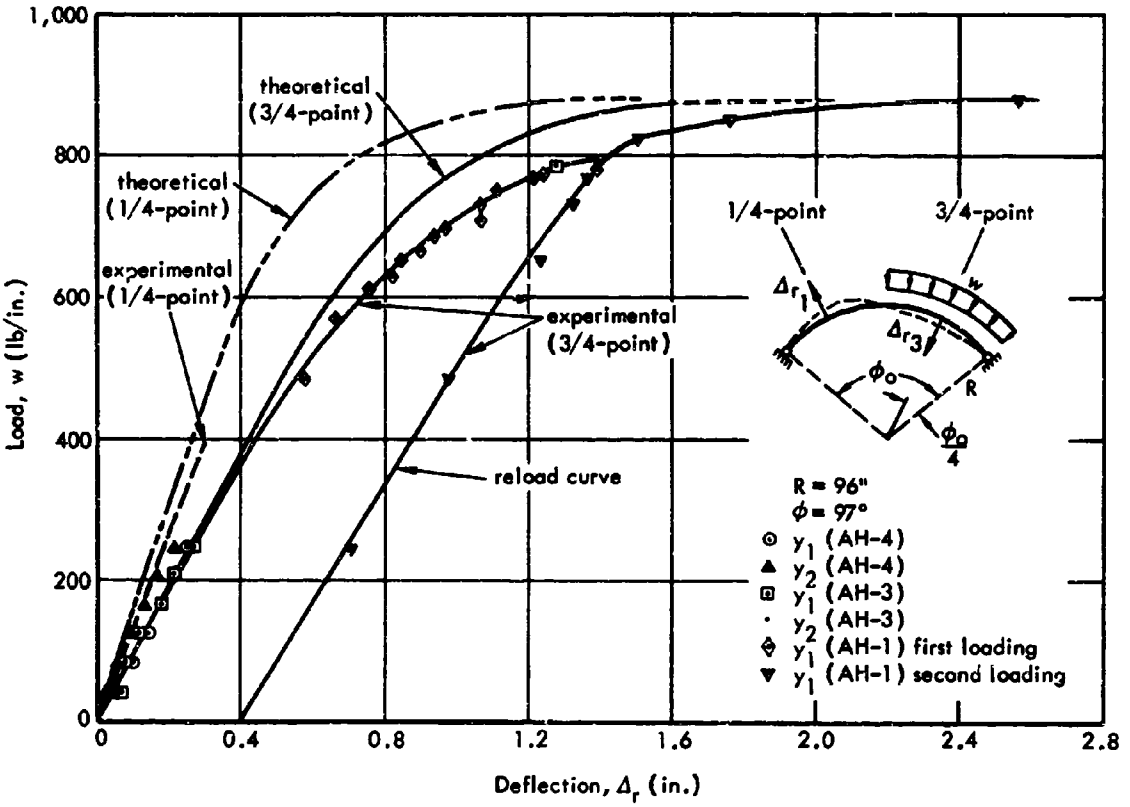

Figure 23. Comparison of theoretical and experimental static load-deflection curves for the antisymmetrically loaded arches.

Arches AH-2, AH-3, and AH-4 were preloaded statically to approximately 60 percent of the yield load prior to dynamic testing. The data from these tests are not included in this report; however, portions of the data are plotted in Figures 23 and 29 along with the data from arch AH-1. The permanent strains experienced in these static preload tests were negligible.

Free-Vibration Tests

Efforts were made to obtain experimental values of natural frequencies of the deflection mode and compression mode. However, only the lowest frequency of the antisymmetrical mode was obtained. These results are presented in Table 4. The average natural frequency from the experimental data was 54 cps, which agrees well with the theoretical natural frequency of the first antisymmetrical mode, 60 cps, as shown in Table D-5 of Appendix D. The theoretical value was obtained from a 40-bar distributed mass system.

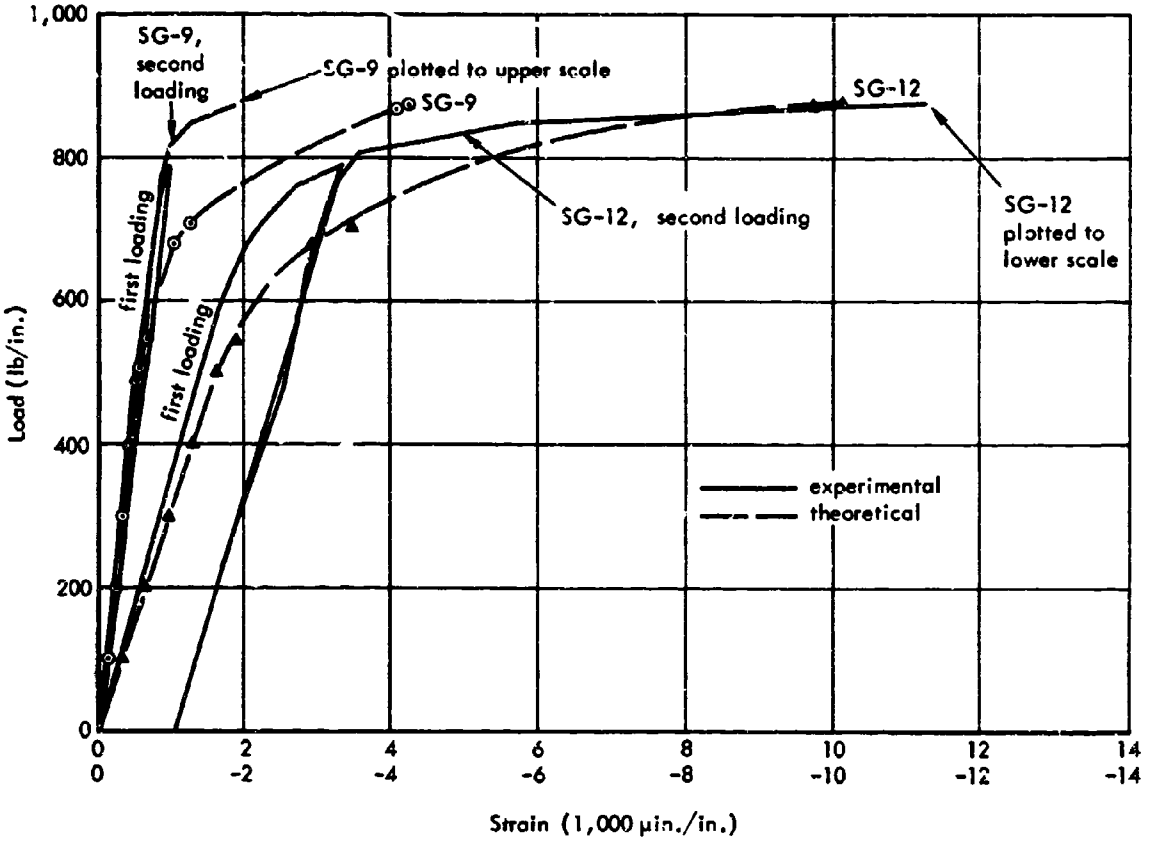

Figure 24. Comparison of theoretical and experimental strains at the 1/4-point of the antisymmetrically loaded arch.

Table 4. Summary of Free-Vibration Test of Antisymmetrically Loaded Arches

Arch No.	Natural Period, Avg T_n (msec)	Natural Frequency ω (cps)	Damping Ratio $\frac{\delta}{c_r}$	Logarithmic Decrement δ	Coulomb Damping Δ
AH-1	18.5	54.1	0.0930	0.587	-0.00507
AH-2	18.0	55.6	0.0975	0.616	0.000597
AH-3	19.1	52.4	---	---	---
Average	18.5	54.0	0.0953	0.602	0.00283

When viscous damping is present in an oscillating structural member, the degree of damping or the rate of decay is measured by means of the logarithmic decrement, δ, which is expressed as follows:

$$\delta = \frac{1}{n} \ln \frac{x_o}{x_n}$$

where x_o is the initial amplitude and x_n is the amplitude at the n^{th} cycle from the initial point. When dry friction or Coulomb damping is also present with the viscous damping, the use of the above equation will lead to erroneous results. A semigraphical trial-and-error method has been presented by Jacobson and Ayre;[10] however, the procedure requires skilled judgment and can lead to inconsistent results. A method presented by DaDeppo[11] applies least-square iteration to determine the damping constants for a dry-friction, viscous-damped system. The method is not well suited to manual computation. A program is presented in Appendix B for calculating the damping constants by means of a digital computer. The experimental decay records of the arches were analyzed by this computer program. The value of the logarithmic decrement, δ, the damping ratio, c_e/c_c, and the Coulomb damping, Δ, are presented in Table 4. The damping ratio is defined as the ratio of the coefficient of viscous damping, c_e, to the critical damping coefficient, c_c. The average value of the damping ratio for the first antisymmetrical mode was 0.095. In the theoretical analysis, the damping factor was expressed in the compression mode, and a corresponding value of 0.018 was used as discussed in Appendix C. A typical free-vibration record is shown in Figure 9.

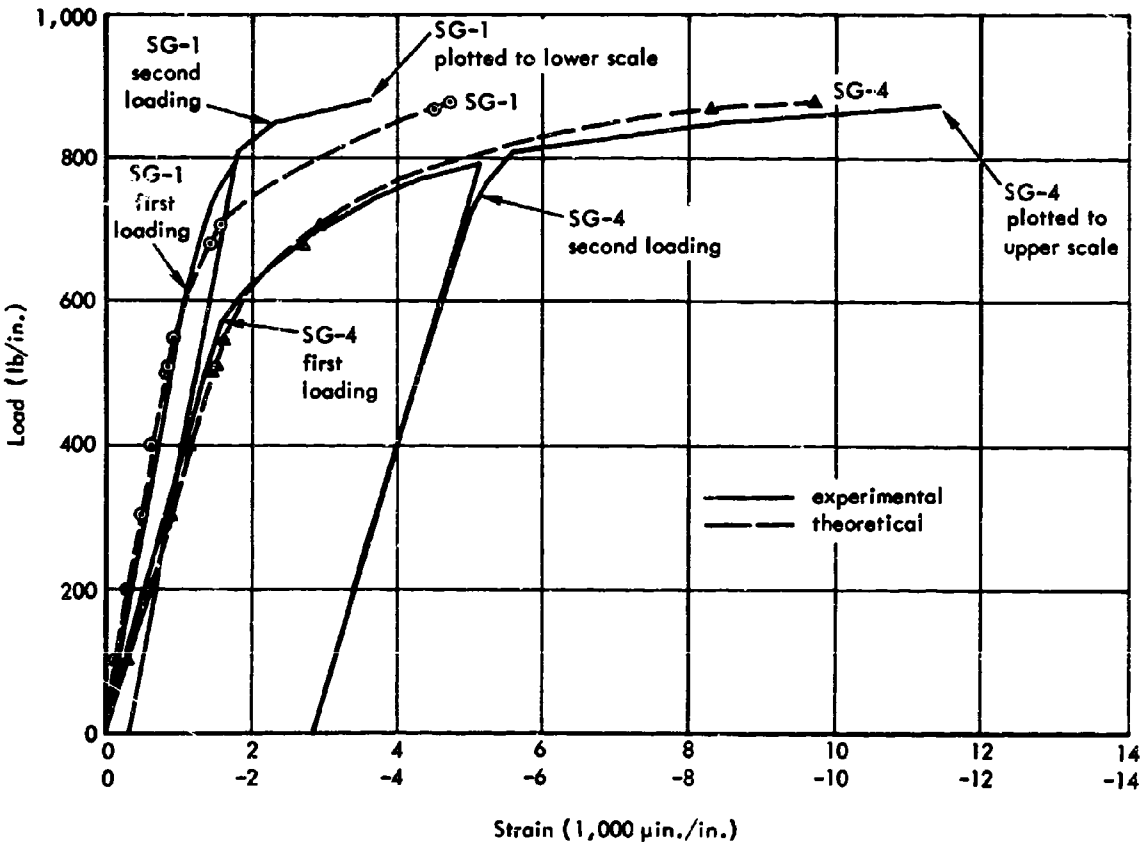

Figure 25. Comparison of theoretical and experimental strains at the 3/4-point of the antisymmetrically loaded arch.

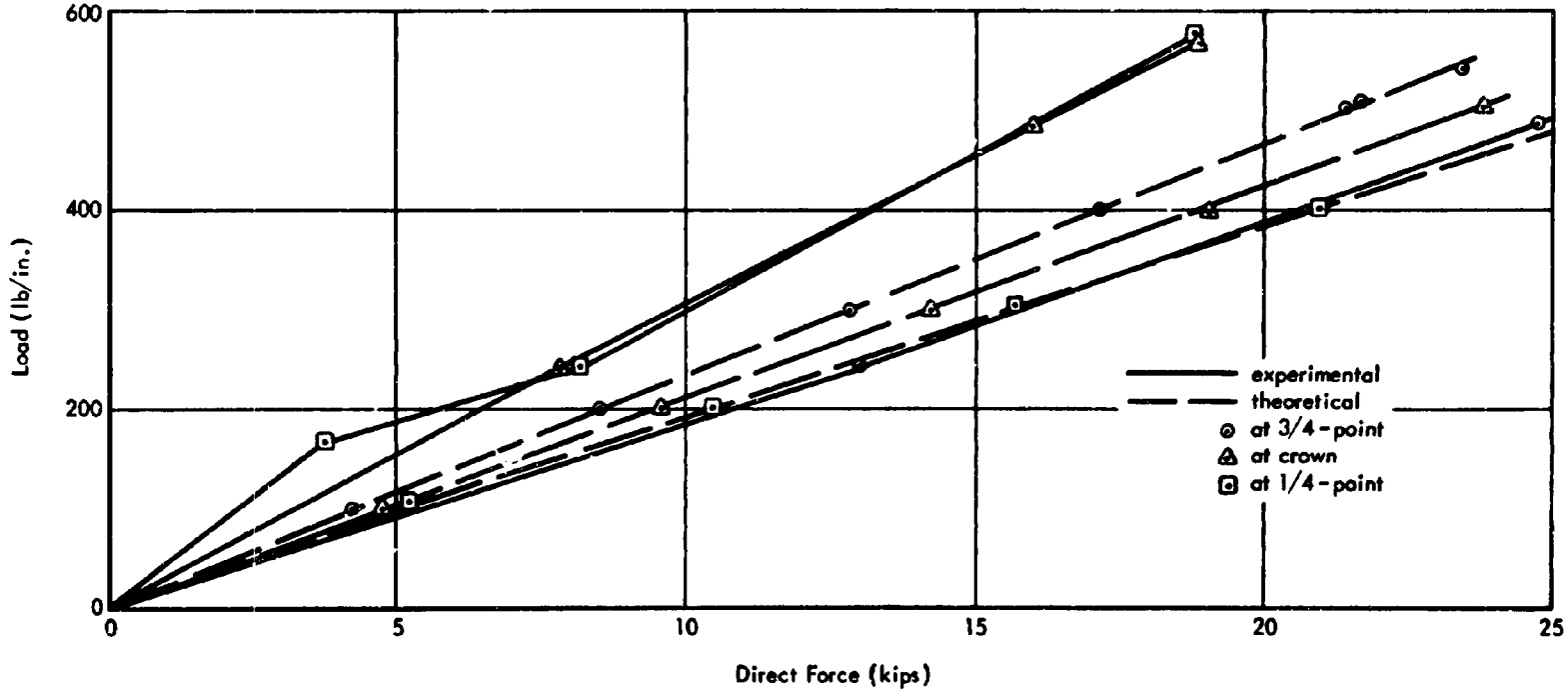

Figure 26. Comparison of theoretical and experimental direct forces in the antisymmetrically loaded arch.

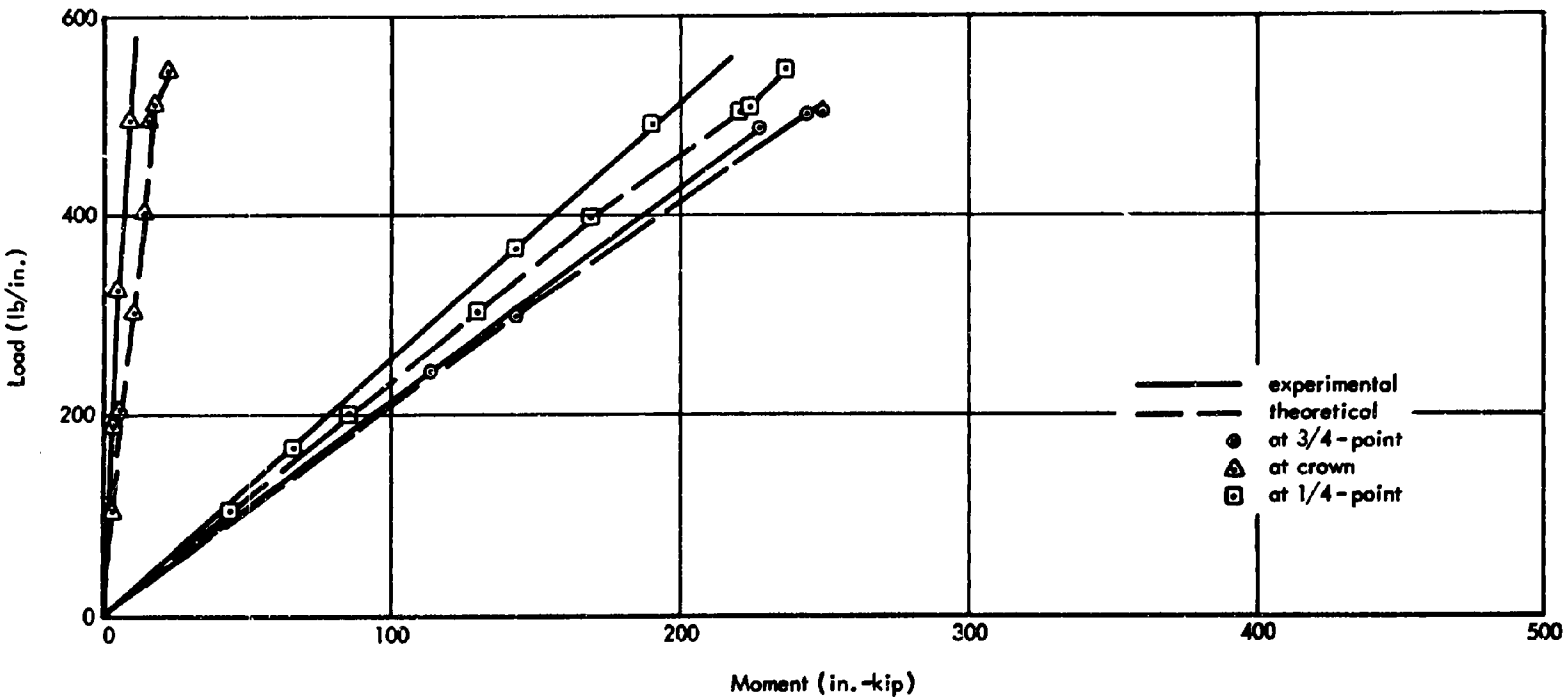

Figure 27. Comparison of theoretical and experimental moment in the antisymmetrically loaded arch.

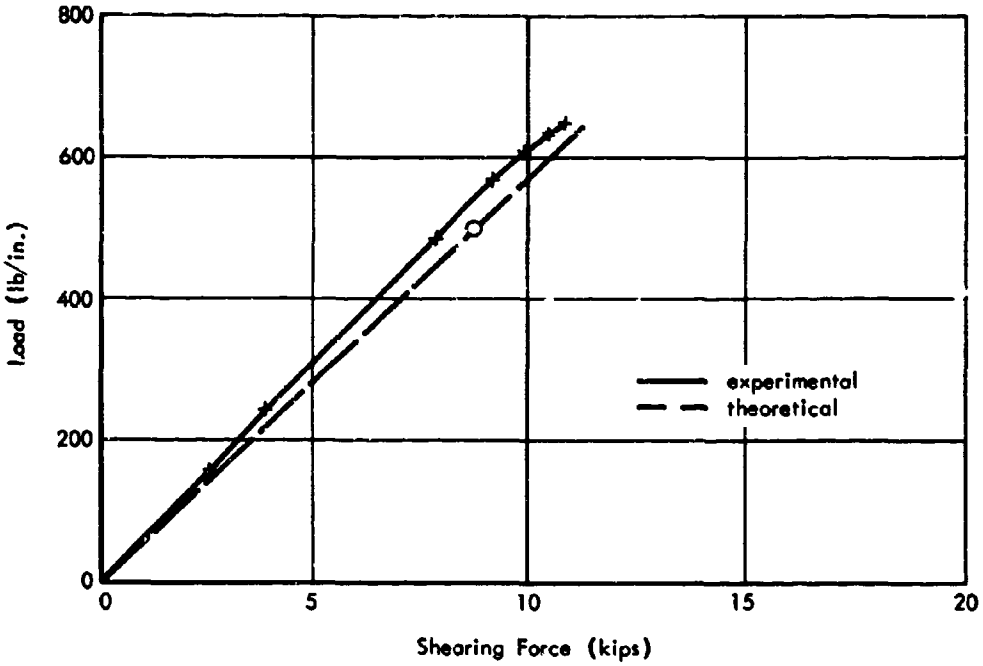

Figure 28. Comparison of theoretical and experimental shearing forces in the antisymmetrically loaded arch at strain rosette SG-13, 14, 15.

Dynamic Tests

After a maximum static load of 243 lb/in. was applied and unloaded, arch AH-2 was subjected to six dynamic loads of increasing magnitudes, with peak loads between 116 lb/in. and 780 lb/in. The postshot view of the arch is shown in Figure F-4. Maximum values of strains, reactions, deflection, and acceleration at the 3/4-point were obtained from data recorded on the oscillograph paper as shown in Figure 10.

Similarly, arches AH-3 and AH-4 were tested dynamically to peak loads of 780 lb/in. and 664 lb/in., respectively. Reduced data of all the dynamic tests are presented in Tables A-4 and A-5.

In comparing the strain values, it was found that the strains at the lower extremity of the 3/4-point were higher than the same location of the 1/4-point for each dynamic load. At a peak load of 780 lb/in., strain gages SG-4 and SG-12 indicated strains of 7,090 μin./in. and 6,940 μin./in., respectively; a similar relationship was observed in the static test data.

It should be noted that certain dynamic tests did not yield valid data and are therefore not recorded in Tables A-4 and A-5. The strain data of Table A-4 were taken at each peak value, which presented a problem in correlation of theoretical and experimental response because all the peak strains did not occur at the same time. Only a portion of the data in the elastic range of arch AH-2 was analyzed, and the resulting moments, direct forces, principal and shearing stresses are summarized in Table A-6 and Figures A-3 and A-4. The strain data of arches AH-2, AH-3, and AH-4 are plotted in Figures A-5, A-6, and A-7, respectively.

The load-deflection curves for both theoretical and experimental results are given in Figure 30. The experimental load-deflection curve represents the mean values of the data taken from the maximum values of each test of arches AH-2, AH-3, and AH-4. The theoretical curve is plotted from the data of Appendix C. Good correlation between the theoretical and experimental curves is evident in Figure 30.

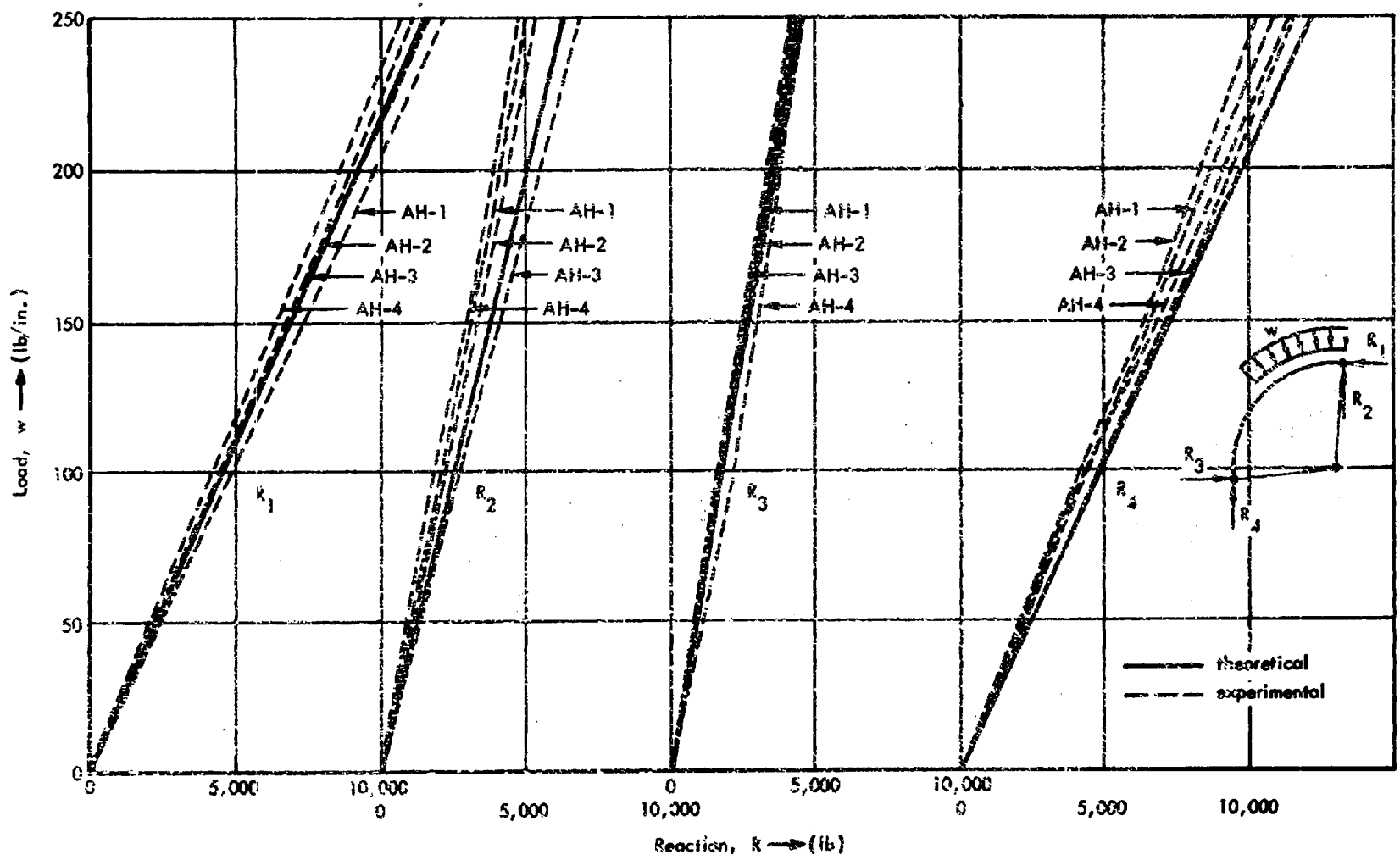

Figure 29. Comparison of theoretical and experimental reactions of the antisymmetrically loaded arch in the elastic range.

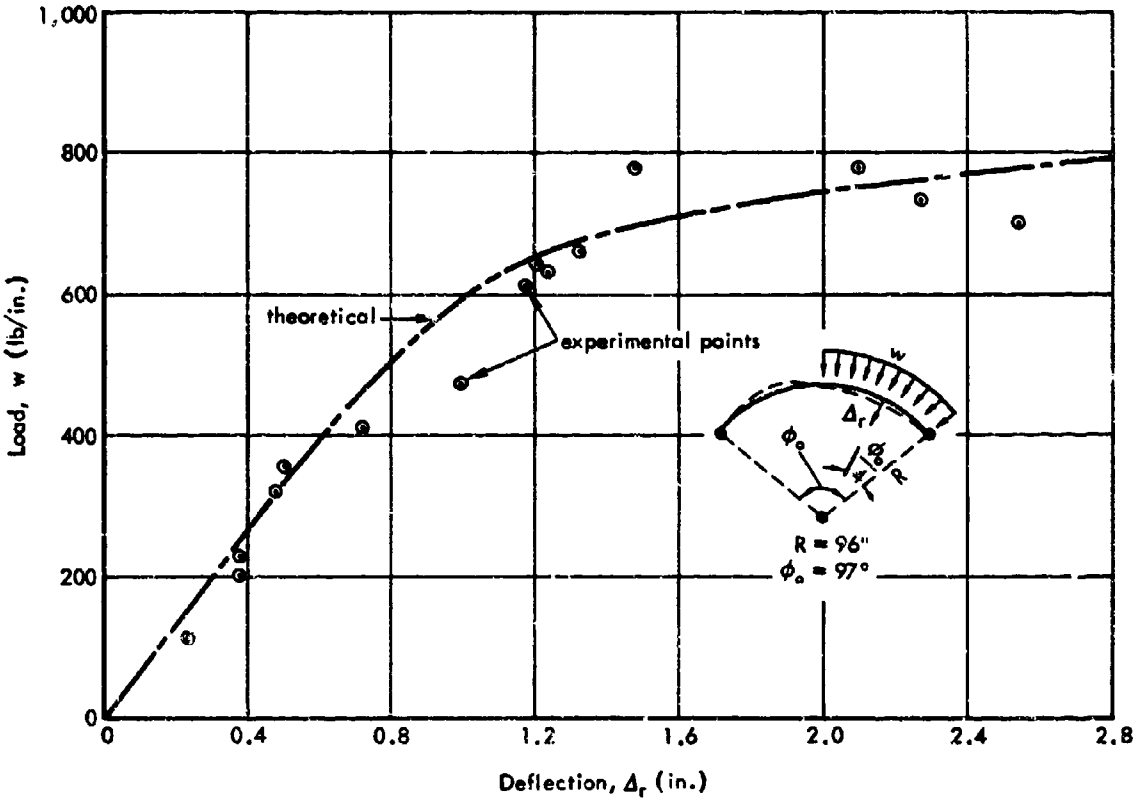

Figure 30. Comparison of dynamic load-deflection curves for the antisymmetrically loaded arch.

Figure 31 shows the comparison of the theoretical and experimental moments of the crown and quarter points of arch AH-2. Only experimental moments in the elastic range are presented for comparison. Moments at the quarter points show good agreement, but the moments at the crown do not agree very well. It is believed that the disagreement of moments at the crown of the arch is due primarily to the inaccuracy of the small strain readings of SG-5 through SG-8. The experimental values of direct forces did not agree with the theoretical values because the peak values of the strains did not occur simultaneously. In the calculation of experimental direct forces, the algebraic sum of different strains at the upper and lower extremities was taken. Small inaccuracies will result in large differences in the direct force.

The axial forces obtained from the simplified analysis (Appendix E) were very close to those obtained from the more rigorous analysis of Appendix C. However, the values of bending moment were notably higher in the same comparison, since the damping was not considered in the simplified analysis. The axial forces have time variations which correspond to the second symmetrical mode and the moment has a time variation which corresponds to the first antisymmetrical mode. Obviously, the damping effect on the moment was much higher than on the axial force.

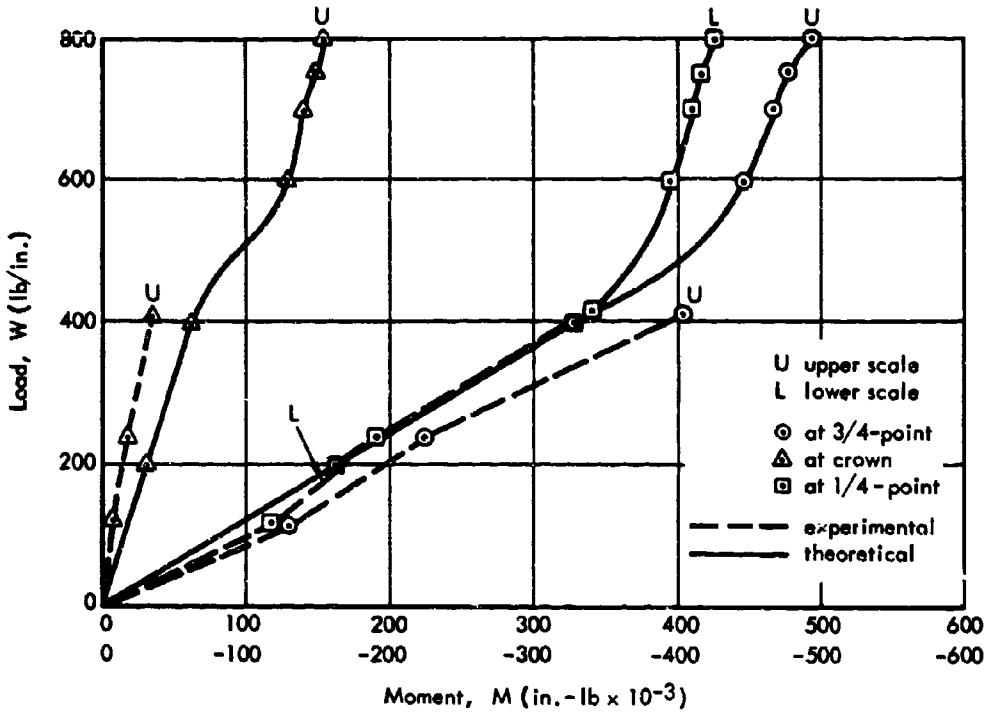

Figure 31. Comparison of theoretical and experimental dynamic moments.

GENERAL DISCUSSION

Design, Behavior, and Analysis of the Arches

The depth and width of the arches were limited to 4 inches and 7-3/4 inches, respectively, because of the physical dimensions and safe-load capacity of the blast simulator. To provide symmetry of the cross section with respect to the neutral axis would have required the use of a thin-gaged steel member. As a compromise, a top-heavy section was selected for the arches, consisting of a 4M13 cold-rolled section with steel strips, 5/8 inch by 1-7/8 inches, welded to each side of the top flange. In the cold-roll process, the 4M13 section was strained beyond yield. The flange strips were cold-rolled separately and then welded to the 4M13 section; as a result the flange strips were inelastically strained less than the 4M13 section. The strain-hardening properties of the flange strips and the 4M13 section were determined by static and dynamic tensile coupon tests.

Because of the strain hardening encountered in the cold-roll process, the static and dynamic stress-strain curves of the material did not exhibit a definite yield point. It was also observed that the total elongation of the tensile specimens was less for strain-hardened steel than for similar material that was not strain hardened. It is believed that the arches would have deflected more at ultimate load if these strain-hardening effects had not been present. Furthermore, the ultimate load of the arch was limited by the ultimate strength of the lower flange. As the lower flange was stressed into the inelastic range, the neutral axis

moved closer to the upper flange which caused the strain in the lower flange to increase more rapidly. As the arch approached the ultimate load, a considerable portion of the arch remained in a low-stress state at the critical section; thus, failure occurred before the full ductile potential of the arch was developed.

In the analysis, it was necessary to consider the nonhomogeneous section created by the 4M13 section and the flange strips. It was desirable to express the stiffness properties of the cross section as the products EI and EA. Separation of the modulus, E, from these product terms would have complicated the analysis.

Due to the lack of a definite yield plateau in the steel used in the arches (particularly the flanges), a trilinear stress-strain curve was used for the static analysis. Ordinarily this would not be necessary since the cold-roll process is not generally used in the fabrication of large arches. The analytic method presented in Appendix B is valid for materials with bilinear or trilinear stress-strain curves or even for a material that does not have an elastic range.

In the elastic range, the static analysis initially involved solving a statically determinate arch without the redundant reactions (the two-hinged arch has one redundant reaction and a fixed-end arch has three). The redundant reaction can then be obtained by satisfying the boundary conditions at the supports. In this analysis, elastic supports as well as rigid supports can be handled.

In the inelastic range, the incremental stress method was used along with an iteration process to determine various locations of yielding until the ultimate strength was reached at some location in the arch. The analysis was carried only as far as the development of the ultimate strength.

Analysis of the two-hinged arch of uniform cross section indicated that moments at the crown were small for a uniform load distributed over one-half the arch. This suggested that the placement of a third hinge at the crown would not substantially alter the behavior of the arch. Thus, a three-hinged arch would support the loads as well as the two-hinged arch. The analysis of a three-hinged arch is much simpler than that of a two-hinged arch. In addition, such a statically determinate arch would not be subjected to the effects of thermal stress, differential settling of the support, and initial misalignment. Furthermore, the variation in cross section could be handled with less difficulty.

Dynamic analysis of the arch employed a discrete framework in both the elastic and inelastic ranges. The mass of the arch was concentrated at the flexible joints, which were connected by rigid bars. An iteration process was used to obtain the forces and displacements at each joint by satisfying the respective equations of motion. The numerical integration method by Newmark was an essential tool in this analysis.[12]

An additional assumption was made for the dynamic analysis in the inelastic range. The cross section of the arch was represented only by the two flanges. This assumption was desirable due to the complexity of the bilinear stress-strain relationship (Figure C-5) in the loading and unloading process. Accuracy of the dynamic analysis by the iteration process depends largely on the simplicity of the idealized stress-strain curve and the number of the joints in the discrete framework. Convergence of iteration is slow if these factors are complicated.

In the determination of natural frequencies and mode shapes (Appendix D), it was found that the distributed-mass system provided better results than the concentrated-mass system for the same number of joints. However, it is believed that the use of a distributed-mass system for the dynamic response theory would undesirably complicate the analysis and increase calculation time.

In the actual arch tests, there were numerous contributions to total damping of the system: viscous damping (internal and external), Coulomb damping, and damping at the supports. To separate the effect of each type of damping would require extensive study of the properties of the material; this study was not justified from an engineering standpoint. The damping factor used in the theoretical development was obtained experimentally from the free-vibration tests in the deflection mode and represented the combined effect from all sources. It is believed that the supports provided a major contribution to the total damping; the number and quality of the support connections greatly influenced the damping characteristics of the arch. Also, it is believed that a three-hinged arch would have higher damping than a two-hinged arch or a hingeless arch, provided other factors remained unchanged.

The simplified dynamic analysis of Appendix E is a rapid, easy method of obtaining information on a portion of the dynamic response of an antisymmetrically loaded arch. This method is limited to the response of the quarter point of the loaded side of the arch. The damping effect was not considered in the analysis and, as a result, the moment values were larger than their counterparts in Appendix C. The values of axial forces obtained from the simplified analysis compared very well with those of the more rigorous analysis.

The digital computer proved indispensable in both the static and dynamic analyses of the arch system, particularly when elastic supports were involved.

Effect of Load History

The effect of load history on the dynamic response of structures has been reported for structural connections and portal frames.[1,2,3] In the static test of arch AH-1, pressure leakage necessitated unloading and reloading the arch after certain portions of the lower flange had been strain-hardened. The load-deflection curve for the reloading was higher, before it became flat, than the initial loading curve. This effect is known as strain aging.[5] When the metal is strained and then aged, the sharp yield and the yield elongation may return and increase the resistance of the material. This phenomenon is accompanied by a decrease in the ductility of the steel.[4,5] Multiple loading of the arch will reduce the flexibility of the arch in the inelastic range, particularly near the ultimate load. The cold-roll fabrication process of the arch can be considered a form of loading; its effects have been discussed in the previous section.

Application of Results

Correlation of the theoretical and experimental data provides a basis for design of arch structures to resist blast loading. The information contained in this report can be used to refine the design and fabrication of arch structures.

This study applies only to the loading, support conditions, and configuration of the arch. Generalization of the results to produce a simplified method for the solution of arch problems should be performed with caution. In relating the results of this investigation to design practice, particular care must be taken to examine the load and mass distributions, stiffness characteristics, and support condition of the structure. The methods and computer program for the theoretical solution of arch behavior provided in this report can be used to study arches of other configurations and loading, provided proper input parameters are employed.

Accuracy of Measurements

The instrumentation used in this experiment was carefully selected and calibrated before testing. The obtained measurements are believed to be accurate within the manufacturer-recommended tolerance of each measuring device. Data reduction, although subject to human error, was carefully performed and checked to eliminate all significant errors. The reduced experimental data are assumed to have the following accuracy:

Data	Accuracy (%)
Static:	
Pressure	2 to 3
Reaction	2 to 3
Deflection	2 to 3
Strain	4 to 5
Dynamic:	
Pressure	4 to 5
Reaction	4 to 5
Deflection	4 to 5
Strain	8 to 10
Strain rate	10 to 12
Acceleration	12 to 15

Conversion of the experimental data for comparison with the theoretical solutions was performed by a computer. The results are believed to be as accurate as the assumptions permit.

FINDINGS AND CONCLUSIONS

The experimental tests and the theoretical solutions included in this report are limited to a specific two-hinged arch with certain loading conditions; however, some of the findings and conclusions are applicable to arches with other loading and support conditions and configurations.

General

1. Tensile coupon tests indicated that the steel used in the arches was strain hardened; the material lacked a definite yield plateau common to structural steel and consequently was better represented by a trilinear stress-strain curve than by the usual bilinear curve.

2. The ductility of the arch material was reduced primarily by the strain resulting from the cold-roll process; the arch failed before the ductile potential was developed.

3. When the material was strain hardened and then aged, as when the arch was unloaded and loaded in the inelastic range, the stress rose above the original stress-strain curve and the ductility of the material was considerably reduced.

4. The failure modes for both the statically and dynamically loaded arches were similar. The governing factor was the ultimate stress at the lower flanges of the quarter points.

Static Tests

1. Good correlation was obtained between experimental behavior and the theoretical analysis in the elastic and inelastic ranges.

2. The deflected shape of the arch was basically antisymmetrical, with a rotation of the chord connecting the two hinges introduced by the yielding supports.

3. Bending moment was the predominant factor in the stress and strain distribution in the arch; the direct axial forces exerted only a minor effect in developing the stress and strain in the arch.

4. The yielding support on the loaded end reduced the axial forces in the arch, increased the bending moment and deflection on the loaded half of the arch, and decreased the moment and deflection on the unloaded half of the arch.

5. The maximum bending moment and deflection occurred very near the quarter points of the arch, where the shearing forces were zero.

6. The maximum stresses occurred in the lower flanges of the quarter points.

7. The crown of the arch, which was very close to the point of contraflexure, maintained a very low bending moment throughout the loading history.

8. Collapse occurred when the ultimate stress at the lower flanges of the quarter points was reached.

Dynamic Tests

1. The theoretical analyses satisfactorily predicted the experimental dynamic behavior of the arches in the elastic and inelastic ranges. The simplified analysis proved to be sufficiently accurate for design purposes.

2. The time-dependent displacements occurred at a frequency corresponding to the first antisymmetrical mode of the free vibration of the arch. This indicated that the first antisymmetrical mode was predominant in the response.

3. The axial force remained essentially uniform along the length of the arch and varied with time according to the frequency of the second symmetrical mode of the arch (breathing mode).

4. The bending moments varied with time at the frequency of the first antisymmetrical mode of the arch. Although some contribution of the third antisymmetrical mode was observed, the first antisymmetrical mode definitely made the main contribution to the moment.

5. Maximum stresses occurred at the lower flanges of the quarter points primarily due to bending action.

6. Bending moment at the crown of the arch was very small for all dynamic tests.

7. Damping of the system had an important effect on the bending response of the arch; its effect on the axial force was small.

DESIGN RECOMMENDATIONS

The methods used in the design of arch structures depend on such factors as the material used, geometry of the arch, conditions of loading and support, and the distribution of mass and stiffness along the arch. The two-hinged arch discussed in this report is only one specific case. However, certain design recommendations can be drawn from the theoretical analyses and experimental data which apply to two-hinged circular arches subjected to overpressure from a traveling blast wave.

Static Design and Analysis

The ultimate strength of the antisymmetrically loaded two-hinged arch is essentially limited by the moment-resisting capacities at the quarter points of the arch. This suggests that special reinforcement of the arch sections in the form of cover plates, or increased depth at the critical sections will considerably increase the ultimate strength at a small increase in fabrication cost.

The bending moment at the crown remained low throughout the entire loading history. This suggests that a three-hinged arch (hinges at the supports and the crown) of the same cross section will respond very much like the two-hinged arch. Thus it would be logical to consider a three-hinged arch as the first alternate design of the two-hinged arch. As a statically determinate structure, the three-hinged arch is less affected by thermal stress, differential settling of supports, and initial misalignment. The stress level is more readily controlled for certain loading conditions.

The arch response is very sensitive to the support conditions. It is essential that proper evaluation of the structural foundation be made before designing the arch. For arches resting on elastic supports, the axial forces in the arch will decrease and the bending moments will increase with increasing flexibility of the supports. In case of uncertainty, the design should be adequate for the two worst conditions.

The unbalanced arch cross section has a tendency to limit the moment-resisting capacity of the arch according to the yield strength of one flange. As the inelastic strain develops, the neutral axis moves away from the flange having higher stress and thus accelerates the straining process. For isotropic materials (most metals can be considered isotropic for design purposes), a balanced cross section is essential for the most economical design.

Strain hardening of the steel reduces its ductility; as a result, collapse of a strain-hardened arch occurs at the ultimate load with little warning. The use of strain-hardened material is not recommended for arch construction. In particular, a cold-roll process should not be used to fabricate arches other than model arches and sheet metal arches.

The use of a digital computer can be of great value in the arch analysis particularly when elastic supports are involved. The programs presented in Appendix B may be readily modified for arches of different geometries and support conditions.

Quasi-pseudo static response may be obtained from the dynamic solution by introducing a high level of damping. A damping factor of 0.3 proved to be satisfactory for the arch under consideration.

Dynamic Design and Analysis

For long-duration loads (in which the ratio of the load duration to the natural period of the arch is greater than ten), dynamic bending moments at the quarter points are equal in magnitude. However, the combination of moment and direct force will cause the lower flange of the quarter point on the loaded portion of the arch to yield first.

Maximum stresses are contributed primarily by bending. Special reinforcement by varying the effective depth of the arch sections at the quarter points is desirable. For dynamically loaded structures, the increased depth is more efficient reinforcement than cover plates because less mass is involved.

Rapidly strained steel exhibits a considerable increase in dynamic yield point; references 2 and 3 report results for initially unstrained specimens of A-7 mild steel. No research has been found which reports the increase in dynamic strength of steel after it had been previously strained into the strain-hardening region. Indications from this investigation are that the percentage increase in dynamic strength properties diminishes after previous inelastic straining has occurred. Specimens from some of these arches exhibit strength increases of about 10 percent for strain rates of 0.5 in./in./sec.

The level of damping is very important for the calculation of dynamic response of the arch. A damping factor of 0.1 will probably be appropriate for most steel arches.

Due to the absence of the damping terms, the use of the simplified analysis in Appendix E is limited to systems of light damping. This is demonstrated in the comparisons of axial force and moment obtained from the simplified and more rigorous dynamic solutions.

Similar to the static response, the bending moment at the crown for dynamic load remains low. Consideration of a three-hinged arch is also valid for dynamically loaded arches. In addition, the damping value will be higher for a three-hinged arch of similar cross-section properties.

The efficient use of a digital computer is essential in obtaining accurate dynamic response of the arch. The dynamic solution by the method of numerical integration is impractical, if not impossible, by manual calculation.

ACKNOWLEDGMENTS

The authors wish to acknowledge the contributions of the following people:

Dr. Bruce G. Johnston of the University of Michigan, for the design of the structural arch and test fixtures and for the preliminary static analysis.

Dr. Richard T. Eppink of the University of Virginia, for the preliminary theoretical analysis of Appendixes C, D, and E.

LIST OF SYMBOLS

General Note:

Superscripts:	Refer to:
ℓ, r	left and right sides of a joint
$\dot{x}$	first derivative of x with respect to time
$\ddot{x}$	second derivative of x with respect to time

Subscripts:

h, i, j, k, ℓ, m	designations for location of joints
x, y	designations for x, y direction
r, t	radial and tangential components
u, ℓ	upper and lower flanges
t, b	top and bottom flanges of the two-flange representation of the cross section

---

A	symmetrical matrix for natural mode and buckling load equation
A_{jm}	static stress amplification factor at joint j
A_m	static amplification factor for the simplified analysis
A_t, A_b	area of top and bottom flanges of the two-flange representation of the cross section (in.)
B	symmetrical matrix for natural mode and buckling load equation
B'	symmetrical matrix for natural mode and buckling load equation
b	instantaneous set
C	constant
C	symmetrical matrix for natural mode and buckling load equation
C_m	initial misalignment of arch supports (in.)
c	parameter used in the equations for natural modes and buckling loads
c_c	critical damping coefficient
c_e	external damping coefficient
c_u, c_ℓ	distances from neutral axis to upper and lower flanges (in.)
D(x)	dynamic amplification factor for simplified analysis
d	depth of arch cross section
E	modulus of elasticity (psi)
E'	inelastic modulus of material (psi)
E_1	second modulus of material (psi)
E_2	third modulus of material (psi)
EA_j	extensional stiffness parameter of joint j (lb)
EI_j	flexural stiffness parameter of joint j (lb-in.^{2})

e	strain (in./in.)
F	external force (lb)
f	stress (psi)
f_n	natural frequency of vibration (cps)
f_y	yield stress (psi)
H	horizontal redundant reaction (lb)
k	parameter used in the equations for natural modes and buckling loads
k	spring constant of elastic support (in./lb)
L	length of bars for the discrete framework (in.)
L_o	span of the arch (in.)
M_j	bending moment at joint j (in.-lb)
M_p	plastic moment (in.-lb)
m_j	mass of joint j (lb-sec^2/in.^{2})
N_j	axial force due to the deformation of bar j (lb)
n	number of bars for the discrete framework (in.)
n	a constant used in the simplified analysis
p_{jx}, p_{jy}	x, y components of external forces acting at joint j (lb)
P_{jx}, P_{jy}	x, y components of internal forces at joint j (lb)
P_{jr}, P_{jt}	radial and tangential forces at joint j (lb)
p	pressure (psi)
R	radius of the arch (in.)
R_1	reaction 1, etc. (lb)
T_n	natural period (msec/cycle)
$T(x)$	natural periods used in the simplified analysis (msec/cycle)
t	time (sec)
t_o	duration of dynamic load (sec)
W_E	total external work (in.-lb)
W_I	total internal work (in.-lb)
W_{jr}, W_{jt}	external resultant forces at joint j in radial and tangential directions (lb)
w	uniform load (lb/in.)

w_{cr}	buckling load used in the simplified analysis (lb/in.)
Z	plastic section modulus ($in.^3$)
Z_{jr}, Z_{jt}	internal resultant forces at joint j in radial and tangential directions (lb)
α	angle between radii of support and a point on the arch (rad)
β	angle between radial of a support and x axis (rad)
β	coefficient of numerical integration
γ	maximum shearing stress in the web
δ	logarithmic decrement
δ_j	deformation of bar j (in.)
$\bar{\delta}_j$	first-order approximation of δ_j (in.)
Δ	deflection (in.)
Δ_{jx}, Δ_{jy}	x, y components of displacement at joint j (in.)
Δ_{jr}, Δ_{jt}	radial and tangential displacements at joint j (in.)
Δt	time increment (sec)
θ_j	angular change, elastic weight at joint j (rad)
$\bar{\theta}_j$	first order approximation of θ_j (rad)
θ_j'	inelastic angular change at joint j (rad)
λ	parameter used in the equations for natural modes and buckling loads
μ	mass per unit length of the arch ($lb\text{-}sec^2/in.^3$)
ν	damping factor
ν'	damping factor associated with "breathing" mode of vibration
ρ	parameter used in the equations for natural modes and buckling loads
$\sigma_{1,\,2}$	principal stresses 1 and 2
ϕ_o	central angle of the arch (rad or deg)
ϕ_j	central angle subtended by bar j (rad)
ϕ_p	angle of principal axes with respect to strain rosette
ψ	angular rotation (rad)
ψ_j	angular rotation of bar j (rad)
$\bar{\psi}_j$	first order approximation of ψ_j (rad)
ω	circular frequency of vibration (rad/sec)

Appendix A

MEASUREMENTS OF PRESSURE, DEFLECTION, AND STRAIN

Table A-1. Static Test Data for Antisymmetrically Loaded Arch AH-1, Test No. 2

Load w (lb/in.)	Deflection y_1 (in.)	Strain, e (μin./in.)									Reaction (lb)	
		SG-1	SG-2	SG-3	SG-4	SG-5	SG-6	SG-7	SG-8	SG-9	R1	R2
0	0	0	0	0	0	0	0	0	0	0	0	0
243	0.27	-440	90	320	690	-40	-50	-70	-60	250	12,270	4,810
486	0.58	-860	180	620	1,370	-70	-110	-150	-140	510	24,310	9,620
568	0.67	-1,000	220	760	1,610	-70	-130	-180	-170	630	28,100	11,110
609	0.76	-1,090	290	880	1,800	-70	-140	-200	-180	660	29,440	11,940
633	0.81	-1,140	360	1,000	2,140	-70	-140	-200	-200	700	30,330	12,270
649	0.85	-1,190	400	1,080	2,310	-70	-150	-210	-200	720	31,000	12,600
665	0.90	-1,230	460	1,180	2,530	-70	-150	-220	-210	740	31,900	12,770
682	0.94	-1,270	500	1,280	2,710	-70	-160	-230	-220	770	32,560	13,100
698	0.98	-1,320	560	1,380	2,940	-70	-160	-240	-230	800	33,230	13,260
714	1.07	-1,360	640	1,510	3,230	-60	-170	-250	-240	830	34,120	13,430
730	1.07	-1,450	710	1,720	3,530	-60	-170	-260	-250	850	34,790	13,760
746	1.12	-1,510	780	1,800	3,790	-60	-180	-270	-260	880	35,460	13,930
763	1.21	-1,560	890	1,990	4,180	-50	-180	-290	-270	910	36,130	14,090
771	1.25	-1,620	950	2,060	4,350	-50	-190	-290	-280	950	36,800	14,260
787	1.34	-1,720	1,120	2,380	5,000	-50	-190	-300	-300	1,000	37,470	14,420
791	1.39	-1,760	1,170	2,460	5,190	-50	-190	-310	-300	1,020	37,470	14,420
perm	0.40	-340	830	390	2,840	-40	-20	-70	-40	10	340	500

Load w (lb/in.)	Deflection y_2 (in.)	Strain, e (μin./in.)									Reaction (lb)	
		SG-10	SG-11	SG-12	SG-13	SG-14	SG-15	SG-16	SG-17	SG-18	R3	R4
0	0	0	0	0	0	0	0	0	0	0	0	0
243	0.27	-180	-370	-670	160	-80	-220	-260	-90	200	4,490	10,730
486	0.58	-370	-740	-1,350	340	-150	-440	-540	-180	390	9,430	21,020
568	0.67	-440	-860	-1,570	390	-150	-520	-640	-200	490	11,180	24,970
609	0.76	-480	-946	-1,710	430	-180	-560	-670	-220	500	11,620	25,840
633	0.81	-500	-1,000	-1,800	450	-180	-590	-700	-220	530	12,170	26,940
649	0.85	-540	-1,040	-1,880	470	-180	-610	-710	-220	560	12,490	27,810
665	0.90	-550	-1,090	-1,960	490	-180	-630	-720	-230	580	12,820	28,250
682	0.94	-580	-1,140	-2,060	510	-180	-650	-720	-230	600	13,260	29,130
698	0.98	-640	-1,200	-2,160	530	-180	-670	-730	-240	600	13,590	29,780
714	1.07	-660	-1,260	-2,250	560	-190	-690	-780	-240	610	14,140	30,440
730	1.07	-700	-1,350	-2,410	580	-190	-720	-800	-240	630	14,580	31,100
746	1.12	-830	-1,440	-2,550	600	-190	-750	-830	-250	660	14,800	31,540
763	1.21	-860	-1,540	-2,720	620	-190	-770	-830	-250	680	15,670	32,630
771	1.25	-920	-1,620	-2,880	630	-190	-790	-850	-260	690	---	---
787	1.34	-1,010	-1,830	-3,210	670	-160	-820	-870	-260	710	---	---
791	1.39	-1,060	-1,900	-3,320	680	-160	-830	-850	-250	720	---	---
perm	0.40	-360	-650	-1,060	120	-100	-80	-30	-20	40	---	---

Table A-2. Summary of Static Data for Arch AH-1, Test No. 2

Load (lb/in.)	SG-5 (μin./in.)	SG-8 (μin./in.)	Moment (in.-kips)	Direct Force (kips)
243	-40	-60	-2.75	7.76
486	-70	-140	-7.60	16.00
568	-70	-170	-10.20	18.90
609	-70	-180	-11.50	19.30
633	-70	-200	-12.60	19.90
	SG-1	SG-4		
243	-440	690	114.00	13.00
486	-860	1,370	227.00	24.70
568	-1,000	1,610	265.00	27.90
	SG-9	SG-12		
243	250	-670	-93.20	8.18
486	510	-1,350	-190.00	15.90
568	630	-1,570	-224.00	14.50
609	660	-1,700	-241.00	18.40

Load (lb/in.)	Principal Stress		Phi (rad)	Max Shear Stress (ksi)	Rad Shear (kips)
	σ_1 (ksi)	σ_2 (ksi)			
243	2.91	-5.20	-0.117	4.05	-3.79
486	6.30	-10.31	-0.126	8.31	-7.80
568	7.20	-12.19	-0.120	9.70	-9.10
609	7.94	-12.90	-0.118	10.40	-9.83
633	8.30	-13.60	-0.105	11.00	-10.40
649	8.77	-13.84	-0.104	11.30	-10.80

Table A-3. Static Test Data for Antisymmetrically Loaded Arch AH-1, Test No. 3

Load w (lb/in.)	Deflection y_1 (in.)	Strain, e (μin./in.)									Reaction (lb)	
		SG-1	SG-2	SG-3	SG-4	SG-5	SG-6	SG-7	SG-8	SG-9	R1	R2
0	0.40	-340	830	390	2,840	-40	-20	-70	-40	10	0	0
243	0.71	-780	910	730	3,510	-70	-70	-150	-160	280	11,850	4,970
487	0.98	-1,220	1,020	1,050	4,270	-100	-120	-230	-270	560	23,700	9,610
649	1.24	-1,520	1,100	1,270	4,780	-120	-160	-280	-350	740	31,920	12,600
730	1.33	-1,660	1,160	1,420	5,040	-130	-180	-300	-390	850	35,870	14,260
771	1.38	-1,760	1,180	1,500	5,240	-130	-190	-360	-410	900	37,850	14,920
811	1.46	-1,880	1,270	1,690	5,600	-140	-200	-340	-430	970	39,490	15,750
852	1.77	-2,350	2,260	3,160	8,510	-130	-210	-380	-490	1,250	41,470	16,240
876	2.57	-3,490	---	6,990	11,430	-100	-220	-430	-560	1,880	43,770	16,580

Load w (lb/in.)	Deflection y_1 (in.)	Strain, e (μin./in.)									Reaction (lb)	
		SG-10	SG-11	SG-12	SG-13	SG-14	SG-15	SG-16	SG-17	SG-18	R3	R4
0	0.40	-360	-650	-1,060	120	-100	-90	-30	-20	40	0	0
243	0.71	-550	-1,030	-1,750	280	-120	-300	-290	-110	230	4,430	10,510
487	0.98	-730	-1,400	-2,590	460	-250	-540	-560	-190	430	9,200	21,020
649	1.24	-870	-1,660	-2,910	580	-310	-690	-750	-250	570	12,470	27,810
730	1.33	-940	-1,800	-3,170	640	-330	-780	-830	-280	640	14,100	31,100
771	1.38	-970	-1,890	-3,320	670	-340	-810	-890	-290	680	14,800	32,850
811	1.46	-1,100	-2,110	-3,630	710	-360	-860	-940	-320	710	16,080	34,820
852	1.77	---	-3,620	-5,790	790	-340	-950	-1,000	-320	760	5,420	35,810
876	2.57	---	-7,320	-11,280	900	-330	-1,070	-1,050	-360	850	---	37,120

Table A-4. Summary of Dynamic Test Data of Antisymmetrically Loaded Arches

Arch No.	Test No.	Load w (lb/in.)	Maximum Strains, e (μin./in.)																	
			SG-1	SG-2	SG-3	SG-4	SG-5	SG-6	SG-7	SG-8	SG-9	SG-10	SG-11	SG-12	SG-13	SG-14	SG-15	SG-16	SG-17	SG-18
AH-2	7	116	-450	---	900	810	-170	-90	-180	-380	370	-200	-410	-760	250	-240	-400	-230	-120	310
	8	235	-800	360	790	1,430	-270	-170	-260	-460	590	-340	-720	-1,260	440	-410	-670	-460	200	610
	9	322	-1,020	470	1,020	1,660	-350	-200	-290	-560	740	-420	-770	-1,390	560	-470	-770	-530	230	690
	10	338	-970	630	960	1,690	-320	-190	-300	-570	660	-380	-800	-1,460	470	-460	-770	-540	190	710
	11	411	-1,480	620	1,260	2,510	-470	-290	-470	-800	1,140	-613	-1,200	-2,200	800	-630	-1,030	-860	-380	930
	12	780	-1,590	---	2,730	7,080	-640	-710	-970	1,760	1,800	-2,940	-4,960	-6,940	1,120	-850	-1,340	-1,050	-660	1,280
	13	618	-2,350	---	4,330	6,080	-450	-340	-490	-760	1,660	-1,380	-2,420	-3,790	970	-860	-1,340	-940	-400	1,220
AH-3	14	---	---	---	---	---	---	---	---	---	---	---	---	---	---	---	---	---	---	---
	15	---	---	---	---	---	---	---	---	---	---	---	---	---	---	---	---	---	---	---
	16	---	---	---	---	---	---	---	---	---	---	---	---	---	---	---	---	---	---	---
	17	474	-1,910	1,000	2,300	4,770	---	-280	-490	---	1,210	-640	-1,580	-3,000	880	-380	-1,080	---	---	---
	18	636	-2,080	1,520	3,010	5,610	---	-280	-430	---	1,410	-1,240	-2,770	-4,370	940	-440	-1,130	---	---	---
	19	---	---	---	---	---	---	---	---	---	---	---	---	---	---	---	---	---	---	---
	20	700	-2,110	3,080	5,820	10,190	---	-330	-650	---	2,170	-3,910	-6,640	-8,760	1,300	-370	-1,450	---	---	---
	21	780	---	2,490	4,280	9,650	---	-310	-720	---	2,170	-3,410	-5,970	---	---	---	---	---	---	---
	22	101	---	---	---	---	---	-40	---	---	300	---	---	---	200	-60	-230	---	---	---
	23	728	---	---	---	---	---	-220	-570	---	2,440	---	---	---	1,320	-450	-1,570	---	---	---
AH-4	24	206	-720	150	570	1,370	-320	-110	-200	420	510	-230	-560	-1,120	400	-230	-530	---	---	---
	25	613	-1,890	1,320	3,060	6,270	-520	-250	330	740	1,350	-830	-1,760	-3,430	830	-460	-1,090	---	---	---
	26	664	-2,140	1,920	4,060	7,490	-410	-370	-570	-1,130	1,660	-1,930	-3,150	-5,750	1,010	-600	-1,310	---	---	---

Table A-5. Summary of Dynamic Test Data of Antisymmetrically Loaded Arches

Arch No.	Test No.	Peak Load w (lb/in.)	Maximum Deflection (in.)	Maximum Reactions (lb)				Acceleration (g)
				Horizontal 1	Vertical 2	Horizontal 3	Vertical 4	
AH-2	7	116	0.22	14,700	5,010	6,450	11,050	108
	8	235	0.38	23,460	10,470	9,680	19,890	677
	9	322	0.48	33,220	12,270	10,690	20,420	254
	10	338	0.51	17,420	10,320	13,100	20,240	224
	11	411	0.73	34,030	16,190	15,830	29,840	255
	12	780	1.44	78,410	11,970	19,110	43,220	225
	13	618	1.09	83,820	16,750	---	41,160	269
AH-3	14	---	---	---	---	---	---	---
	15	---	---	---	---	---	---	---
	16	---	---	---	---	---	---	---
	17	474	0.99	54,630	16,180	15,810	40,090	214
	18	636	1.22	57,880	12,890	26,360	41,960	263
	19	---	---	---	---	---	---	---
	20	700	2.83	54,110	18,580	26,610	46,780	248
	21	780	2.10	51,590	31,850	19,960	48,110	---
	22	101	---	9,730	5,500	6,250	6,180	---
	23	728	2.28	68,600	18,220	23,950	49,460	---
AH-4	24	206	0.38	21,380	9,980	11,530	18,980	174
	25	613	1.18	57,390	19,960	26,610	43,660	266
	26	664	1.34	55,700	20,350	24,180	48,950	357

Table A-6. Summary of Maximum Dynamic Data for Arch AH-2

Load (lb/in.)	SG-1 (μin./in.)	SG-4 (μin./in.)	Moment (in.-kips)	Direct Force (kips)
116	-460	810	129.0	8.29
235	-800	1,430	227.0	14.10
411	-1,480	2,510	406.0	34.50
	SG-5	SG-8		
116	-170	-380	-20.8	42.60
235	-270	-460	-18.5	59.00
411	-470	-800	-33.8	103.00
	SG-9	SG-12		
116	370	-760	-116.0	-0.55
235	590	-1,260	-189.0	-1.71
411	1,140	-2,200	-340.0	-10.20

Load (lb/in.)	Principal Stress		Phi (rad)	Max Shear Stress (ksi)	Rad Shear (kips)
	σ_1 (ksi)	σ_2 (ksi)			
116	4.63	-10.20	-0.238	7.44	-6.15
235	8.64	-17.20	-0.243	12.90	-10.90
411	17.20	-26.00	-0.255	21.60	-19.40

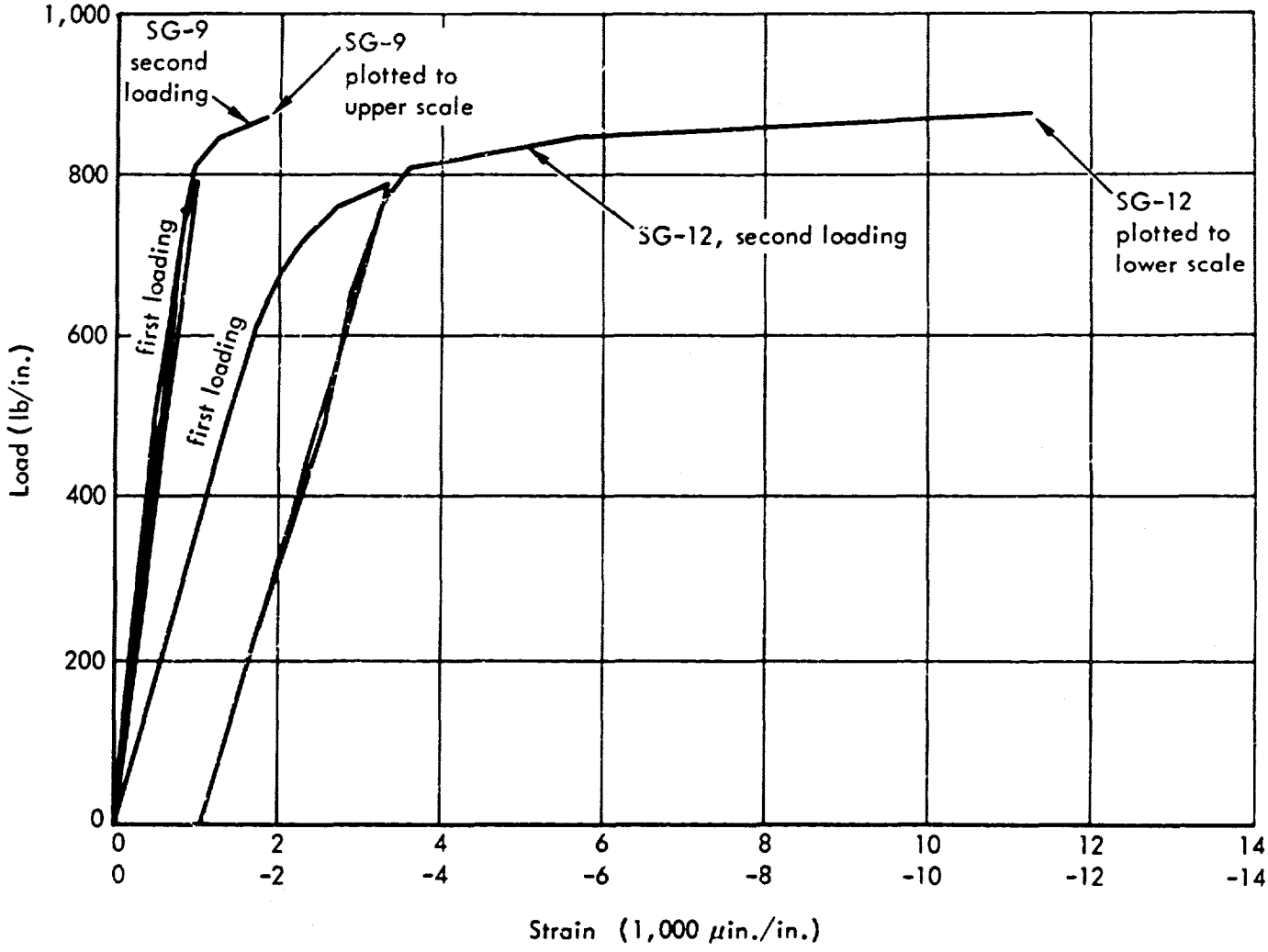

Figure A-1. Accumulative strains, SG-9 and SG-12, of antisymmetrically loaded arch AH-1.

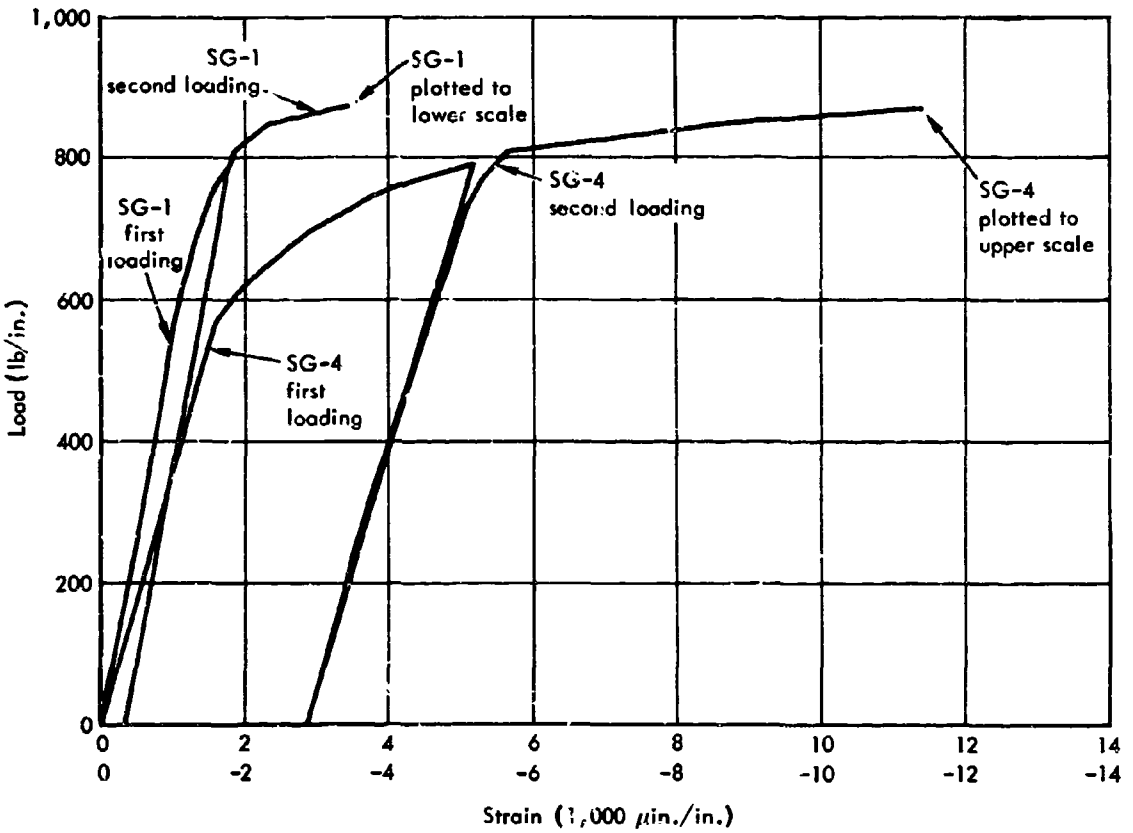

Figure A-2. Accumulative static strains, SG-1 and SG-4, of antisymmetrically loaded arch AH-1.

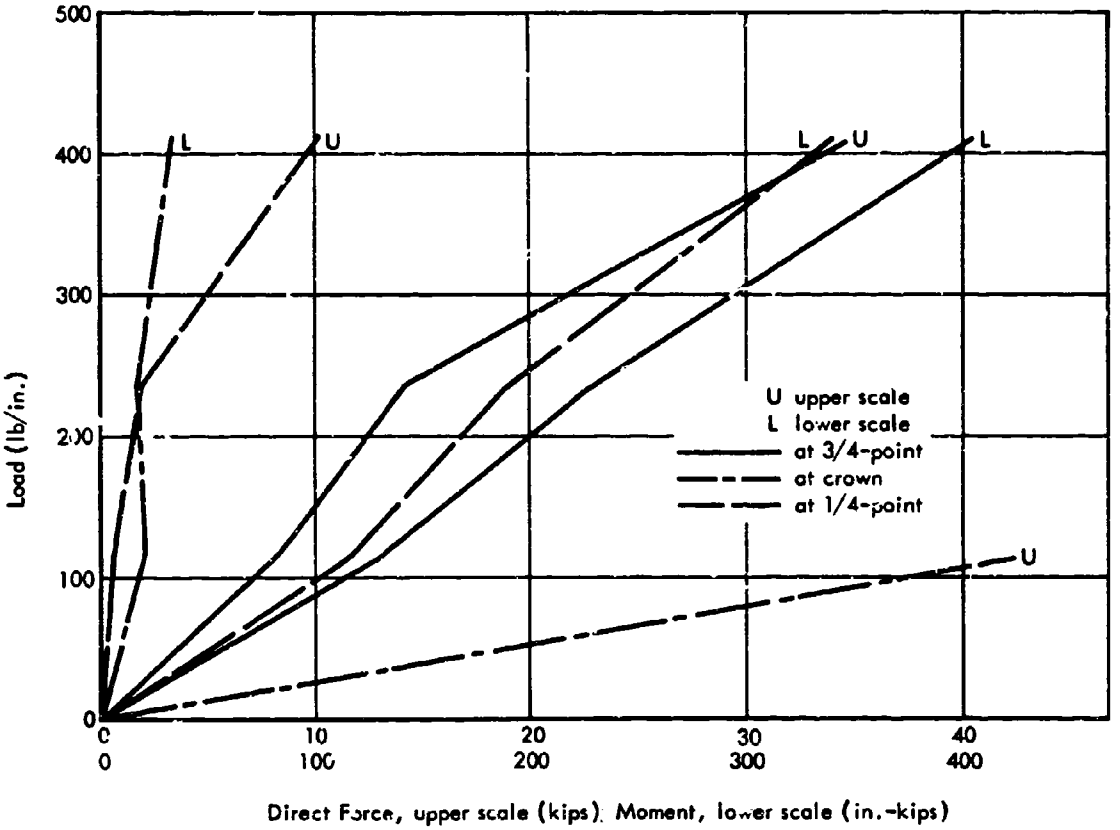

Figure A-3. Maximum values of experimental moment and direct force for dynamically loaded arch AH-2.

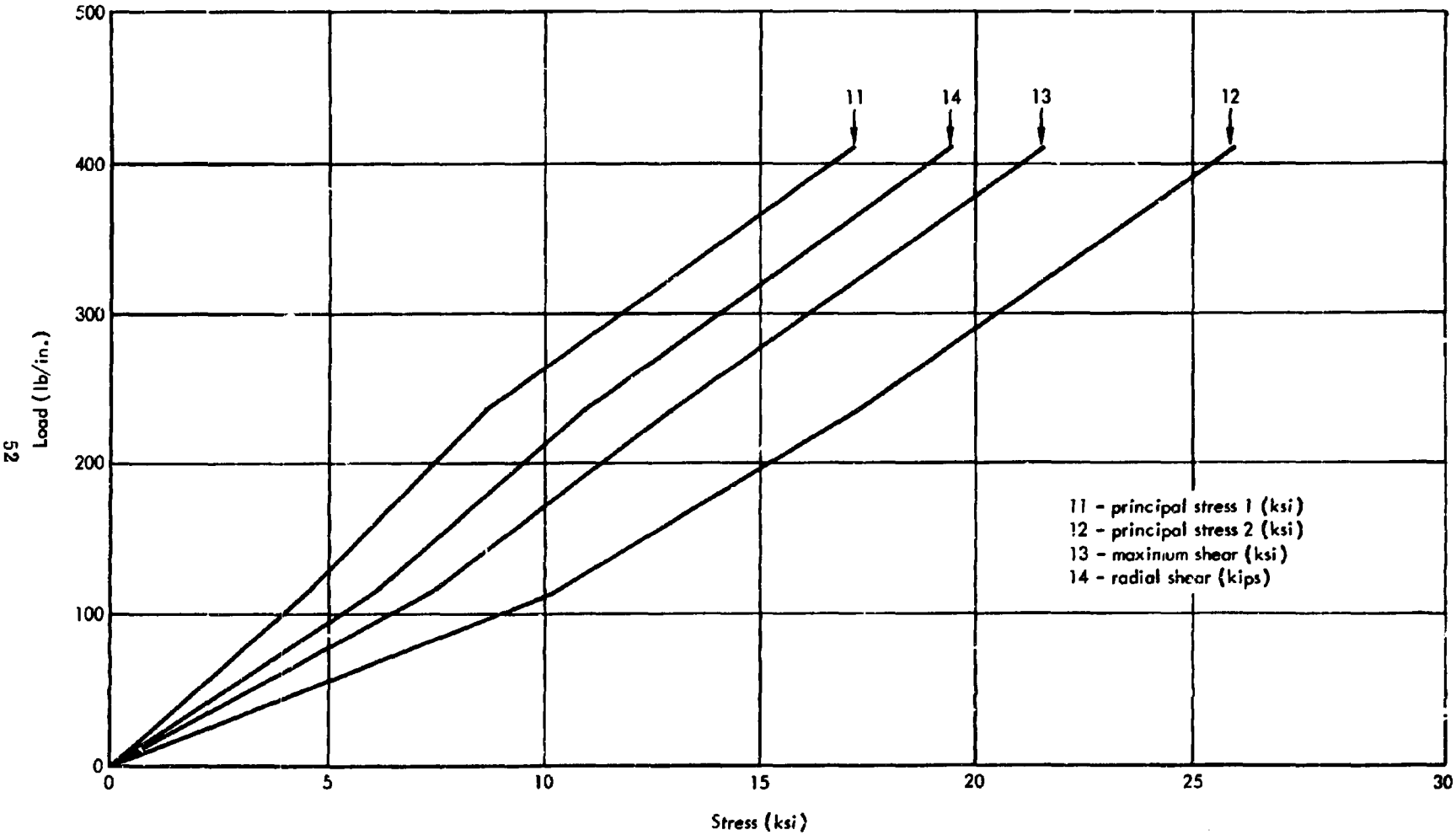

Figure A-4. Maximum values of experimental shear and principal stress for dynamically loaded arch AH-2 at SG-13, 14, 15.

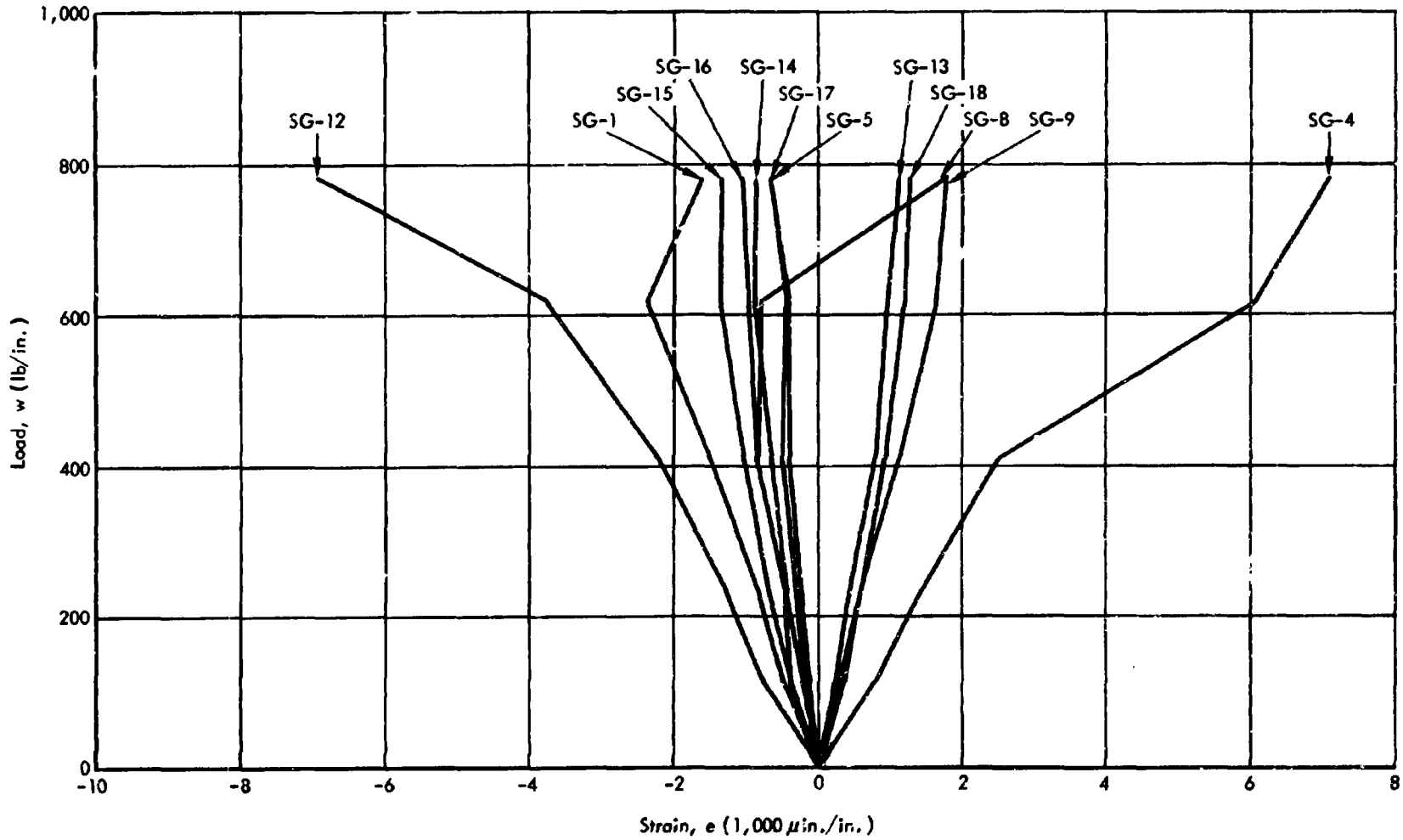

Figure A-5. Maximum dynamic strains for antisymmetrically loaded arch AH-2.

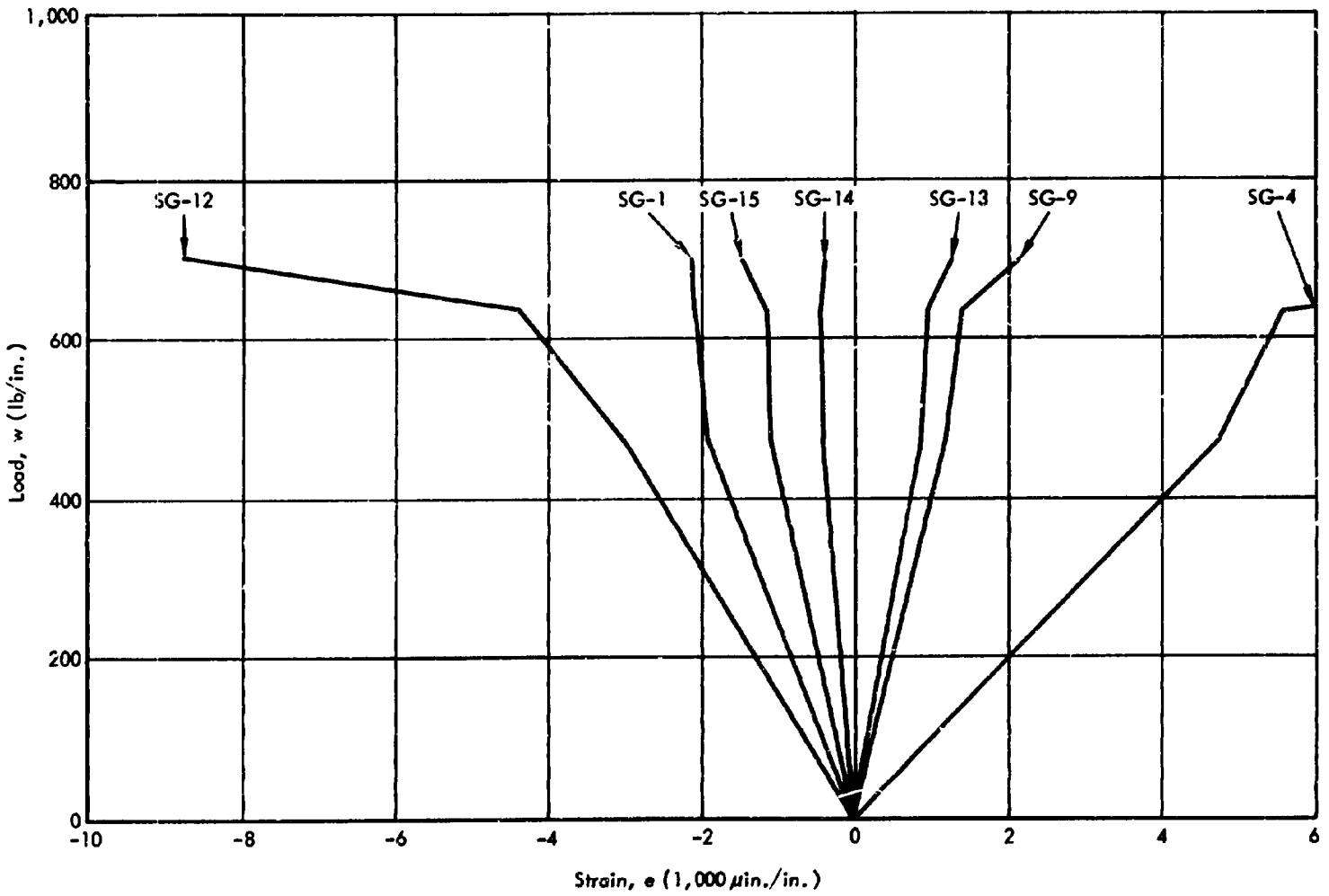

Figure A-6. Maximum dynamic strains for antisymmetrically loaded arch AH-3.

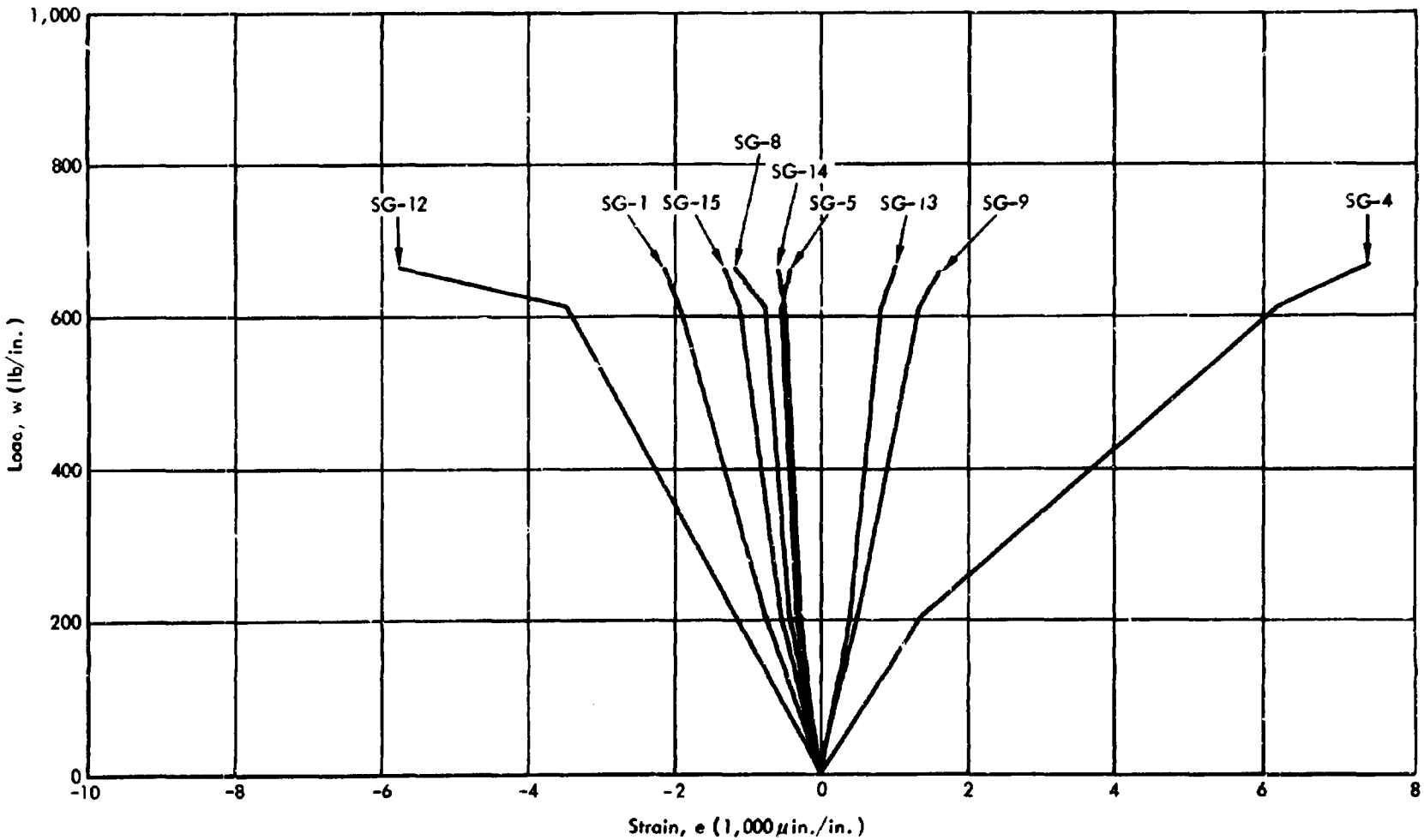

Figure A-7. Maximum dynamic strains for antisymmetrically loaded arch AH-4.

Appendix B

STATIC ANALYSIS OF TWO-HINGED CIRCULAR ARCH

General

The static analysis of the two-hinged circular arch with a uniform load, w, distributed over one-half the span (Figure B-1), includes theoretical solutions in both the elastic and inelastic ranges. To simplify the numerical solution, an idealized arch (Figure B-2) is taken along the centerline of the actual arch. The elastic characteristics are represented by the flexible joints connected by rigid bars.[13] This substitute framework is shown in Figure B-3.

Elastic Range

In determining the theoretical behavior of the circular arch in the elastic range, the following assumptions were made:

a. A linear distribution of stress and strain is maintained at any cross section of the entire arch.

b. The arch cross sections are uniform between any two adjacent joints.

c. Segments of the arch are assumed to be straight.

d. Continuity of the arch is maintained in the elastic range.

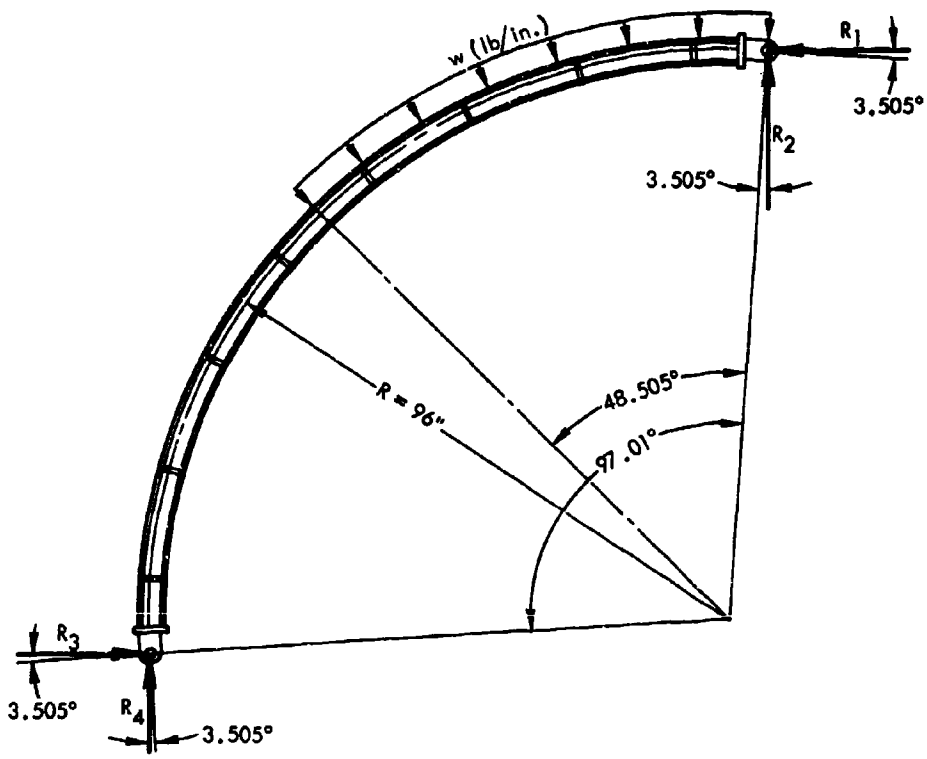

Figure B-1. Geometry and loading condition of the circular arch.

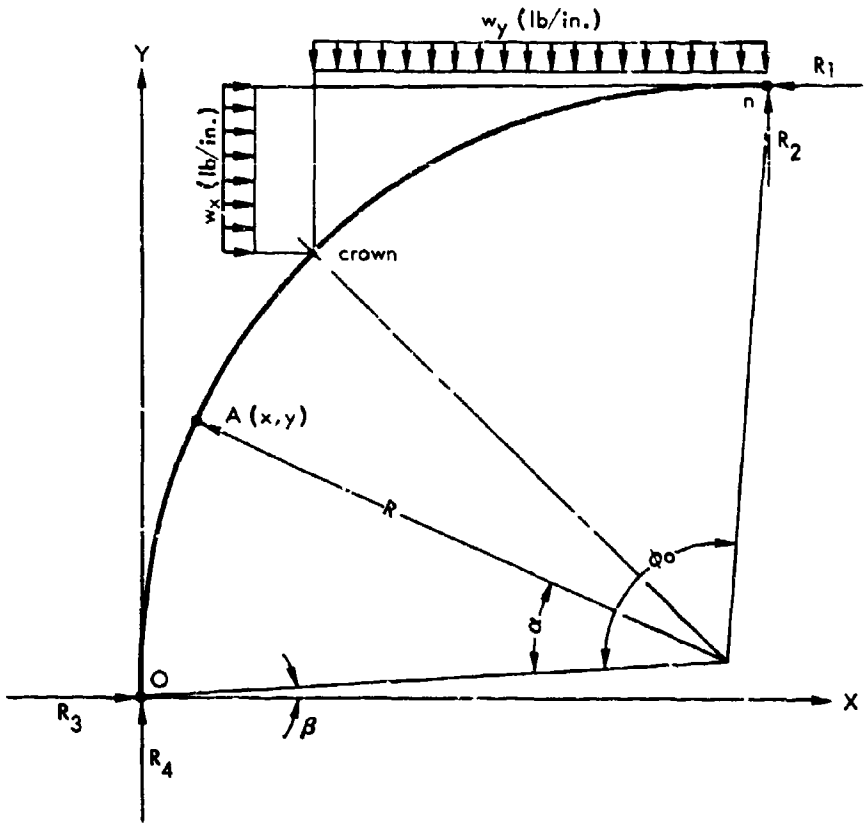

Figure B-2. Coordinate system and loading condition for static analysis of the circular arch.

e. The applied loads are assumed uniform between any two adjacent joints and can be represented by components of concentrated loads.

f. Rotations due to elastic strain take place at the joint.

g. The elastic support is represented by a linear spring.

h. The effect of dead load is negligible.

Assumption g is due to the horizontal movement of the right support during the static tests. The horizontal permanent displacements recorded were 1.16 inch. It is believed that the elastic displacement during the test was larger. The elastic constant was taken to be 6.25×10^{-6} in. lb in the static analysis.

The two-hinged arch considered is a statically indeterminate structure with a redundant reaction. If the horizontal restraint at n is removed, the structure becomes readily solvable by the principles of statics. The deformed structure is shown in Figure B-4. The simulated structure, obtained by the addition of the redundant reaction, H, is shown in Figure B-5. By applying the principle of superposition, the magnitude of H is obtained for the nonyielding support by equating the horizontal deflection at n ($\Delta x''$ in Figure B-5) to the deflection $\Delta x'$ in Figure B-4. For structures with yielding supports, special boundary conditions must be satisfied.

The slope-deflection relationship of a segment of the arch may be expressed by the moment-area method.

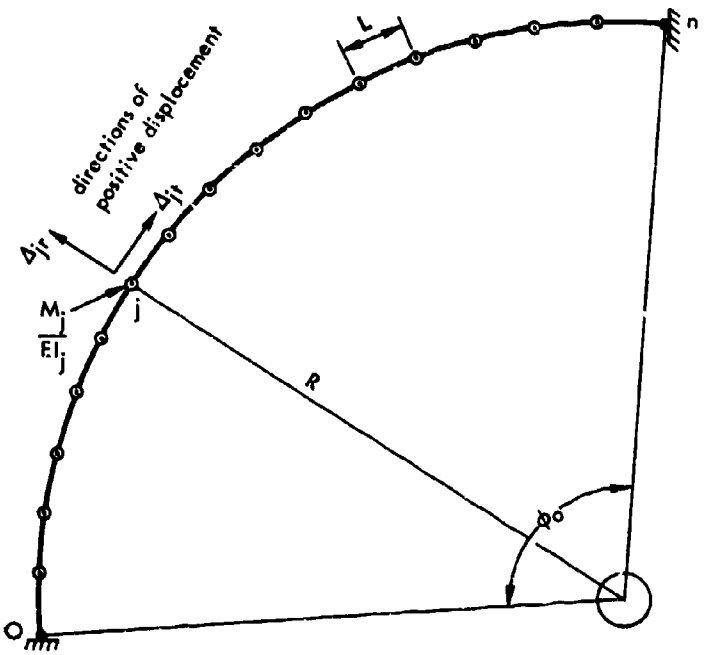

Figure B-3. Discrete framework of the arch.

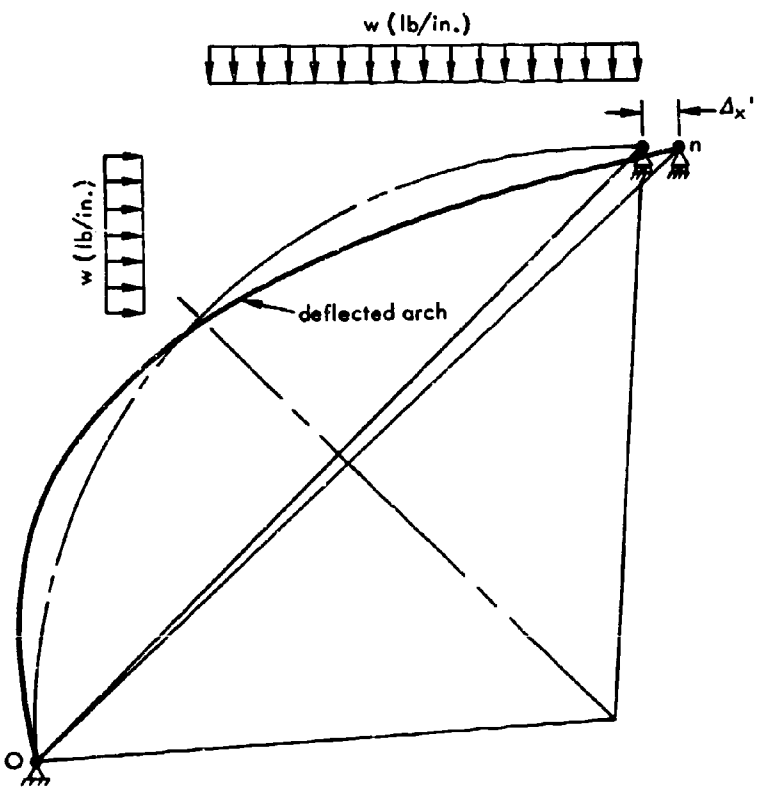

Figure B-4. Deflection of the statically determinate base structure.

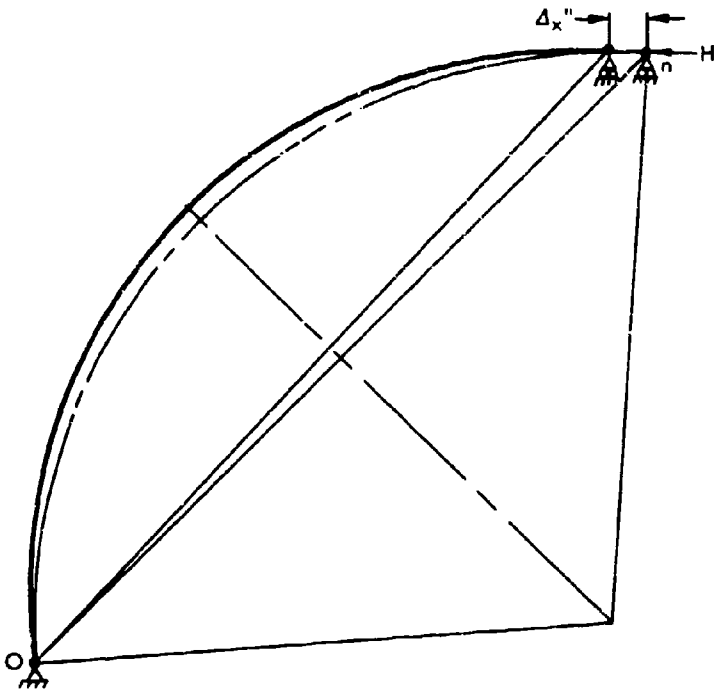

Figure B-5. Original arch simulated by addition of redundant reaction H.

For the entire arch, the origin of the coordinate system is taken at the left support of the arch as shown in Figure B-2. Note that the x and y axes coincide with the direction of reactions, R_3 and R_4, respectively. By trigonometry, the coordinates of any joint j on the arch may be established as follows:

$$x_j = R\left[\cos\beta\,(1 - \cos\alpha) - \sin\beta\,\sin\alpha\right] \tag{B-1}$$

$$y_j = R\left[\sin\beta + \sin(\alpha - \beta)\right] \tag{B-2}$$

where β is the initial angle between the radial line of the arch at point 0 and the horizontal axis. Because of symmetry at the crown of the arch

$$\beta = \frac{1}{2}\left(\phi_o - \frac{\pi}{2}\right) \tag{B-3}$$

where ϕ_o is the central angle of the arch.

Consider a discrete system with a finite number of joints connected by straight bars. Let the angle between radii to two adjacent joints be ϕ and the central angle of the arch be ϕ_o; then

$$\phi = \frac{\phi_o}{n}$$

where n is the number of bars used in the discrete system. The bar length is

$$L = 2R \sin \frac{\phi}{2} \tag{B-4}$$

The x and y components of the bar connecting joints j and i are

$$x_{jx} = x_j - x_i \tag{B-5}$$

$$y_{jy} = y_j - y_i \tag{B-6}$$

where joint i is the joint j-1.

Proceeding on the assumption that the applied loads are uniformly distributed along each segment of the arch, it is convenient to resolve the distributed loads into x and y components of a concentrated load acting at the centroid of the segment. If the segment is sufficiently small to warrant the assumption of the member being straight for the segment, the uniform load, w, may be resolved into components as follows:

$$p_{jx} = w y_{jy} \tag{B-7}$$

and

$$p_{jy} = w x_{jx} \tag{B-8}$$

The conditions of equilibrium require that

$$P_{nx} + P_{ox} + \sum_{j=o}^{n} w y_{jy} = 0 \tag{B-9}$$

$$P_{ny} + P_{oy} + \sum_{j=o}^{n} w x_{jx} = 0 \tag{B-10}$$

and

$$M_n = M_o + P_{ox}\, y_n + P_{oy}\, x_n + \sum_{j=o}^{n} \left[p_{jx} \left(y_n - y_j + \frac{y_{jy}}{2} \right) + p_{jy} \left(x_n - x_j + \frac{x_{jx}}{2} \right) \right]$$

$$= M_o + P_{ox}\, y_n + P_{oy}\, x_n + \sum_{j=o}^{n} w \left[y_{jy} \left(y_n - y_j + \frac{y_{jy}}{2} \right) + x_{jx} \left(x_n - x_j + \frac{x_{jx}}{2} \right) \right] \quad \text{(B-11)}$$

where the subscripts o and n denote beginning and ending points of the free body considered for equilibrium. It is important to note that point j can be an ending point as well. A review of the statically determinate structure of Figure B-4 indicates that the x component of reaction n is zero.

$$P_{nx} = 0$$

$$P_{ox} + \sum_{j=o}^{n} w y_{jy} = 0 \quad \text{(B-12)}$$

or

$$P_{ox} = - \sum_{j=o}^{n} w y_{jy} \quad \text{(B-13)}$$

The summation of moments at joint 0 is zero.

$$P_{ny}\, x_n + \sum_{j=o}^{n} w \left(y_j\, y_{jy} + x_j\, x_{jx} \right) = 0$$

$$P_{ny} = -\frac{1}{x_n} \sum_{j=o}^{n} w \left(y_j\, y_{jy} + x_j\, x_{jx} \right) \quad \text{(B-14)}$$

Summing up all forces in the y direction, we obtain

$$P_{oy} = - P_{ny} - \sum_{j=o}^{n} w x_{jx} \quad \text{(B-15)}$$

Substituting Equations B-13 and B-15 into Equation B-11, the bending moment at any joint can be calculated.

Consider an arbitrary moment distribution in the vicinity of joint j as shown in Figure B-6, and subdivide the moment diagram into a number of triangular portions. The segment size is chosen so that the variation of moment can be adequately approximated by straight lines between adjacent joints. The bending moments tributary to joint j can be represented by the triangle abc and the area of the triangle is

$$\theta_j = \frac{M_j L}{E I_j} \tag{B-16}$$

where θ_j denotes angular change at j due to elastic strain between dg. The areas abc and defg are equivalent, and M_j/EI can be taken as the average elastic weight between d and g.

For small angular changes, the relative displacement of joint j with respect to any point A, shown in Figure B-7, may be expressed in component terms as follows: [14]

$$\Delta_y = \theta_j x_j = \frac{M_j L}{E I_j} x_j$$

$$\Delta_x = \theta_j y_j = \frac{M_j L}{E I_j} y_j$$

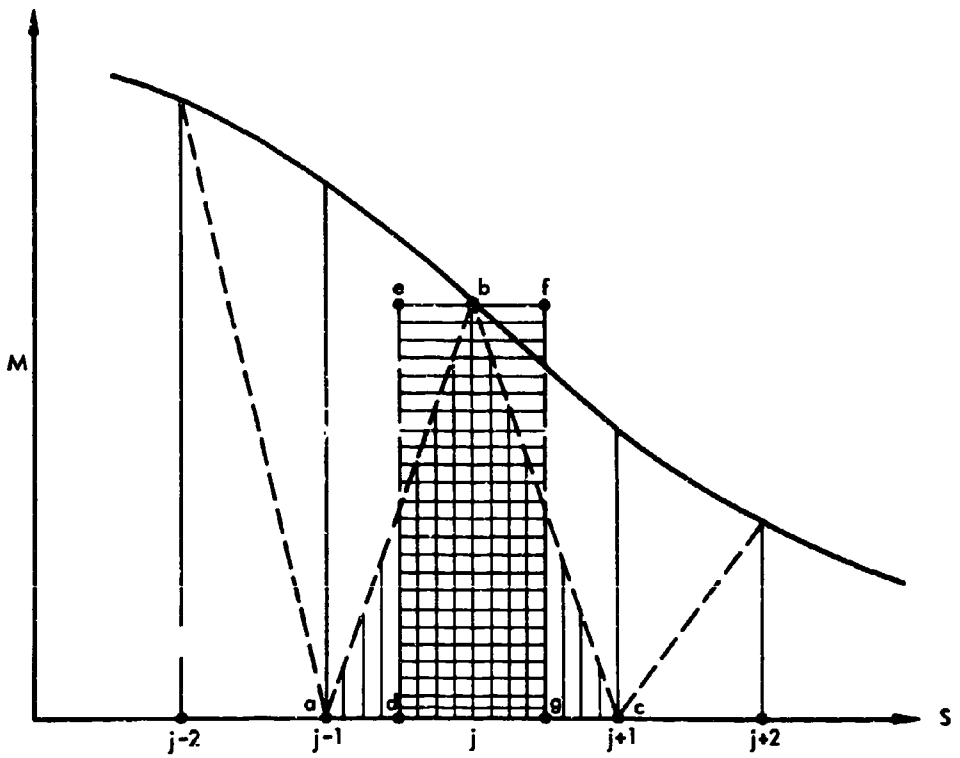

Figure B-6. Moment at the vicinity of joint j.

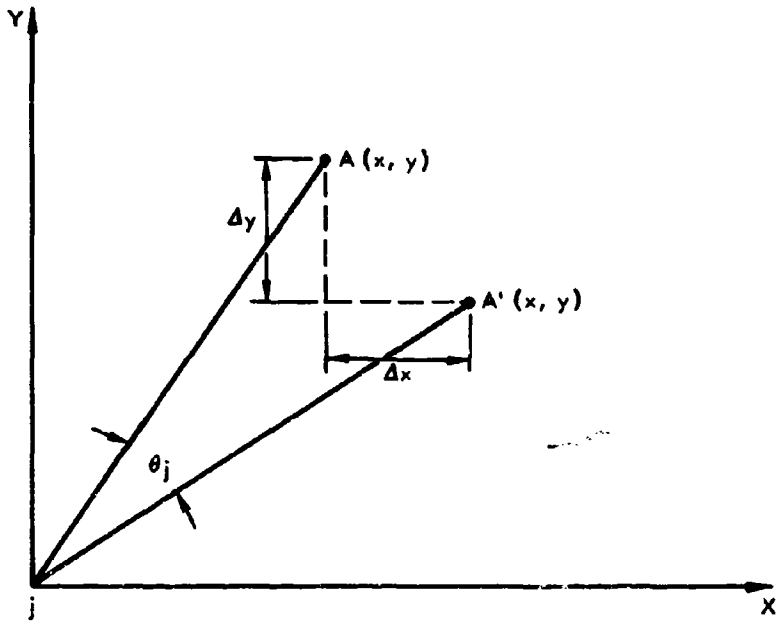

Figure B-7. Joint rotation due to elastic strains.

Summing from 0 to n and adding the initial displacement terms, the x- and y-components of final displacement become

$$\Delta_{ny} = \Delta_{oy} + \theta_o x_n + \sum_{j=o}^{n} \frac{M_j L}{E I_j} x_j \qquad \text{(B-17)}$$

$$\Delta_{nx} = \Delta_{ox} + \theta_o y_n + \sum_{j=o}^{n} \frac{M_j L}{E I_j} y_j \qquad \text{(B-18)}$$

It should be noted that M_j may be obtained from Equation B-11 by substituting j for n.

To maintain continuity, the sum of total angular changes between 0 and n must be equal to zero and Equations B-17 and B-18 must be satisfied. This results in

$$\theta_o + \theta_n + \sum_{j=o}^{n} \frac{M_j L}{E I_j} = 0 \qquad \text{(B-19)}$$

For the structure shown in Figure B-4, $\Delta_{ny} = \Delta_{oy} = 0$. It follows from Equation B-17 that

$$\theta_o = -\frac{1}{x_n} \sum_{j=o}^{n} \frac{M_j L}{E I_j} x_j \tag{B-20}$$

Substituting Equation B-20 into B-18 and noting that $\Delta_{ox} = 0$

$$\Delta_{nx} = -\frac{x_n}{x_n} \sum_{j=o}^{n} \frac{M_j L}{E I_j} x_j + \sum_{j=o}^{n} \frac{M_j L}{E I_j} y_j$$

By symmetry

$$\frac{y_n}{x_n} = 1$$

The above equation is then reduced to

$$\Delta_{nx} = \sum_{j=o}^{n} \frac{M_j L}{E I_j} \left(y_j - x_j \right) = \Delta_x' \tag{B-21}$$

This equation gives the horizontal displacement of the statically determinate arch shown in Figure B-4.

In order for this arch to act as a two-hinged arch, the horizontal restraining force, H, must be provided as shown in Figure B-5. For simplicity of presentation, let H be unity.

The equilibrium in the x direction requires that

$$P_{ox} = -P_{nx} = 1 \tag{B-22}$$

Taking moments about point 0 and noting the geometric symmetry and equilibrium condition in the y direction, it is clear that

$$P_{oy} = -P_{ny} = 1 \tag{B-23}$$

Substituting Equations B-22 and B-23 into Equation B-11 for new bending moment terms

$$M_j = y_j - x_j \tag{B-24}$$

Substituting Equation B-24 into Equation B-21 for horizontal displacement in the direction of the unit load at n, and introducing the redundant reaction, H

$$\Delta_x'' = -H \sum_{j=0}^{n} \frac{L}{E I_j} \left(y_j - x_j\right)^2 \tag{B-25}$$

In the case of a nonyielding support

$$\Delta_x' + \Delta_x'' = 0 \tag{B-26}$$

By substituting Equations B-21 and B-25 into Equation B-26, one obtains the following expression for the redundant, H

$$H = \sum_{j=0}^{n} \frac{M_j}{\left(y_j - x_j\right)} \tag{B-27}$$

For elastic support represented by a linear spring with constant k in the direction of H

$$\Delta_x' + \Delta_x'' = kH \tag{B-28}$$

therefore

$$H = \frac{\sum_{j=0}^{n} \frac{M_j L}{E I_j} \left(y_j - x_j\right)}{k + \sum_{j=0}^{n} \frac{L}{E I_j} \left(y_j - x_j\right)^2} \tag{B-29}$$

Note that Equation B-27 is a special case of Equation B-29 with k = 0.

Once the redundant, H, is known, the two-hinged arch can be solved as a statically determinate structure as outlined above.

The bending moment and the x- and y-components of forces at each joint can be calculated by Equations B-9, B-10, and B-11. It is desirable to convert the x- and y-components of the forces at each joint into radial and tangential forces as follows:

$$P_{jr} = P_{jx} \cos(\alpha - \beta) + P_{jy} \sin(\alpha - \beta) \tag{B-30}$$

$$P_{jt} = P_{jy} \cos(\alpha - \beta) - P_{jx} \sin(\alpha - \beta) \tag{B-31}$$

where P_{jr} and P_{jt} are the radial and tangential forces at the joint j, generally known as radial shear and direct forces in the arch.

The stress and strain of upper and lower fibers at each section can be calculated from the bending moment and direct forces of Equations B-11 and B-13. The expressions for strains, e_u and e_ℓ, for the upper fiber and the lower fiber are as follows:

$$e_u = -\left(\frac{P_{jt}}{EA_j} + \frac{M_j c_u}{EI_j}\right) \tag{B-32}$$

$$e_\ell = -\frac{P_{jt}}{EA_j} + \frac{M_j c_\ell}{EI_j} \tag{B-33}$$

where c_u and c_ℓ are distances from the neutral axis to the upper and lower fibers, respectively. The stresses f_u and f_ℓ for the upper and the lower fibers may be expressed in terms of strains as follows:

$$f_u = e_u E_u \tag{B-34}$$

$$f_\ell = e_\ell E_\ell \tag{B-35}$$

where E_u and E_ℓ are the elastic moduli of the upper and lower fibers, respectively.

The x- and y-components of deflection can be obtained from Equations B-21 and B-22 and can be converted into radial and tangential components, Δ_{jr} and Δ_{jt}, as follows:

$$\Delta_{jr} = \Delta_{jx} \cos(\alpha - \beta) + \Delta_{jy} \sin(\alpha - \beta) \tag{B-36}$$

$$\Delta_{jt} = \Delta_{jy} \cos(\alpha - \beta) - \Delta_{jx} \sin(\alpha - \beta) \tag{B-37}$$

Secondary bending moments are produced by direct forces acting on the radial displacements, Δ_{jt}, and initial misalignment of the arch. The secondary stresses are ordinarily neglected in structural analysis; however, in this arch analysis they are quite significant.

$$M_j' = \Gamma_{jt}\left(\Delta_{jt} + C_m\right) \tag{B-38}$$

M_j' denotes the secondary bending, and C_m is the initial misalignment. It is evident that the deflections, stresses, and strains are amplified by M_j' as follows:

$$A_{jm} = \frac{M_j + M_j'}{M_j} \tag{B-39}$$

The amplification factor, A_{jm}, should be used as a coefficient in Equations B-36, B-37, B-11, B-32, B-33, B-34, and B-35 for the final deflections, moment, strains, and stresses at each joint.

Inelastic Range

The procedures described in the elastic range may be extended to cover the inelastic range by introducing the variable inelastic modulus, E', when the stress in the section exceeds the yield stress. Equation B-16 becomes

$$\theta_j' = \frac{M_j L}{E' I_j} \tag{B-40}$$

The solutions can be obtained by small increments of stress at each joint. When the yield stress is reached, the inelastic modulus becomes effective at that joint. The forces, moment, stresses, strains, and deflections are calculated at the point by the equations shown in the elastic program. The stress increments can continue until the ultimate stress is reached.

For each change of slope in the stress-strain curve, a corresponding yield stress is given. Since the strain-hardening materials do not have a definite plastic range, it becomes necessary to represent the stress-strain curve by a series of lines (more than two). Figure B-8 shows the idealized stress-strain curve for the circular arch tested. The variable inelastic modulus, E', is represented by E_1 and E_2 in this case.

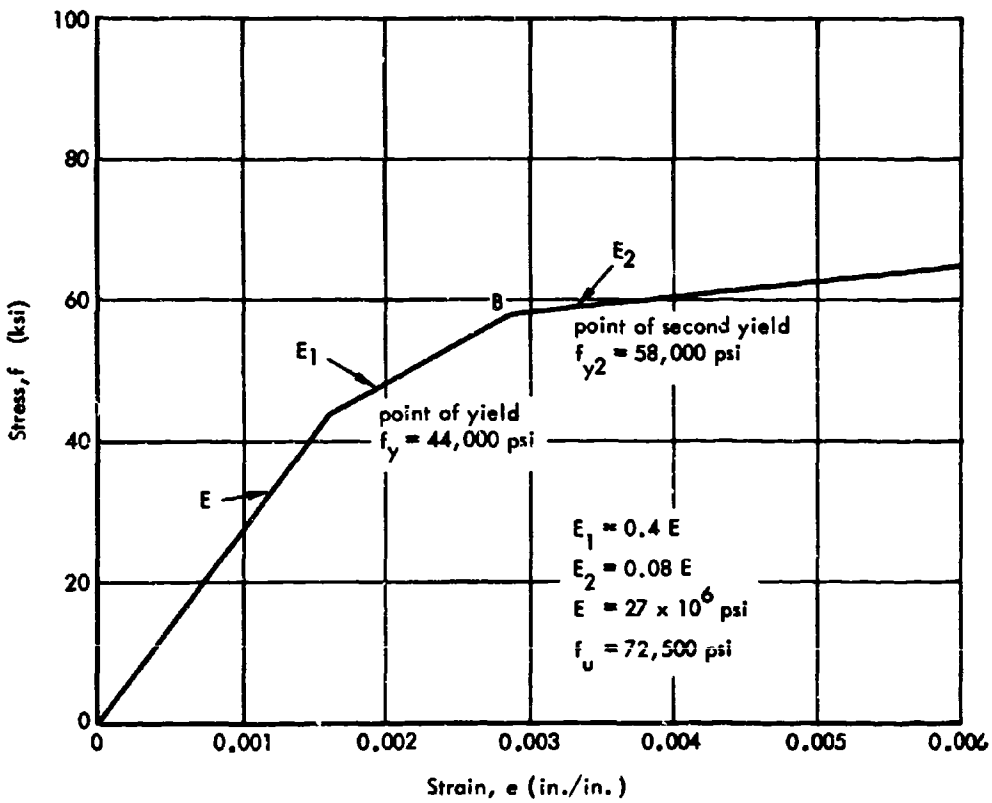

Figure B-8. Idealized stress-strain curve for static analysis.

Computer Programs

Computer programs (B-1 and B-2) were used for the analysis of the circular arch for the elastic and inelastic ranges. The programs follow the theoretical derivation of equations given in this appendix. The source programs are written in FORTRAN language and can be carried out on an IBM 1620 or IBM 1620II computer. A flow chart showing the sequence of operations of Program B-1 is given in Figure B-9. Program B-2 is relatively simple, and no flow chart is needed. The input specifications for the programs are as follows:

Number of bars:	variable but subject to the limitations of the computer memory system
Stiffness parameters:	can be varied from joint to joint
Elastic support constant:	variable
Loading:	uniformly distributed over any portion of the arch

Presentation of Numerical Results

The static properties for materials used in the arches are given in Table 2. Due to the strain-hardening properties of some specimens, particularly the bottom flanges, the idealized stress-strain relationship is represented by the trilinear curve of Figure B-8 instead of by the usual bilinear stress-strain curve.

The average elastic modulus of 27×10^6 psi was used; the inelastic moduli, E_1 and E_2, were 0.4E and 0.08E, respectively. The average ultimate stress for the bottom flange was 72,500 psi. Other input parameters for static analysis of the arch were as follows:

Number of bars	$n = 16$
Angle of segments	$\phi = 0.1\ldots082$ radian
Offset angle	$\beta = 0.06117$ radian
Radius of arch	$R = 96.0$ in.
Stiffness parameter	$EI = 407.1 \times 10^6$ lb-in.^{2}
Stiffness parameter	$EA = 177.4 \times 10^6$ lb
E of top flange	$E_u = 27.9 \times 10^6$ psi
E of bottom flange	$E_\ell = 26.7 \times 10^6$ psi
Initial misalignment	$C_m = 0.0195$ in.
Elastic support constant	$k = 6.25 \times 10^{-6}$ in./lb
Upper fiber from neutral axis	$c_u = 1.29$ in.
Lower fiber from neutral axis	$c_\ell = 2.71$ in.

Loading was considered uniformly distributed over one-half the arch length. The magnitudes of the uniform loads used in the analyses were increased by increments of 100 lb/in. from zero to 500 lb/in. The yield stress of 44,000 psi was first reached in the bottom flange at the 1/4-point of the arch, where the stresses caused by axial force and flexure were of the same sign; the load causing this yielding was 507 lb/in. At a load of 545 lb/in., the yield stress was developed in the bottom flange at the 3/4-point. Higher loads of 680 and 704 lb/in. produced stresses of 58,000 psi (point B in Figure B-8) in the bottom flanges at the 1/4-point and 3/4-point, respectively.

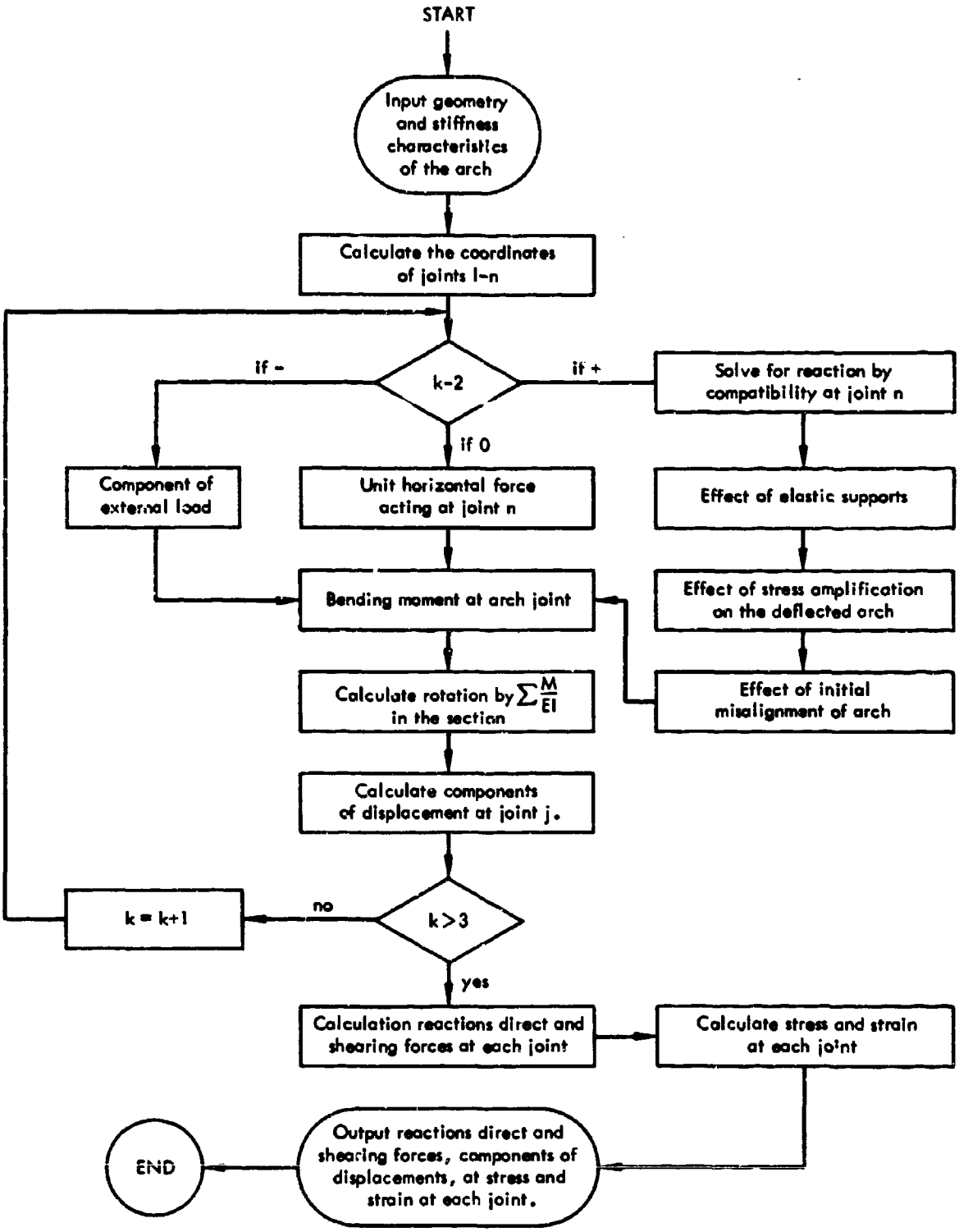

Figure B-9. Flow chart for the static analysis of the circular arch.

Program B-1. Analysis of the Statically Loaded Arch, Part I

```
C       ANALYSIS OF ARCHES BY VIRTUAL WORK METHOD
C       PROGRAMED / RICHARD H. CHIU / MARCH 1965
        DIMENSION  XI(17),SM(17),EW(17),X(17),Y(17),XX(17),YY(17),W(17)
        DIMENSION  DRX(17),DRY(17),FXM(17),T(17),ST(17,2)
      1 FORMAT(I4,6F12.6,I4)
      2 FORMAT(I3,5F15.4)
      3 FORMAT(I3,5F15.8)
C     4 FORMAT(/6H JOINT7X1HA14X1HX14X1HY14X2HXX13X2HYY/)
C     5 FORMAT(/6H JOINT7X2HXW13X2HYW12X3HSXW12X3HSYW12X2HXM/)
C     6 FORMAT(/6H JOINT6X4HE.W.10X4H SFW12X4HDEFX/)
C     7 FORMAT(/6H JOINT7X1HH14X1HV12X5HEW(I)12X3HSYM13X2HMX/)
      8 FORMAT (6HJOINT 7X1HH14X1HV14X1HS14X1HT13X4HM(I))
     10 FORMAT(/6HJOINT 6X2HDX13X2HDY13X2HDR13X2HDT10X6HFXM(I)/)
    102 FORMAT (6HJOINT 6X2HFT13X2HFB13X2HST13X2HSB)
    100 READ 1,N,DA,B,R,CSA,EC,SPRC,N1
        READ 1, N3,DW,C1,C2,E,E1
C       GEOMETRY OF CIRCULAR ARCH
        DO 9 I=1,N,6
      9 READ1,N2,XI(I),XI(I+1),XI(I+2),XI(I+3),XI(I+4),XI(I+5)
        DO 110 I=1,N
    110 W(I)=0.
        X(1)=0.
        Y(1)=0.
        XX(1)=0.
        YY(1)=0.
C       ESTABLISH THE COORDINATES OF JOINTS 1 THRU N
     11 A=DA
        XM=0.
C       PUNCH 4
     13 DO 14 I=2,N
        X(I)=R*(COS(B)*(1.-COS(A))-SIN(A)*SIN(B))
        Y(I)=R*(SIN(B)+SIN(A-B))
C       SECTIONAL COMPONENTS IN X AND Y DIRECTIONS
     15 XX(I)=X(I)-X(I-1)
        YY(I)=Y(I)-Y(I-1)
C       PUNCH 2, I,A,X(I),Y(I),XX(I),YY(I)
     14 A=A+DA
C       X AND Y COMPONENTS OF THE APPLIED LOADS
C       MOMENTS ABOUT O
C       PUNCH 5
        DO 19 J=1,N1
        SXW=0.
        SYW=0.
        DO 16 I=N3,N
        W(I)=W(I)+DW
        YW=XX(I)*W(I)
        XW=YY(I)*W(I)
        SXW=SXW+XW
        SYW=SYW+YW
        XM=XM+XW*(Y(I)-YY(I)/2.)+YW*(X(I)-XX(I)/2.)
C       PUNCH 2, I,XW,YW,SXW,SYW,XM
     16 CONTINUE
        PUNCH 2, J,W(N)
        VN=XM/X(N)
        VO=SYW-VN
        HO=SXW
        RSX=0.
        RSY=0.
        DO 19 K=1,3
        XM=0.
        SMX=0.
        SYM=0.
        A=-B
        DO 20 I=2,N
```


Continued

Program B-1. Analysis of the Statically Loaded Arch, Part I (Contd)

```
C       MOMENT AT SECTION X
C       ACCUMULATIVE AREA OF THE MOMENT DIAGRAM
        DS=R*DA/(E*XI(I))
        IF(K-2) 118,117,117
  117 XM=XM+YY(I)*(HO-W(I)*YY(I)/2.)+XX(I)*(VO-W(I)*XX(I)/2.)
        GO TO 119
  118 XM =  X(I)-Y(I)
  119 EW(I)=XM*DS
        SMX=SMX+EW(I)
        SYM=SYM+EW(I)*X(I)
        IF(K-2)  20,121,121
  121 HO=HO-W(I)*YY(I)
        VO=VO-W(I)*XX(I)
        IF(K-2) 20,20,17
   17 A=A+DA
        DRX(I)=-HO*XX(I)/(CSA*E)
        RSX=RSX+DRX(I)
        DRY(I)=-VO*YY(I)/(CSA*E)
        RSY=RSY+DRY(I)
        RR=HO*COS(A)+VO*SIN(A)
        RT=VO*COS(A)-HO*SIN(A)
        T(I)=RT
        FXM(I)=XM
        ST(I,1)=RT/CSA+XM*C1/XI(I)
        ST(I,2)=RT/CSA-XM*C2/XI(I)
   25 PUNCH 2, I,HO,VO,RR,RT,XM
C       GO TO 20
C   18 PUNCH 2, I,HO,VO,EW(I),SYM,XM
   20 CONTINUE
  131 EW(N)=-SYM/X(N)
        EW(1)=-(EW(N)+SMX)
        SXM=0.
        SEW=EW(1)
C       PUNCH 6
C       PUNCH 3, N2,EW(1),SEW,SXM
        DO 24  I=2,N
        SXM=SXM+SEW*YY(I)
C       PUNCH 3, I,EW(I),SEW,SXM
   24 SEW=SEW+EW(I)
        IF(K-2) 22,21,141
C       DEFLECTION OF THE ARCH
  141 A=-B
        PUNCH 102
        DO 26 I=2,N
        STT=ST(I,1)/E
        STB=ST(I,2)/E1
   26 PUNCH 3, I,ST(I,1),ST(I,2),STT,STB
        DX=0.
        DY=0.
        SEW=EW(1)
        ROX=-RSX/Y(N)
        ROY=-RSY/X(N)
        PUNCH 10
        DO 23 I=2,N
        DX=DX+SEW*YY(I)+ROX*YY(I)+DRX(I)
        DY=DY+SEW*XX(I)+ROY*XX(I)+DRY(I)
        SEW=SEW+EW(I)
        A=A+DA
        DR=DX*COS(A)+DY*SIN(A)
        DT=DY*COS(A)-DX*SIN(A)
C       EFFECTS OF STRESS AMPLIFICATION
        AMPF=FXM(I)/(FXM(I)+T(I)*(DR-CC))
        FXM(I)=FXM(I)*AMPF/100.
        IF (AMPF-0.5) 142,142,143
```


Continued

Program B-1. Analysis of the Statically Loaded Arch, Part I (Contd)

```
  142 ADX=DX
      ADY=DY
      GO TO 23
  143 ADX=DX*AMPF
      ADY=DY*AMPF
      DR=DR*AMPF
      DT=DT*AMPF
   23 PUNCH 3, I,ADX,ADY,DR,DT,FXM(I)
      GO TO 19
C     EFFECTS OF HORIZONTAL ELASTIC SUPPORT
   21 XR=(SXM*SPRC/SXM1-SXM)/SXM1
      HO=SXW-XR
      VO=XR+VO+SYW
      PUNCH 8
C     AXIAL AND SHEAR STRESSES IN THE ARCH
  133 RR=HO*COS(B)-VO*SIN(B)
      RT=HO*SIN(B)+VO*COS(B)
      XM=0.
      PUNCH 4, N2,HO,VO,RR,RT,XM
      GO TO 19
   22 SXM1=SXM
C     PUNCH 7
   19 CONTINUE
      IF(SENSE SWITCH 1) 100,101
  101 PAUSE
      END
```

Program B-2. Analysis of the Statically Loaded Arch, Part II

```
      DIMENSION X(9,17),SX(9,9),R(4),SR(4)
    1 FORMAT (3X,4F15.8)
    2 FORMAT (33X,3F15.8)
    3 FORMAT (I4,2F8.0,3F9.0,2F8.0,F8.4)
    4 FORMAT (3X,4F15.8/)
    5 FORMAT ( //3X)
    6 FORMAT (/4H BAR,5X,1HW,6X,4HR(1),4X,4HR(2),5X,4HR(3),5X,4HR(4),
     14X,5HV(SR)/)
    7 FORMAT (/4H JT.,2X,6HDIR. F,3X,5HSHEAR,3X,6HMOMENT,7X,8HSTRESSES,
     110X,7HSTRAINS,6X,10HDEFLECTION)
    8 FORMAT (4H NO.,3X,4H(LB),5X,4H(LB),9H  (IN-LB),3X,6HT(PSI),3X,
     16HB(PSI),17H  T IN/IN B IN/IN,2X,5HR(IN),3X,5H(IN)/)
    9 FORMAT (3X, F15.8/)
      DO 111 J=1,9
      DO 111 I=1,9
  111 SX(I,J)=0.
      DO 112 I=1,4
  112 SR(I)=0.
      SW=0.
  100 READ 3, M,C5,C13,S
      READ 9,W
      READ 1,R(3),R(4),X(2,1),X(1,1)
      DO 11 J=2,16
   11 READ 2,X(2,J),X(1,J)
      READ 4,R(1),R(2),X(2,17),X(1,17)
      V=X(2,1)+0.763*(X(2,2)-X(2,1))
      DO 12 I=1,4
   12 R(I)=ABS(R(I))
      DO 21 J=2,4
   21 READ 1, X(4,J),X(5,J),X(6,J),X(7,J)
      READ 1, X(4,5),X(5,5),X(6,5),X(7,5)
      X(4,5)=X(4,5)*C5
      X(5,5)=X(5,5)*C5
      DO 22 J=6,12
   22 READ 1, X(4,J),X(5,J),X(6,J),X(7,J)
      READ 1, X(4,13),X(5,13),X(6,13),X(7,13)
      X(5,13)=X(5,13)*C13
      X(4,13)=X(4,13)*C13
      DO 23 J=14,17
   23 READ 1, X(4,J),X(5,J),X(6,J),X(7,J)
      DO 24 I=4,7
      DO 25 J=2,17
   25 X(I,J)=-X(I,J)
   24 X(I,1)=X(I,17)
      READ 5
      DO 31 I=8,9
   31 X(I,1)=0.
      X(3,1)=0.
      DO 32 J=2,17
   32 READ 2, X(8,J),X(9,J),X(3,J)
      DO 42 J=1,17
      DO 41 I=6,7
   41 X(I,J)=X(I,J)*1.0E+6
   42 X(3,J)=X(3,J)*1.0E+3
      GO TO (45,51,52),M
   45 SW=W
      SV=V
      DO 44 I=1,4
   44 SR(I)=R(I)
      DO 43 J=1,9
      DO 43 I=1,9
      K=1+2*(J-1)
   43 SX(I,J)=X(I,K)
      GO TO 60
```


Continued

Program B-2. Analysis of the Statically Loaded Arch, Part II (Contd)

```
 51 FAC=-(S+SX(5,3))/X(5,5)
    GO TO 53
 52 FAC=(S-SX(5,7 ))/X(5,13)
 53 W=FAC*W
    V=FAC*V
    DO 54 I=1,4
 54 R(I)=R(I)*FAC
    DO 55 J=1,17
    DO 55 I=1,9
 55 X(I,J)=X(I,J)*FAC
    SW=SW+W
    SV=SV+V
    DO 57 I=1,4
 57 SR(I)=SR(I)+R(I)
    DO 56 J=1,9
    DO 56 I=1,9
    K=1+2*(J-1)
 56 SX(I,J)=SX(I,J)+X(I,K)
 60 NJ=(J-2)*2
    PUNCH 6
    PUNCH 3, NJ, W, R(1), R(2), R(3), R(4),V
    PUNCH 7
    PUNCH 8
    DO 61 J=1,17
    K=J-1
 61 PUNCH 3, K, X(1,J), X(2,J), X(3,J), X(4,J), X(5,J), X(6,J),
   1 X(7,J), X(8,J), X(9,J)
    PUNCH 6
    NJ=NJ/2
    PUNCH 3, NJ,SW,SR(1),SR(2),SR(3),SR(4),SV
    PUNCH 7
    PUNCH 8
    DO 62 J=1,9
    K=J-1
 62 PUNCH 3, K,SX(1,J),SX(2,J),SX(3,J),SX(4,J),SX(5,J),SX(6,J),
   1SX(7,J),SX(8,J),SX(9,J)
    IF (SENSE SWITCH 2) 100,101
101 CALL EXIT
    END
```

A load of 866 lb/in. developed the ultimate stress of 72,500 psi in the bottom flange at the 1/4-point. At a load of 877 lb/in., the bottom flange at the 3/4-point also attained the ultimate stress. If this load were maintained, the arch would continue to deflect until collapse occurred.

The results of the theoretical response in the elastic and inelastic ranges are given in Tables B-1 through B-4. Table B-1 summarizes the reactions and radial shear at strain rosette SG-13-14-15. The location of the rosette is shown in Figure 6; the directions of the reactions are shown in Figure B-1.

Table B-2 summarizes the theoretical results at the 1/4-point of the arch. At this section the direct forces are maximum and the shearing forces are minimum for each level of load. Maximum stress and strain values occur at this location in the bottom flange. Positive radial deflections are in the outward direction.

Table B-3 summarizes the theoretical results at the crown of the arch. The positive shear and tangential displacements are maximum at this location. The direction of positive tangential displacement is shown in Figure B-3.

Table B-4 summarizes the theoretical results at the 3/4-point of the arch. The bending moments and the radial deflections are maximum at this location; the axial and shearing forces are small.

Table B-1. Summary of Elastic and Inelastic Reactions and Shears of the Statically Loaded Arch

Load (lb/in.)	R(1) (lb)	R(2) (lb)	R(3) (lb)	R(4) (lb)	V(SR)* (lb)
Elastic					
100	4,590	2,520	1,800	4,860	-1,700
200	9,180	5,040	3,600	9,720	-3,400
300	13,800	7,560	5,400	13,580	-5,100
400	18,400	10,080	7,200	19,440	-6,800
500	23,000	12,600	9,000	24,300	-8,500
507	23,300	12,800	9,120	24,600	-8,630
Inelastic					
545	25,000	13,800	9,760	26,400	-9,230
680	31,200	17,200	12,200	33,000	-11,600
704	32,200	17,900	12,500	34,100	-11,900
866	39,700	21,900	15,500	42,000	-14,700
877	40,200	22,200	15,700	42,600	-14,900

*V(SR) are shearing forces at strain rosette SG-13-14-15.

Table B-2. Summary of Elastic and Inelastic Responses at the 1/4-Point of the Statically Loaded Arch

Load (lb/in.)	Direct Force (lb)	Shear (lb)	Moment (in.-lb)	Stresses		Strains		Deflection	
				T (psi)	B (psi)	T (μin./in.)	B (μin./in.)	R (in.)	T (in.)
Elastic									
100	5,180	38	-42,800	2,900	-8,700	100	-320	0.062	-0.018
200	10,400	77	-86,200	5,900	-17,300	210	-650	0.125	-0.037
300	15,500	115	-130,000	8,800	-26,000	320	-970	0.189	-0.056
400	20,700	154	-175,000	11,800	-34,700	420	-1,300	0.254	-0.075
500	25,900	192	-221,000	14,700	-43,400	530	-1,620	0.320	-0.095
507	26,300	195	-224,000	14,900	-44,000	530	-1,650	0.324	-0.096
Inelastic									
545	28,200	234	-239,000	16,100	-46,800	640	-1,910	0.356	-0.105
680	35,200	277	-297,000	20,800	-58,000	1,060	-2,960	0.489	-0.140
704	36,320	347	-304,000	21,300	-59,300	1,320	-3,550	0.538	-0.152
866	44,800	372	-378,000	27,500	-72,500	4,080	-9,750	1.107	-0.283
877	45,370	374	-383,000	27,900	-73,400	4,270	-10,160	1.150	-0.291

Table B-3. Summary of Elastic and Inelastic Responses at the Crown of the Statically Loaded Arch

Load (lb/in.)	Direct Force (lb)	Shear (lb)	Moment (in.-lb)	Stresses		Strains		Deflection	
				T (psi)	B (psi)	T (μin./in.)	B (μin./in.)	R (in.)	T (in.)
Elastic									
100	4,710	2,160	3,080	-1,010	-176	-40	-6	-0.030	-0.030
200	9,410	4,320	6,460	-2,020	-353	-70	-13	-0.062	-0.062
300	14,100	6,490	10,200	-3,030	-529	-110	-19	-0.100	-0.100
400	18,800	8,650	14,300	-4,040	-706	-140	-26	-0.138	-0.137
500	23,500	10,800	18,900	-5,050	-883	-180	-33	-0.182	-0.181
507	23,900	11,000	19,200	-5,120	-896	-180	-33	-0.184	-0.184
Inelastic									
545	25,600	11,800	22,300	-5,660	-900	-202	-22	-0.200	-0.198
680	32,000	14,700	25,800	-6,970	-967	-249	-36	-0.237	-0.260
704	33,000	15,200	31,300	-7,610	-104	-272	-3	-0.248	-0.279
866	40,700	18,700	33,300	-9,000	-952	-322	-35	-0.294	-0.526
877	41,200	19,000	33,500	-9,090	-1,010	-325	-37	-0.297	-0.543

Table B-4. Summary of Elastic and Inelastic Responses at the 3/4-Point of the Statically Loaded Arch

Load (lb/in.)	Direct Force (lb)	Shear (lb)	Moment (in.-lb)	Stresses		Strains		Deflection	
				T (psi)	B (psi)	T (μin./in.)	B (μin./in.)	R (in.)	T (in.)
Elastic									
100	4,200	-38	47,200	-4,820	8,020	-172	300	-0.103	0.004
200	8,500	-77	95,300	-9,640	16,000	-345	600	-0.208	0.008
300	12,700	-115	144,000	-14,500	24,100	-518	901	-0.314	0.012
400	17,000	-154	194,000	-19,300	32,100	-690	1,200	-0.423	0.016
500	21,200	-192	245,000	-24,100	40,100	-863	1,500	-0.534	0.020
507	21,600	-195	249,000	-24,500	40,700	-876	1,520	-0.542	0.020
Inelastic									
545	23,100	-234	268,000	-26,400	44,000	-940	1,650	-0.585	0.020
680	28,900	-277	332,000	-32,300	55,300	-1,480	2,710	-0.774	0.015
704	29,800	-347	347,000	-33,700	58,000	-1,600	2,960	-0.821	0.010
866	36,700	-372	423,000	-40,300	71,600	-4,570	9,320	-1.460	-0.084
877	37,200	-374	428,000	-40,800	72,500	-4,760	9,750	-1.500	-0.090

Computations of direct force, shear, bending moment, stresses, strains, and deflections were made for all joints. However, Tables B-2 through B-4 tabulate those values for only the 1/4-point, the crown, and the 3/4-point. The distribution of direct forces along the arch varied from a maximum at the 1/4-point to a minimum at the 3/4-point (e.g., from 10,400 lb to 8,500 lb at a load of 200 lb/in.). The 1/4-point and 3/4-point had maximum bending moments and nearly zero shear. The fact that the shear was not zero at these points indicates that the maximum bending moment does not occur exactly at either quarter point. This would tend to provide a theoretical stiffness of the arch that is slightly higher than it would be if a greater number of bars was considered in the theoretical solution.

A theoretical curve of load versus deflection is shown in Figure 23.

Appendix C

DYNAMIC ANALYSIS OF A CIRCULAR ARCH

The dynamic response of a two-hinged circular arch subjected to dynamic load distributed uniformly over one-half the arch length was calculated for the elastic and inelastic ranges. A substitute discrete framework was used in the analysis, and the numerical results were obtained by the iterative method of numerical integration. The original investigation was performed under contract by Eppink (References 15, 16, and 17). Variations and additional comments were made primarily for clarity and continuity of this report.

Analogous Framework

As pointed out in the static analysis of the circular arch of Figure B-1, the exact solution of the continuous arch with distributed mass is impracticable. This is even more so in the dynamic analysis of the circular arch. In order to simplify the solution, it is desirable to represent the original continuous arch by a discrete framework consisting of a series of rigid bars and flexible joints. The following assumptions are made regarding the analogous framework in the elastic range:

1. The rigid bars are assumed to be massless and straight.

2. The flexible joints have the elastic properties of the arch section included between the midpoints of the adjoining segments.

3. The distributed mass of the segment is lumped into a concentrated mass at the joint.

Due to the complexity of the stress-strain relationship in the inelastic range, further assumptions regarding the section properties of the arch are needed:

1. The cross-sectional area of the arch is composed of two flanges and a thin web of zero area.

2. The web is assumed to be rigid in shear but resists no axial force.

Schematic representations of the circular arch and the analogous framework are shown in Figures C-1 and C-2, respectively. The joints of the discrete framework are numbered consecutively from 0 at the left support to n at the right support, and the bars are numbered from 1 to n. A subscript notation is used to identify the locations of joints along the arch. A representative joint is designated by subscript j; joints j-2, j-1, j+1, j+2, and j+3 are designated by h, i, k, ℓ, and m, respectively. The same system is also used for bars such that bar j connects joints i and j.

The deformed arch is represented by the radial and tangential components, Δ_{jr} and Δ_{jt}, of the displacement of the joints. All displacements are measured from the undeformed position of the joints, and the directions of positive displacements are shown in Figure C-2.

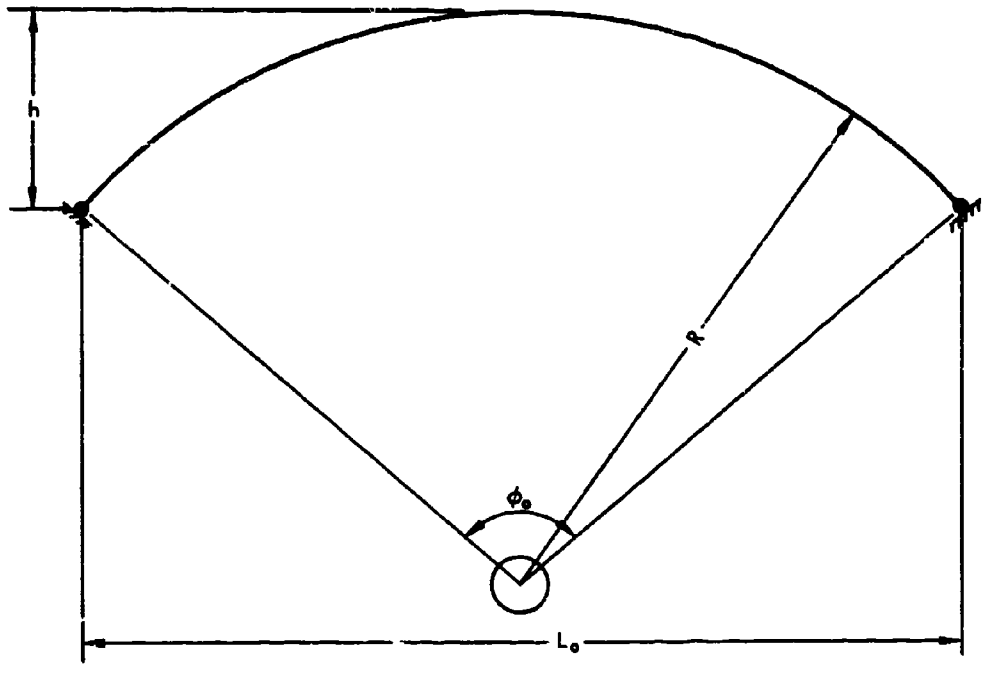

Figure C-1. The original arch.

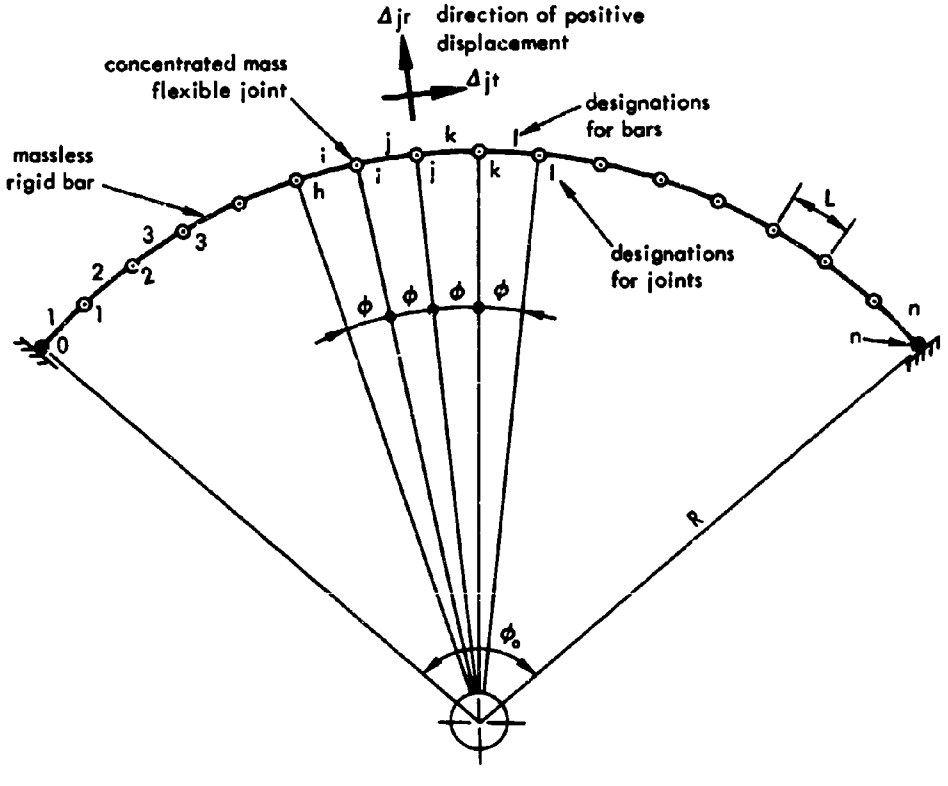

Figure C-2. The analogous framework.

Development of Equations of Motion

The forces acting at the ends of a typical bar and joint are shown in Figure C-3. They include the axial force, P_{jt}; the transverse shearing force, P_{jr}; the bending moment, M_j; the damping forces, $c_e\dot{\Delta}_{jt}$ and $c_e\dot{\Delta}_{jr}$; and the applied force, P_j. The applied force is expressed in terms of its components, P_j^{ℓ} and P_j^{r}, to the left and right of the joint j, respectively. Summing the components of all internal forces in the radial direction, one obtains the following expression for internal resulting force in the radial direction, Z_{jr}

$$Z_{jr} = -P_{jt}\sin\left(\frac{\phi}{2} - \psi_j\right) - P_{kt}\sin\left(\frac{\phi}{2} + \psi_k\right)$$

$$+ P_{jr}\cos\left(\frac{\phi}{2} - \psi_j\right) - P_{kr}\cos\left(\frac{\phi}{2} + \psi_k\right)$$

where ψ_j denotes the rotation of bar j and ψ_k denotes the rotation of bar k. Considering a small deformation such that $\sin\psi \cong \psi$ and $\cos\psi \cong 1$, the above equation can be written in the following form:

$$Z_{jr} = -\left(P_{jt} + P_{kt}\right)\sin\frac{\phi}{2} + \left(P_{jt}\,\psi_j - P_{kt}\,\psi_k\right)\cos\frac{\phi}{2}$$

$$+ \left(P_{jr} - P_{kr}\right)\cos\frac{\phi}{2} + \left(P_{jr}\,\psi_j + P_{kr}\,\psi_k\right)\sin\frac{\phi}{2} \qquad \text{(C-1)}$$

Similarly, the tangential component of the internal resulting force, Z_{jt}, may be obtained by summing all the internal forces in the tangential direction as follows:

$$Z_{jt} = -P_{jt}\cos\left(\frac{\phi}{2} - \psi_j\right) + P_{kt}\cos\left(\frac{\phi}{2} + \psi_k\right)$$

$$- P_{jr}\sin\left(\frac{\phi}{2} - \psi_j\right) - P_{kr}\sin\left(\frac{\phi}{2} + \psi_k\right)$$

and for a small deformation this reduces to

$$Z_{jt} = -\left(P_{jt} - P_{kt}\right)\cos\frac{\phi}{2} - \left(P_{jt}\,\psi_j + P_{kt}\,\psi_k\right)\sin\frac{\phi}{2}$$

$$- \left(P_{jr} + P_{kr}\right)\sin\frac{\phi}{2} + \left(P_{jr}\,\psi_j - P_{kr}\,\psi_k\right)\cos\frac{\phi}{2} \qquad \text{(C-2)}$$

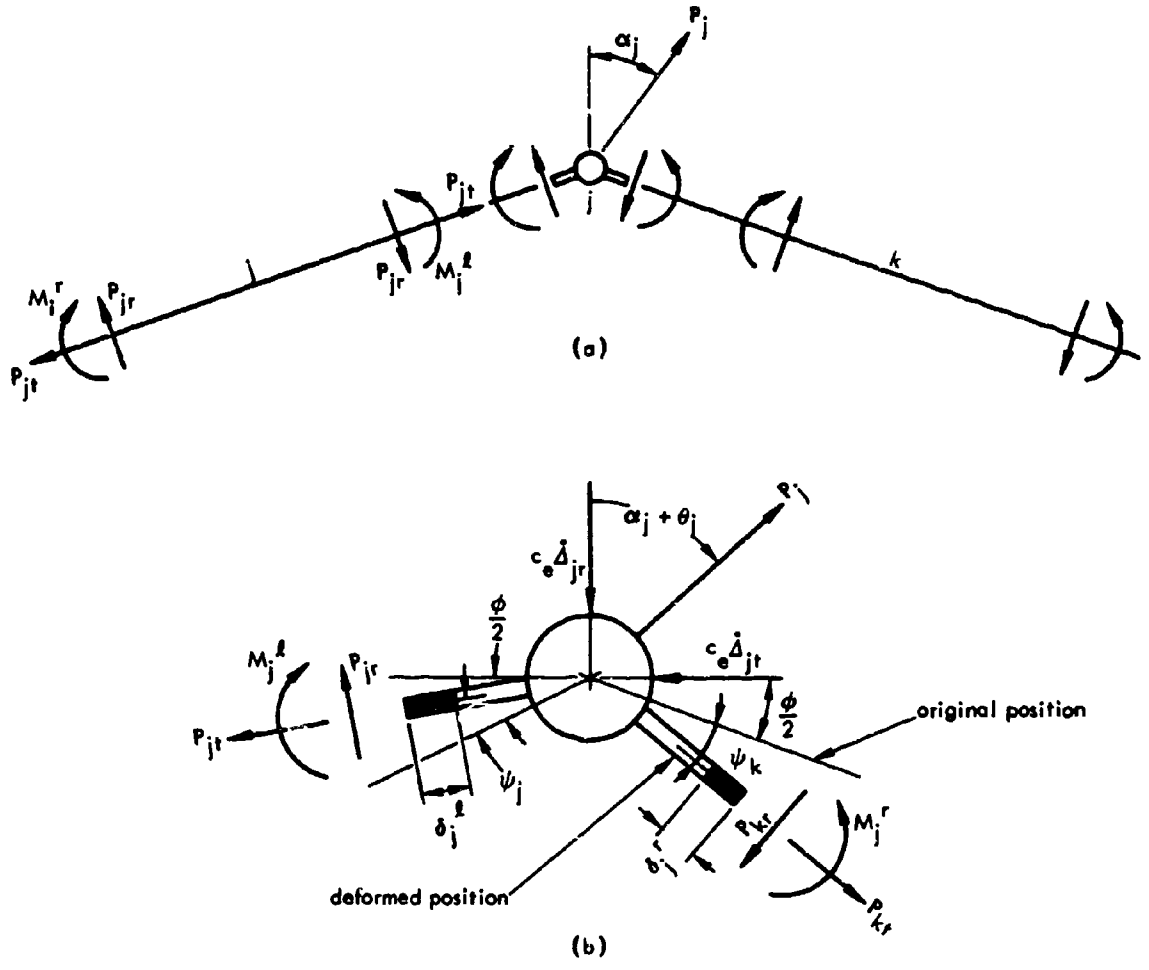

Figure C-3. Free body diagrams for a typical bar and joint.

The shearing forces P_{jr} and P_{kr} in the above equations are related to the bending moments M_i, M_j, and M_k as follows:

$$P_{jr} = \frac{M_j - M_i}{L + \delta_j} \quad , \quad P_{kr} = \frac{M_k - M_j}{L + \delta_k} \tag{C-3}$$

where δ_j and δ_k are deformations of the bar j and bar k, respectively. The axial forces, P_{jt}, and shearing forces, P_{jr}, are taken at the center of the bars, and the bending moments, M_j, are taken at the centers of the joints.

The external pressure is considered to act normal to the arch surface. The distributed load is represented by a series of concentrated forces acting at the joints. For convenience, the concentrated forces are represented by their components, P_j^{ℓ} and P_j^{r}, which are positive in the outward direction. By summing the external forces in the radial direction, one obtains the expression for the external resultant force in the radial direction, W_{jr}, as follows:

$$W_{jr} = P_j^{\ell} \cos\left(\frac{\phi}{2} - \psi_j\right) + P_j^{r} \cos\left(\frac{\phi}{2} + \psi_k\right) - c_e \dot{\Delta}_{jr}$$

where c_e is the coefficient of external viscous damping, and a dot superscript denotes differentiation with respect to time. In the absence of specific information regarding the internal damping of various types, the external damping is taken to be the total damping of the system. The coefficient c_e is obtained from experimental sources. For small displacement, the above equation becomes

$$W_{jr} = \left(P_j^{\ell} + P_j^{r}\right) \cos\frac{\phi}{2} + \left(P_j^{\ell}\psi_j - P_j^{r}\psi_k\right) \sin\frac{\phi}{2} - c_e \dot{\Delta}_{jr} \qquad \text{(C-4)}$$

Similarly, by summing the external forces in the tangential direction, one obtains the expression for the external resultant force in the tangential direction, W_{jt}, as follows:

$$W_{jt} = -P_j^{\ell} \sin\left(\frac{\phi}{2} - \psi_j\right) + P_j^{r} \sin\left(\frac{\phi}{2} + \psi_k\right) - c_e \dot{\Delta}_{jt}$$

and for a small displacement, it becomes

$$W_{jt} = -\left(P_j^{\ell} - P_j^{r}\right) \sin\frac{\phi}{2} + \left(P_j^{\ell}\psi_j + P_j^{r}\psi_k\right) \cos\frac{\phi}{2} - c_e \dot{\Delta}_{jt} \qquad \text{(C-5)}$$

The equations of motion for mass m_j in the radial and tangential directions are as follows:

$$m_j \ddot{\Delta}_{jr} = Z_{jr} + W_{jr} \qquad \text{(C-6)}$$

$$m_j \ddot{\Delta}_{jt} = Z_{jt} + W_{jt} \qquad \text{(C-7)}$$

where $\ddot{\Delta}_{jr}$ and $\ddot{\Delta}_{jt}$ are the radial and tangential accelerations of the mass m_j.

The schematic representation of the displacement-deformation relationships is shown in Figure C-4, where ab and a'b' are the positions of bar j before and after deformation. Let the projection a'c' on ab be designated by $L + \bar{\delta}_j$; then $\bar{\delta}_j$ can be expressed in terms of the displacements of joints i and j as follows:

$$\bar{\delta}_j = \left(\Delta_{jt} - \Delta_{it}\right) \cos\frac{\phi}{2} + \left(\Delta_{jr} + \Delta_{ir}\right) \sin\frac{\phi}{2} \qquad \text{(C-8)}$$

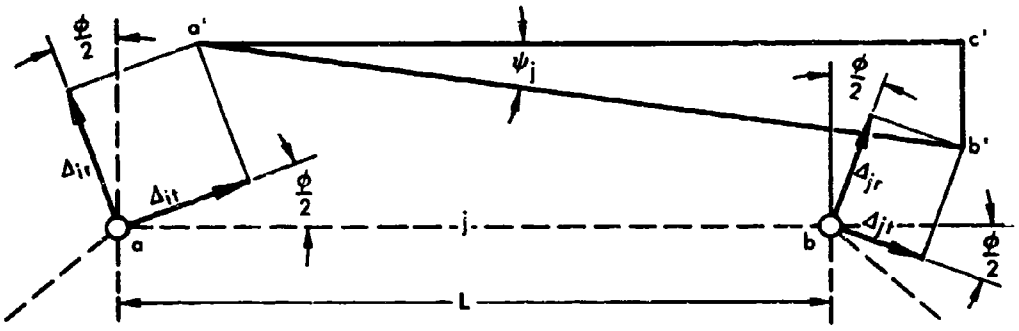

Figure C-4. Schematic representation of displacement-deformation relationships.

Let the projection c'b' in the direction normal to ab be designated by $L\bar{\psi}_j$; then

$$\bar{\psi}_j = \frac{1}{L}\left[\left(\Delta_{jt} + \Delta_{it}\right)\sin\frac{\phi}{2} - \left(\Delta_{jr} - \Delta_{ir}\right)\cos\frac{\phi}{2}\right] \qquad \text{(C-9)}$$

The length of the deformed bar, a'b', can be expressed in terms of the deformation, δ_j, as follows:

$$L + \delta_j = L\sqrt{\bar{\psi}_j^{\,2} + \left(1 + \frac{\bar{\delta}_j}{L}\right)^2}$$

The deformation of the bar j is then

$$\delta_j = L\left[-1 + \sqrt{\bar{\psi}_j^{\,2} + \left(1 + \frac{\bar{\delta}_j}{L}\right)^2}\right] \cong \bar{\delta}_j + \frac{1}{2}L\bar{\psi}_j^{\,2} \qquad \text{(C-10)}$$

Similarly, the rotation of the bar j, ψ_j, can be expressed in terms of $\bar{\delta}_j$ and $\bar{\psi}_j$ as follows:

$$\psi_j = \tan^{-1}\frac{\bar{\psi}_j}{1 + \frac{\bar{\delta}_j}{L}} \cong \bar{\psi}_j\left(1 - \frac{\bar{\delta}_j}{L}\right) \qquad \text{(C-11)}$$

Similarly,

$$\sin \psi_j = \frac{\bar{\psi}_j}{\sqrt{\bar{\psi}_j^2 + \left(1 + \frac{\bar{\delta}_j}{L}\right)^2}} \cong \bar{\psi}_j \left(1 - \frac{\bar{\delta}_j}{L}\right)$$

$$\cos \psi_j = \frac{1 + \frac{\bar{\delta}_j}{L}}{\sqrt{\bar{\psi}_j^2 + \left(1 + \frac{\bar{\delta}_j}{L}\right)^2}} \cong 1 - \frac{1}{2}\bar{\psi}_j^2$$

where $\bar{\delta}_j$ and $\bar{\psi}_j$ are the first-order approximations of δ_j and ψ_j. The angular change at joint j, θ_j, is

$$\theta_j = \psi_k - \psi_j \tag{C-12}$$

and its first-order approximation, $\bar{\theta}_j$, is

$$\bar{\theta}_j = \bar{\psi}_k - \bar{\psi}_j \tag{C-13}$$

The geometric relationships and the equations of motion developed in the preceding paragraphs are general; they are valid irrespective of the material properties. In order to formulate the force-deformation relationship, distinctions between the material properties in the elastic and inelastic ranges must be made.

Elastic Range. Taken from midpoints of the adjacent bars, the deformation to the left and to the right of joint j can be expressed in terms of internal forces and section properties of the joint as follows:

$$\left.\begin{aligned} \delta_j^{\ell} &= \frac{1}{2}\frac{L P_{jt}}{E A_j} \\ \delta_j^{r} &= \frac{1}{2}\frac{L P_{kt}}{E A_j} \end{aligned}\right\} \tag{C-14}$$

where $E A_j$, the extensional stiffness parameter, is the product of the elastic modulus and cross-sectional area of joint j. The total deformation of bar j is expressed as follows:

$$\delta_j = \delta_i^{r} + \delta_j^{\ell} \tag{C-15}$$

Combining the above expression with Equation C-14 and solving for the axial force due to elastic strain, N_j, one obtains

$$N_j = 2 \frac{EA_j}{1 + \frac{EA_j}{EA_i}} \left(\frac{\delta_j}{L}\right) \qquad \text{(C-16)}$$

In the absence of extensional damping, the total axial force, P_{jt}, equals N_j.

Similarly, the bending moment, M_j, is expressed in terms of angular change, θ_j, and the flexural stiffness parameter, EI_j, of joint j as follows:

$$M_j = \frac{EI_j}{L} \theta_j \qquad \text{(C-17)}$$

Inelastic Range. In the inelastic range, the actual arch cross sections are approximated by a section consisting of two flanges. For simplicity, the idealized bilinear stress-strain curve of Figure C-5 is used to correlate the force-deformation relationships. The curve is shown in dimensionless form such that the slope of the elastic portion is unity and yielding occurs when the value of f/f_y is equal to one. The slope of the inelastic portion is E_1/E, the ratio of the inelastic modulus to the elastic modulus of the arch material. Unloading is assumed to take place along a line, AB, parallel to the elastic line. The intercept of AB on the e/e_y axis is the instantaneous set, b/e_y. Unloading will continue along this line until a new "elastic" limit is reached at B. The projected length of AB on the vertical axis is $2f/f_y$. Further unloading will occur along a line with a slope of E_1/E. A possible path of a loading and unloading cycle is represented by OABCD in Figure C-5.

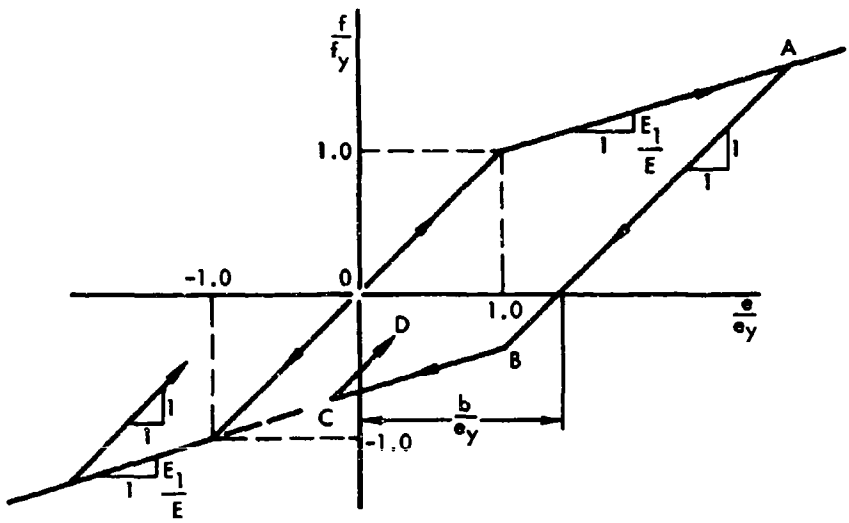

Figure C-5. Bilinear stress-deformation relationship.

In the inelastic range, the stress-deformation relationship is rather complicated. It becomes necessary to determine the deformations in the flanges before the stress, moment, and axial force in each joint can be calculated. A schematic representation of the flange deformations is shown in Figure C-6. Additional subscript notations, t and b, are introduced to designate the top and bottom flanges, respectively.

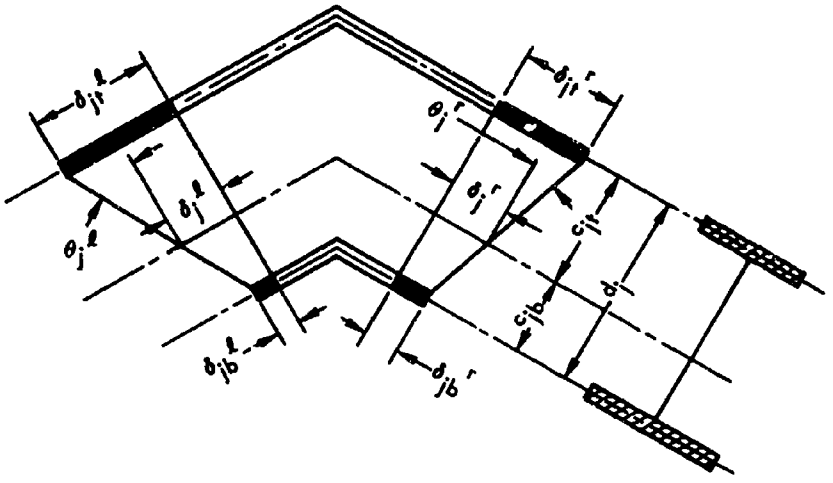

Figure C-6. Schematic representation of deformed joint.

To avoid the time-consuming process of solving numerous simultaneous equations, additional approximations are needed. The distribution of angular change to the left and to the right of a joint is inversely proportional to the relative stiffness, EI/L, of the adjacent bars; the distribution of axial deformation is inversely proportional to the equivalent cross-sectional areas, EA, of two joints. Considering the arch to have uniform cross section along its length, the deformations are given by the following equations:

$$\left.\begin{aligned} \delta_{jt}^{\ell} &= \tfrac{1}{2}\left(\delta_j + c_{jt}\,\theta_j\right) \\ \delta_{jb}^{\ell} &= \tfrac{1}{2}\left(\delta_j - c_{jb}\,\theta_j\right) \\ \delta_{jt}^{r} &= \tfrac{1}{2}\left(\delta_k + c_{jt}\,\theta_j\right) \\ \delta_{jb}^{r} &= \tfrac{1}{2}\left(\delta_k - c_{jb}\,\theta_j\right) \end{aligned}\right\} \qquad \text{(C-18)}$$

where c_{jt} and c_{jb} are the distances from the neutral axis of joint j to the top and bottom flanges, respectively. Equations C-18 give exact results for all deformations in the elastic range. Specialized conditions must be used to account for the boundary condition at the support. For hinged supports the elastic angular change, θ, is zero. The following expressions are obtained for joints o and n:

$$\left.\begin{aligned} \delta_{ot}{}^{r} &= \delta_{ob}{}^{r} = \frac{\delta_1}{2} \\ \delta_{nt}{}^{\ell} &= \delta_{nb}{}^{\ell} = \frac{\delta_n}{2} \end{aligned}\right\} \qquad \text{(C-19)}$$

As a result of the assumptions used to obtain Equations C-18, the equilibrium conditions at the joints can only be met by introducing the average axial forces and moments as follows:

$$P_{jt} = \frac{1}{2}\left(P_{it}{}^{r} + P_{ib}{}^{r} + P_{jt}{}^{\ell} + P_{jb}{}^{\ell}\right) \qquad \text{(C-20)}$$

$$M_j = \frac{1}{2}\left(P_{jb}{}^{\ell} c_{jb} - P_{jt}{}^{\ell} c_{jt} + P_{jb}{}^{r} c_{jb} - P_{jt}{}^{r} c_{jt}\right) \qquad \text{(C-21)}$$

Method of Numerical Integration

Equations C-6 and C-7 may be expressed in terms of the radial and tangential components of displacement for joints 1 through n-1 by using the relationships established in the preceding section. The solution of the dynamic response of the arch is obtained by satisfying a set of 2 (n-1) simultaneous nonlinear differential equations of motion. To accomplish this, a method of iteration and numerical integration is used.

The process of iteration begins at time, t_n, with known values of displacements, velocities, and accelerations of all joints in the system and proceeds to solve for the corresponding quantities for a time, t_{n+1}, at a small time interval, Δt, from t_n. It should be noted that the initial values of displacements, velocities, and accelerations may be estimated or assumed. However, good estimates will ensure a speedier convergence. A step-by-step operation of this method will be shown in the following paragraphs. Each of the following operations is to be repeated for the components of displacement at each joint of the system.

1. Assume or estimate a set of values of displacements, velocities, and accelerations at a chosen time t_n. For example, at initial time, t_o, all quantities may be taken to be zero; at time t_n the quantities may be assumed as the corresponding quantities at time t_{n-1}.

2. Assume a function for accelerations for the small time interval and evaluate the values of velocities and displacements at the end of the time interval in terms of the accelerations, velocities, and displacements at the beginning of the interval. To accomplish this, the following equations obtained from Newmark[12] are used:

$$\left.\begin{aligned} \dot{x}_{n+1} &= \dot{x}_n + \frac{1}{2}(\Delta t)\,\ddot{x}_n + \frac{1}{2}(\Delta t)\,\ddot{x}_{n+1} \\ x_{n+1} &= x_n + (\Delta t)\,\dot{x}_n + \left(\frac{1}{2} - \beta\right)(\Delta t)^2\,\ddot{x}_n + \beta\,(\Delta t)^2\,\ddot{x}_{n+1} \end{aligned}\right\} \qquad \text{(C-22)}$$

where x may be taken to be either component Δ_{jr} or Δ_{jt} of displacement at joint j. The dots denote differentiation with respect to time; the subscripts n and n+1 correspond to times t_n and t_{n+1}, respectively; β depends on the assumed variation of the accelerations within the time interval, Δt. β is 1/6 for a linear variation of the accelerations.

3. Calculate δ_j, ψ_j, and $\bar{\theta}_j$ of Equations C-10, C-11, and C-13 using the values of displacement at the end of the time interval.

4. Evaluate W_{jr} and W_{jt} of Equations C-4 and C-5 for external force components.

5. Evaluate P_{jt} and M_j of Equations C-16 and C-17 for the elastic response of axial force and moment at joint j. The corresponding quantities can be evaluated from Equations C-20 and C-21 using information from the stress-strain curve and Equations C-18 and C-19.

6. Evaluate P_{jr}, Z_{jr}, and Z_{jt} of Equations C-3, C-1, and C-2 for shearing force and the components of internal forces at joint j.

7. Determine a new set of accelerations of Equations C-6 and C-7 with the results of W_{jr}, W_{jt}, Z_{jr}, and Z_{jt}.

8. Compare the derived accelerations with the assumed accelerations.

9. Substitute the derived accelerations for the corresponding assumed accelerations if the agreement is not satisfactory, and repeat steps 2 through 9. Proceed to the next time interval when a satisfactory degree of agreement is reached, and repeat steps 1 through 9.

The above iterative procedure was intended for the dynamic arch response. However, a quasi-static response can also be obtained from the dynamic program by introducing a relatively high level of damping.

Computer Program

A computer program was prepared for the procedures described in the previous section. The source program is written in ALGOL language and can be carried out on the Burroughs B-5000 computer at the University of Virginia. The general capabilities and features of the programs are as follows:

Number of bars:	variable but subject to the limitations of the computer memory system
Stiffness parameters:	can be varied from joint to joint
Support conditions:	varying from fully hinged to fully fixed supports*
Loading conditions:	arbitrary in distribution and magnitude. The time variation of load is considered linear
Output quantities:	axial force, bending moment, radial and tangential components of displacement, stress, and strain

Properties of the Circular Arch and Load Function

The geometry of the two-hinged circular arch and the distribution of loads are shown in Figure B-1. The parameters of the arch are as follows:

Radius of arch $R = 96.0$ inches

Span of arch $L_0 = 143.8$ inches

Angle of opening $\phi_0 = 97.01$ degrees

*See Reference 15 for derivations of moment-resisting supports.

The curvature of the circular arches was obtained by the cold-roll process, and the flanges of the 4M13 rolled section were strained beyond the yield point. The dynamic stress-strain curves do not show the familiar yield plateau. For simplicity, the idealized dynamic stress-strain curves for the component parts of the arch cross section are taken to be bilinear as shown in Figure C-7.

The idealized time variation of the dynamic load is represented by a triangular decaying function with initial peak load, p_o, as shown in Figure C-8. The load duration, t_o, is taken to be 1.6 seconds for all magnitudes of the peak loads.

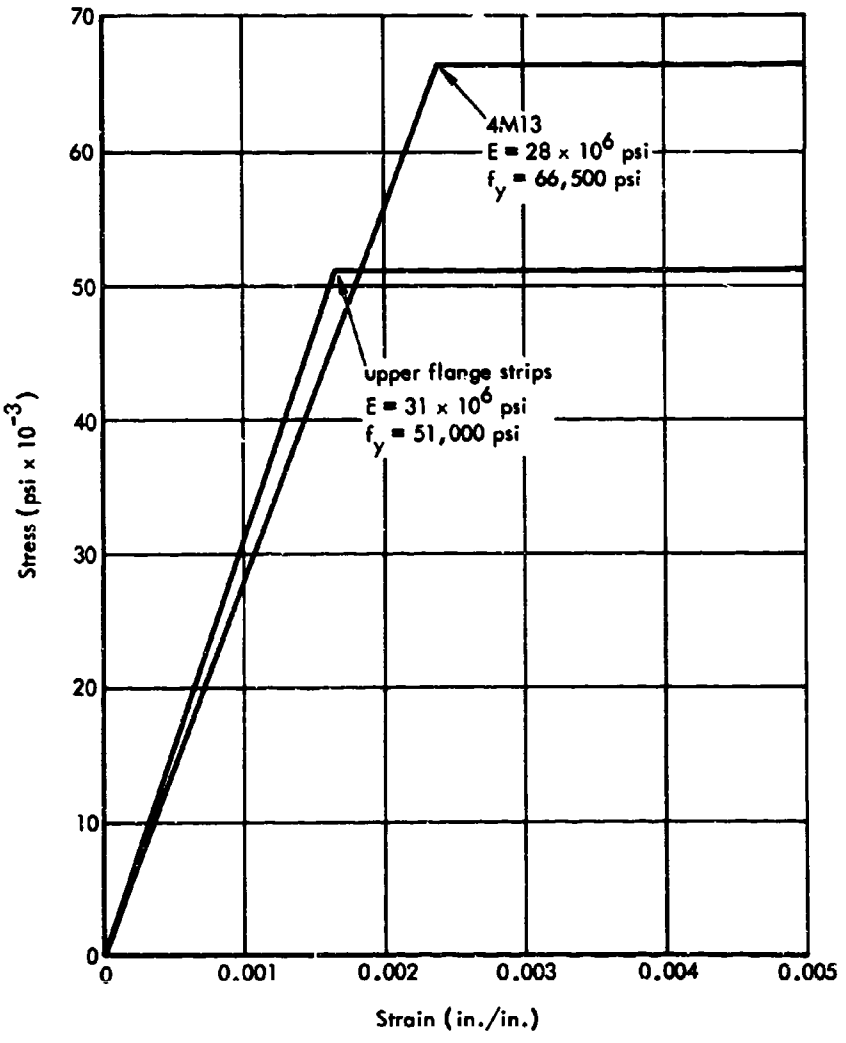

Figure C-7. Idealized dynamic stress-strain relationship.

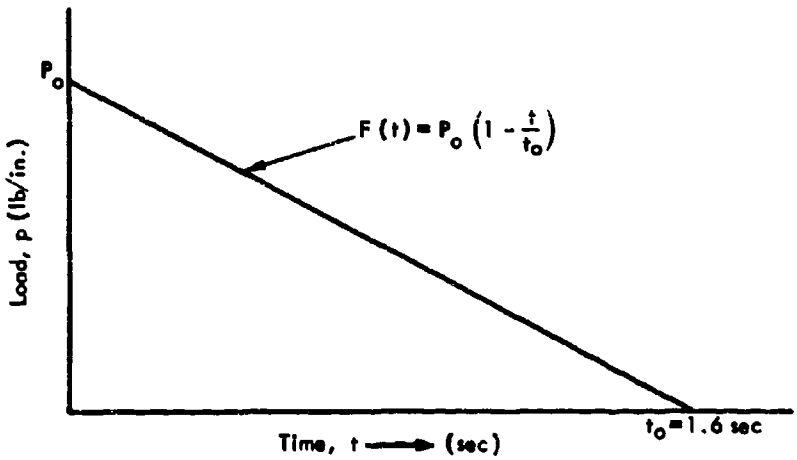

Figure C-8. Load-time relationship.

The cross-sectional properties of the arch in the elastic range are represented by the stiffness parameters, EA and EI, as follows:

$$EA = 177.4 \times 10^6 \text{ lb}$$

$$EI = 407.1 \times 10^6 \text{ lb-in.}^2$$

The cross-sectional properties of the arch in the inelastic range are more complicated; the actual cross section is represented by two flanges. Attempts were made to provide the closest approximations of the actual cross-sectional properties. The following set of parameters were used:

Area of top flange	$A_t = 3.815 \text{ in.}^2$
Area of bottom flange	$A_b = 2.288 \text{ in.}^2$
Modulus of elasticity of top flange	$E_t = 30 \times 10^6$ psi
Modulus of elasticity of bottom flange	$E_b = 28 \times 10^6$ psi
Yield strength of top flange	$f_{yt} = 55,300$ psi
Yield strength of bottom flange	$f_{yb} = 66,500$ psi
Distance between flanges	$d = 3.15$ in.

In the absence of specific information on the damping characteristics of the arch material, it was assumed that the external damping measured by experimental means represented the total damping of the system. An average damping factor, ν, of 0.095 was observed from the fundamental antisymmetrical mode of the free vibration tests. In order to conform with the damping term used in the computer program, the above damping factor was converted to that of a complete ring oscillating at the frequency corresponding to the "breathing" mode.

As shown in Appendix D, the first antisymmetrical frequency of the arch was 59.9 cps, and the "breathing" mode frequency of a complete ring was 317.3 cps. The equivalent damping factor, ν', was as follows:

$$\nu' = \frac{59.9}{317.3}(0.095) = 0.018$$

Presentation of Numerical Results

Dynamic responses of the arch in the elastic range were obtained for peak loads of 200 lb/in. and 400 lb/in. For loads above 400 lb/in., the inelastic behavior of the arch was anticipated and the inelastic program was used. As a comparison, the load of 400 lb/in. was repeated in the inelastic solution. The loading was increased in increments of 100 lb/in. up to 700 lb/in. and then increased in 50-lb/in. increments. A maximum dynamic load of 800 lb/in. was used in the solutions.

The results of dynamic solutions for elastic response for peak loads of 200 lb/in. and 400 lb/in. are given in Table C-1, along with the maximum values of bending moments, axial forces, radial and tangential displacements, and the corresponding times when the maximum values occurred. The inelastic responses for loading between 400 lb/in. and 800 lb/in. are given in Tables C-2, C-3, and C-4. All solutions were based on a 16-bar system; however, data are presented for intervals of one-eighth of the arch length. At the maximum load of 800 lb/in., the convergence of radial and tangential displacements was slow. The maximum displacements were not obtained at several locations of the arch as indicated in Table C-4.

The maximum elastic and inelastic values of moments, axial forces, and radial and tangential displacements at the quarter points and the crown of the arch are presented in graphic form in Figures C-9 through C-12. The bending moment curves for the quarter points coincide with each other in the elastic range, but their signs are different. Bending moments at the crown are comparatively low. The maximum values of axial forces do not vary appreciably at the quarter points and at the crown of the arch, as shown in Figure C-10. The maximum radial displacements occur at the 3/4-point and the maximum tangential displacements occur at the crown of the arch.

The time interval within which the maximum values of various response functions are attained is only a very small fraction of the entire load duration. The decrease of the load from its peak value is very small within this time interval.

The time-variant traces of moment and displacements show that the major contribution came from the first antisymmetrical mode of vibration. This observation can be made from the moment curves and displacement curves of Figures C-13 and C-14 for a peak load of 200 lb/in. The period of major oscillations corresponds to the period of the first antisymmetrical mode of the arch in free vibration. It should be noted that the influence of the third symmetrical mode is also present, but the effects are comparatively small.

The predominant oscillation of the axial forces occurs at a frequency corresponding to the second symmetrical mode of vibration, which is close to the "breathing" mode for a complete ring. The time variant traces of axial forces near the crown and supports of the arch are shown in Figure C-15. It can be seen that the variation of axial forces along the arch is small.

In the inelastic range, the response frequencies and modes of various functions are modified. Increases in the natural period of the response curves are expected as the stiffness of the arch decreases.

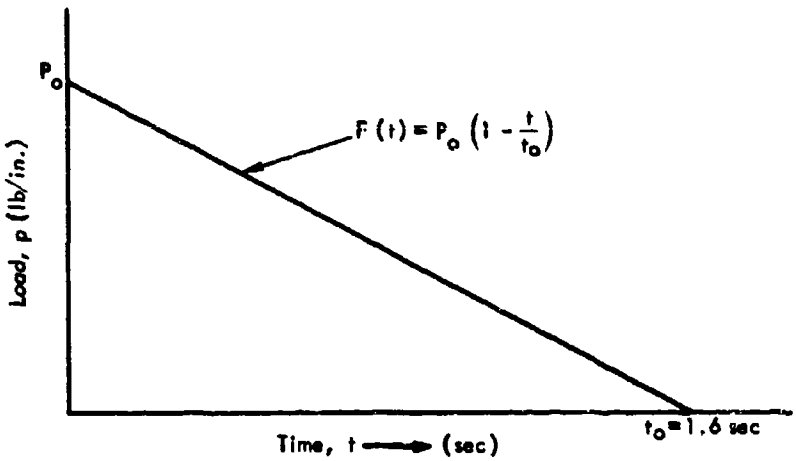

Figure C-8. Load-time relationship.

The cross-sectional properties of the arch in the elastic range are represented by the stiffness parameters, EA and EI, as follows:

$$EA = 177.4 \times 10^6 \text{ lb}$$

$$EI = 407.1 \times 10^6 \text{ lb-in.}^2$$

The cross-sectional properties of the arch in the inelastic range are more complicated; the actual cross section is represented by two flanges. Attempts were made to provide the closest approximations of the actual cross-sectional properties. The following set of parameters were used:

Area of top flange	$A_t = 3.815 \text{ in.}^2$
Area of bottom flange	$A_b = 2.288 \text{ in.}^2$
Modulus of elasticity of top flange	$E_t = 30 \times 10^6$ psi
Modulus of elasticity of bottom flange	$E_b = 28 \times 10^6$ psi
Yield strength of top flange	$f_{yt} = 55,300$ psi
Yield strength of bottom flange	$f_{yb} = 66,500$ psi
Distance between flanges	$d = 3.15$ in.

In the absence of specific information on the damping characteristics of the arch material, it was assumed that the external damping measured by experimental means represented the total damping of the system. An average damping factor, ν, of 0.095 was observed from the fundamental antisymmetrical mode of the free vibration tests. In order to conform with the damping term used in the computer program, the above damping factor was converted to that of a complete ring oscillating at the frequency corresponding to the "breathing" mode.

As shown in Appendix D, the first antisymmetrical frequency of the arch was 59.9 cps, and the "breathing" mode frequency of a complete ring was 317.3 cps. The equivalent damping factor, ν', was as follows:

$$\nu' = \frac{59.9}{317.3}(0.095) = 0.018$$

Presentation of Numerical Results

Dynamic responses of the arch in the elastic range were obtained for peak loads of 200 lb/in. and 400 lb/in. For loads above 400 lb/in., the inelastic behavior of the arch was anticipated and the inelastic program was used. As a comparison, the load of 400 lb/in. was repeated in the inelastic solution. The loading was increased in increments of 100 lb in. up to 700 lb/in. and then increased in 50-lb/in. increments. A maximum dynamic load of 800 lb/in. was used in the solutions.

The results of dynamic solutions for elastic response for peak loads of 200 lb/in. and 400 lb/in. are given in Table C-1, along with the maximum values of bending moments, axial forces, radial and tangential displacements, and the corresponding times when the maximum values occurred. The inelastic responses for loading between 400 lb/in. and 800 lb/in. are given in Tables C-2, C-3, and C-4. All solutions were based on a 16-bar system; however, data are presented for intervals of one-eighth of the arch length. At the maximum load of 800 lb/in., the convergence of radial and tangential displacements was slow. The maximum displacements were not obtained at several locations of the arch as indicated in Table C-4.

The maximum elastic and inelastic values of moments, axial forces, and radial and tangential displacements at the quarter points and the crown of the arch are presented in graphic form in Figures C-9 through C-12. The bending moment curves for the quarter points coincide with each other in the elastic range, but their signs are different. Bending moments at the crown are comparatively low. The maximum values of axial forces do not vary appreciably at the quarter points and at the crown of the arch, as shown in Figure C-10. The maximum radial displacements occur at the 3/4-point and the maximum tangential displacements occur at the crown of the arch.

The time interval within which the maximum values of various response functions are attained is only a very small fraction of the entire load duration. The decrease of the load from its peak value is very small within this time interval.

The time-variant traces of moment and displacements show that the major contribution came from the first antisymmetrical mode of vibration. This observation can be made from the moment curves and displacement curves of Figures C-13 and C-14 for a peak load of 200 lb/in. The period of major oscillations corresponds to the period of the first antisymmetrical mode of the arch in free vibration. It should be noted that the influence of the third symmetrical mode is also present, but the effects are comparatively small.

The predominant oscillation of the axial forces occurs at a frequency corresponding to the second symmetrical mode of vibration, which is close to the "breathing" mode for a complete ring. The time variant traces of axial forces near the crown and supports of the arch are shown in Figure C-15. It can be seen that the variation of axial forces along the arch is small.

In the inelastic range, the response frequencies and modes of various functions are modified. Increases in the natural period of the response curves are expected as the stiffness of the arch decreases.

Table C-1. Maximum Response From Dynamic Loading (Elastic Program)

Location	Moment (in. -lb)	Time (msec)	Axial Force (lb)	Time (msec)	Radial Displace-ment (in.)	Time (msec)	Tangential Displace-ment (in.)	Time (msec)
P_o = 200 lb/in.								
Left support	0				0		0	
1/8 point	-124,000	9.0	-19,100	1.5	0.202	8.9	-0.025	8.3
1/4 point	-161,000	8.5	-19,500	8.0	0.278	8.6	-0.080	8.3
3/8 point	-116,000	7.9	-19,100	8.0	0.187	7.4	-0.134	8.2
Crown	30,000	3.2	-18,800	1.5	-0.027	10.3	-0.155	8.1
5/8 point	118,000	9.0	-18,700	1.5	-0.221	8.0	-0.131	8.0
3/4 point	161,000	7.2	-19,100	1.7	-0.302	7.8	-0.075	7.6
7/8 point	123,000	7.7	-19,800	1.8	-0.215	7.8	-0.021	7.1
Right support	0		-20,300	1.8	0		0	
P_o = 400 lb/in.								
Left support	0				0		0	
1/8 point	-254,000	9.0	-38,100	1.4	0.410	8.9	-0.053	8.3
1/4 point	-328,000	8.5	-39,200	8.0	0.560	8.6	-0.165	8.4
3/8 point	-233,000	8.0	-38,400	8.0	0.374	7.4	-0.272	8.3
Crown	61,000	3.2	-37,500	1.5	-0.062	10.2	-0.314	8.2
5/8 point	242,000	9.0	-37,400	1.5	-0.456	8.0	-0.368	8.1
3/4 point	327,000	7.2	-38,100	1.7	-0.617	7.9	-0.151	8.0
7/8 point	250,000	7.7	-39,600	1.8	-0.438	7.8	-0.041	7.1
Right support	0		-40,500	1.8	0		0	

Table C-2. Maximum Response From Dynamic Loading (Inelastic Program)

Location	Moment (in. -lb)	Time (msec)	Axial Force (lb)	Time (msec)	Radial Displace-ment (in.)	Time (msec)	Tangential Displace-ment (in.)	Time (msec)
P_o = 400 lb/in.								
Left support	0				0		0	
1/8 point	-254,000	9.1	-38,000	1.5	0.405	9.0	-0.053	8.4
1/4 point	-326,000	8.5	-39,000	8.1	0.552	8.6	-0.162	8.4
3/8 point	-234,000	8.0	-38,400	8.1	0.371	7.2	-0.270	8.3
Crown	61,000	3.3	-37,500	1.5	-0.062	10.2	-0.312	8.2
5/8 point	242,000	9.1	-37,400	1.5	-0.454	8.1	-0.263	8.0
3/4 point	326,000	7.2	-38,100	1.8	-0.614	7.9	-0.151	7.4
7/8 point	251,000	7.8	-39,700	1.8	-0.434	7.8	-0.041	7.2
Right support	0		-40,500		0		0	
P_o = 500 lb/in.								
Left support	0				0		0	
1/8 point	-287,000	9.2	-47,500	1.5	0.517	9.2	-0.066	8.5
1/4 point	-371,000	6.4	-47,000	1.5	0.724	9.1	-0.211	8.7
3/8 point	-269,000	6.6	-47,000	1.5	0.461	7.0	-0.350	8.6
Crown	95,000	10.2	-46,800	1.5	-0.122	10.5	-0.398	8.5
5/8 point	307,000	9.2	-46,700	1.5	-0.580	8.4	-0.334	8.2
3/4 point	408,000	7.8	-47,600	1.8	-0.783	7.9	-0.190	7.5
7/8 point	306,000	7.7	-49,500	1.8	-0.546	7.9	-0.050	7.2
Right support	0		-50,700	1.8	0		0	

Table C-3. Maximum Response From Dynamic Loading (Inelastic Program)

Location	Moment (in. -lb)	Time (msec)	Axial Force (lb)	Time (msec)	Radial Displacement (in.)	Time (msec)	Tangential Displacement (in.)	Time (msec)
P_o = 600 lb/in.								
Left support	0				0		0	
1/8 point	-301,000	9.8	-56,900	1.5	0.690	9.8	-0.090	10.5
1/4 point	-393,000	6.4	-56,400	1.5	0.991	9.6	-0.296	10.2
3/8 point	-278,000	5.5	-56,400	1.5	0.555	9.1	-0.480	9.9
Crown	129,000	9.8	-56,200	1.5	-0.191	10.9	-0.530	9.8
5/8 point	354,000	10.4	-56,000	1.5	-0.785	10.6	-0.437	9.1
3/4 point	442,000	8.0	-57,100	1.8	-1.007	8.3	-0.243	8.9
7/8 point	330,000	6.0	-59,400	1.8	-0.672	8.3	-0.062	9.0
Right support	0		-60,800	1.8	0		0	
P_o = 700 lb/in.								
Left support	0				0		0	
1/8 point	-313,000	12.9	-66,400	1.5	1.010	12.8	-0.137	13.2
1/4 point	-408,000	9.8	-65,700	1.5	1.428	12.8	-0.460	13.1
3/8 point	-278,000	5.1	-65,700	1.5	0.756	15.3	-0.719	13.1
Crown	139,000	9.8	-65,500	1.5	-0.261	11.5	-0.792	13.3
5/8 point	388,000	10.7	-65,400	1.5	-1.147	14.1	-0.656	13.4
3/4 point	464,000	8.0	-66,500	1.8	-1.524	14.2	-0 352	13.3
7/8 point	352,000	5.6	-69,300	1.8	-0.960	14.0	-0.081	12.9
Right support	0		-70,900	1.8	0		0	

Table C-4. Maximum Response From Dynamic Loading (Inelastic Program)

Location	Moment (in. -lb)	Time (msec)	Axial Force (lb)	Time (msec)	Radial Displacement (in.)	Time (msec)	Tangential Displacement (in.)	Time (msec)
P_o = 750 lb/in.								
Left support	0				0		0	
1/8 point	-317,000	12.9	-71,100	1.5	1.314	19.1	-0.187	19.4
1/4 point	-413,000	9.7	-70,400	1.5	1.880	19.1	-0.603	19.3
3/8 point	-279,000	5.0	-70,400	1.5	0.990	19.0	-0.968	19.3
Crown	148,000	9.7	-70,200	1.5	-0.546	20.0	-1.068	19.2
5/8 point	399,000	11.1	-70,000	1.5	-1.561	18.0	-0.887	19.1
3/4 point	473,000	14.3	-71,300	1.8	-2.055	17.8	-0.462	19.2
7/8 point	355,000	5.6	-74,200	1.8	-1.262	17.6	-0.098	19.2
Right support	0		-75,900	1.8	0		0	
P_o = 800 lb/in.								
Left support	0				0		0	
1/8 point	-326,000	12.7	-75,700	1.5	1.876	38.8	0.291	40.0*
1/4 point	-426,000	9.6	-75,000	1.5	2.645	39.0	-0.898	40.0*
3/8 point	-279,000	4.9	-74,900	1.5	1.344	38.8	-1.423	40.0*
Crown	152,000	10.0	-74,800	1.5	-0.558	40.0*	-1.567	39.2
5/8 point	407,000	11.1	-74,600	1.5	-2.345	40.0*	-1.320	40.0*
3/4 point	492,000	8.0	-76,000	1.8	-3.062	40.0*	-0.657	39.0
7/8 point	364,000	5.4	-79,200	1.8	-1.845	40.0*	-0.120	38.8
Right support	0		-81,000	1.8	0		0	

*End of solution; maximum values were not obtained.

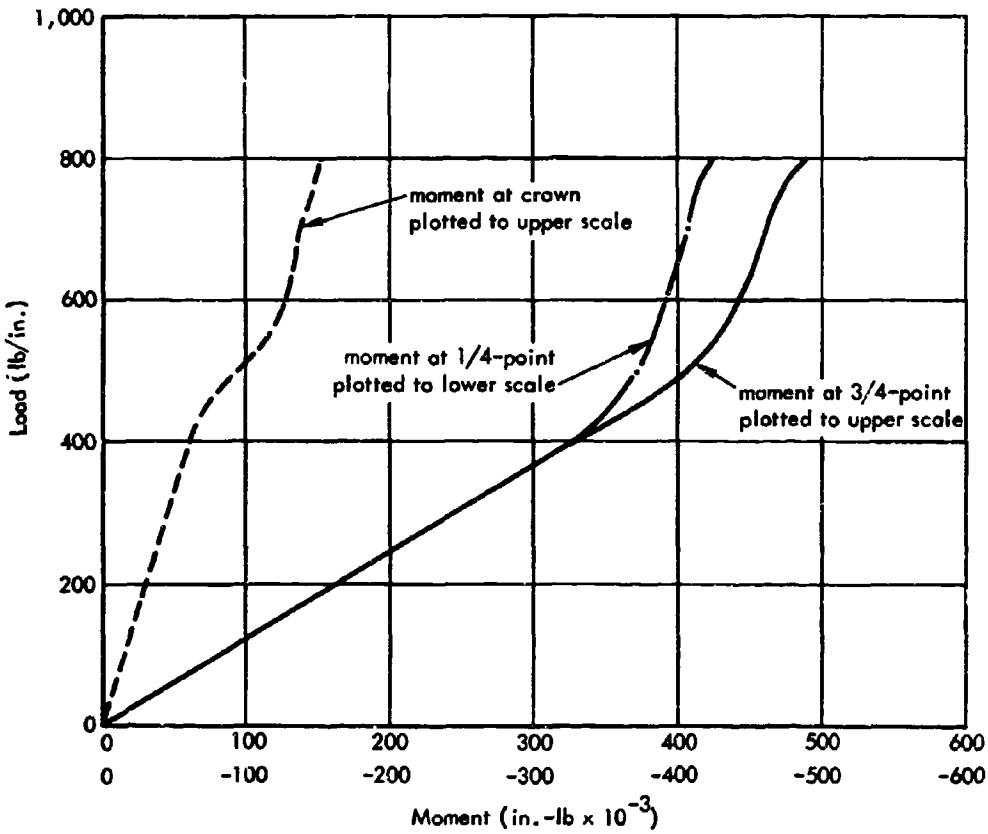

Figure C-9. Maximum dynamic moments.

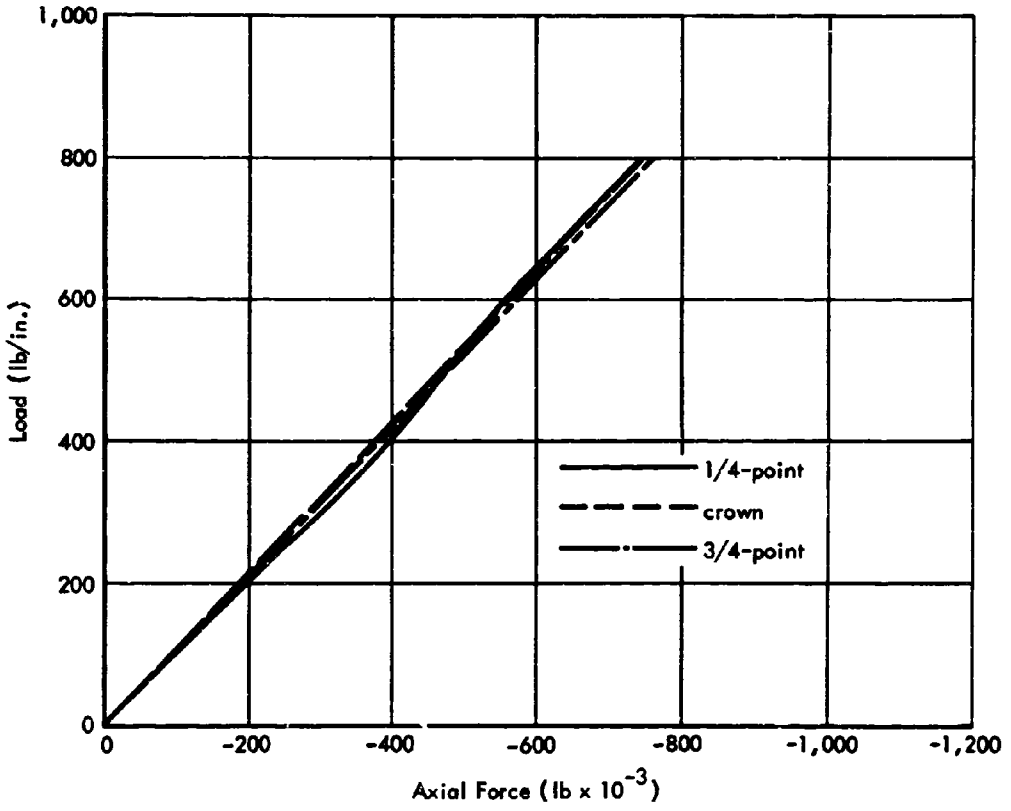

Figure C-10. Maximum dynamic axial forces.

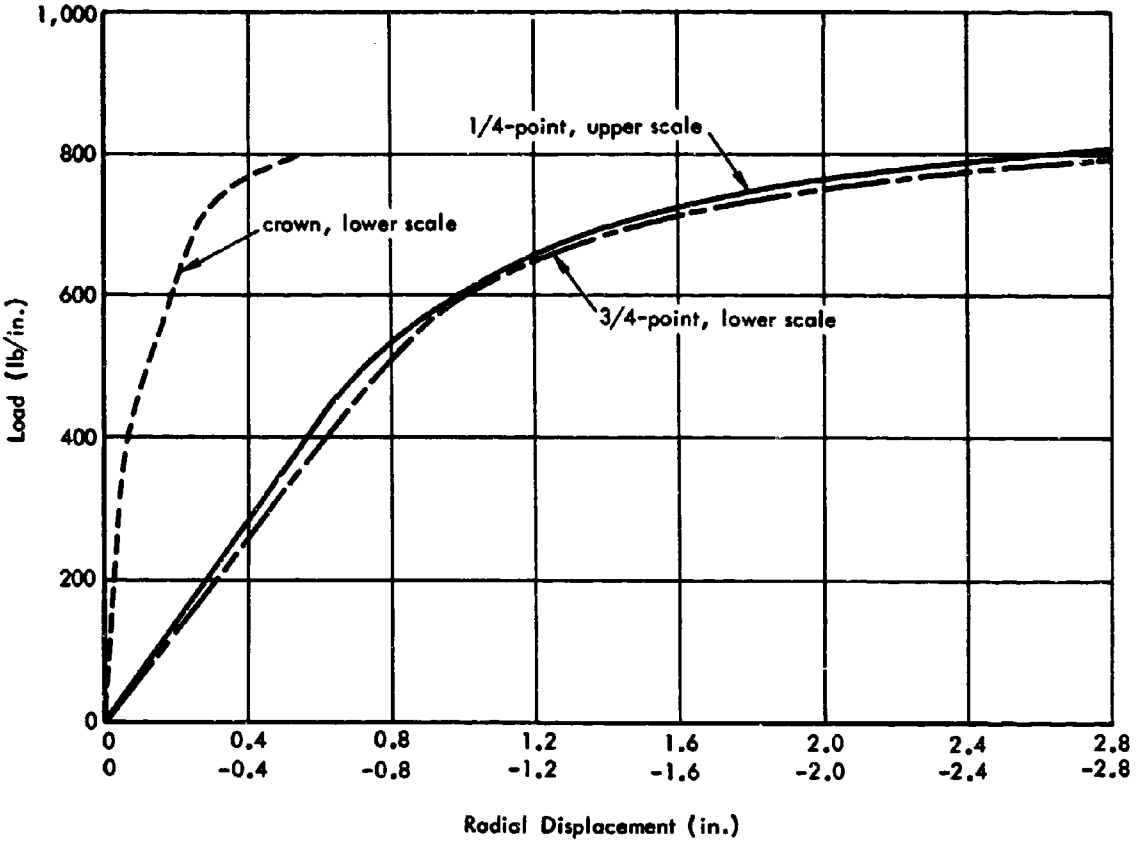

Figure C-11. Maximum radial displacement for dynamic loads.

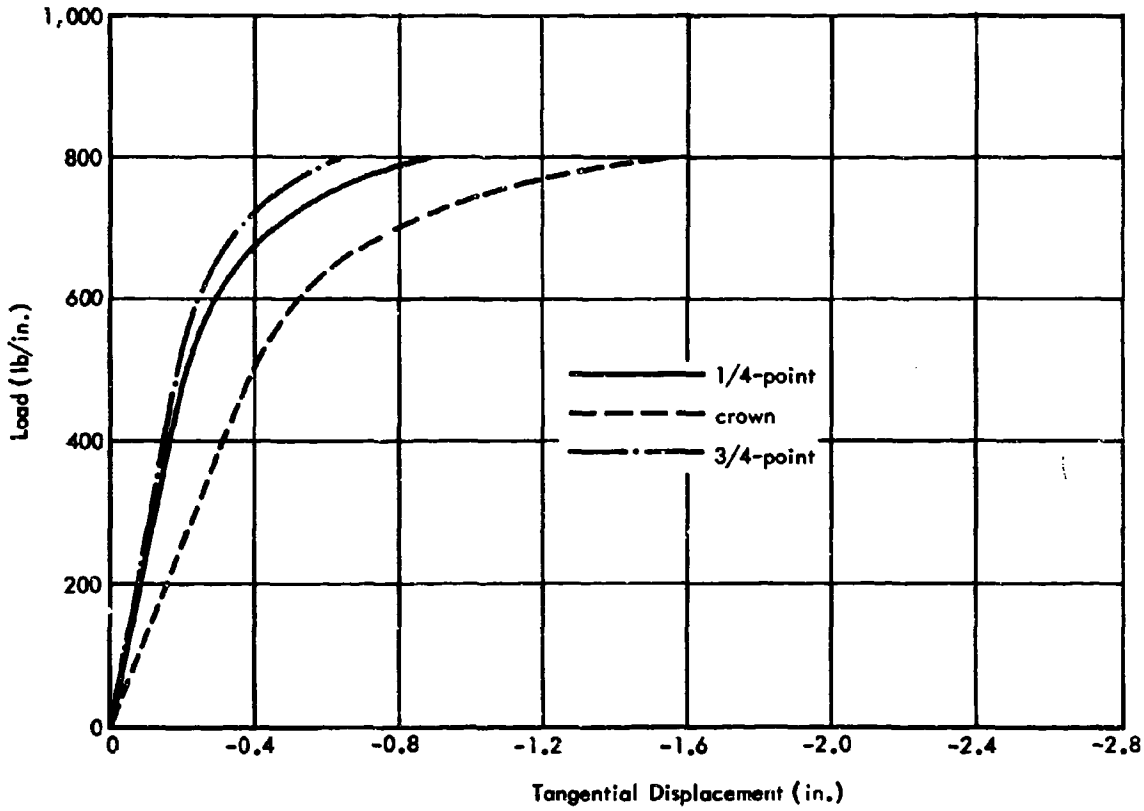

Figure C-12. Maximum tangential displacement for dynamic loads.

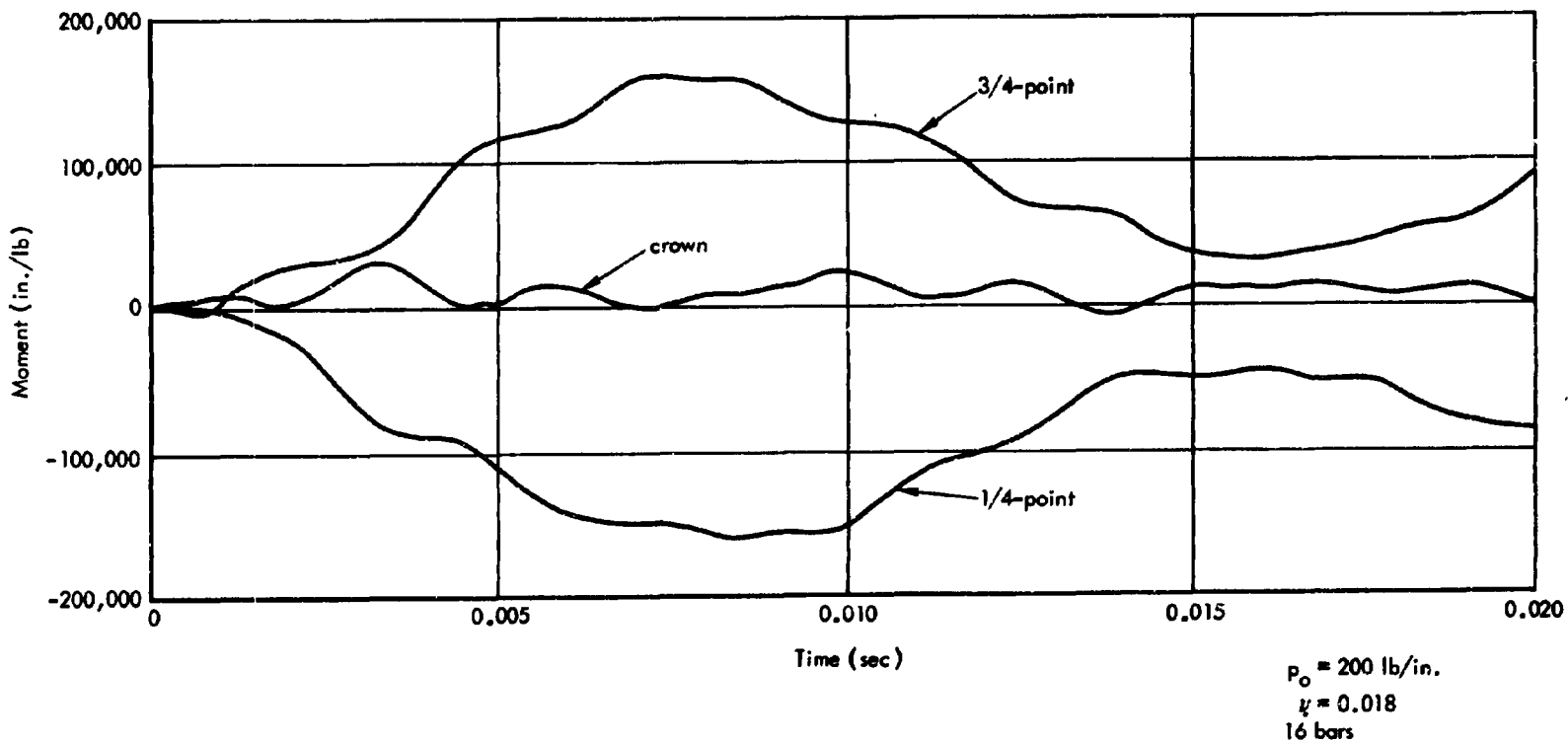

Figure C-13. Bending moments versus time.

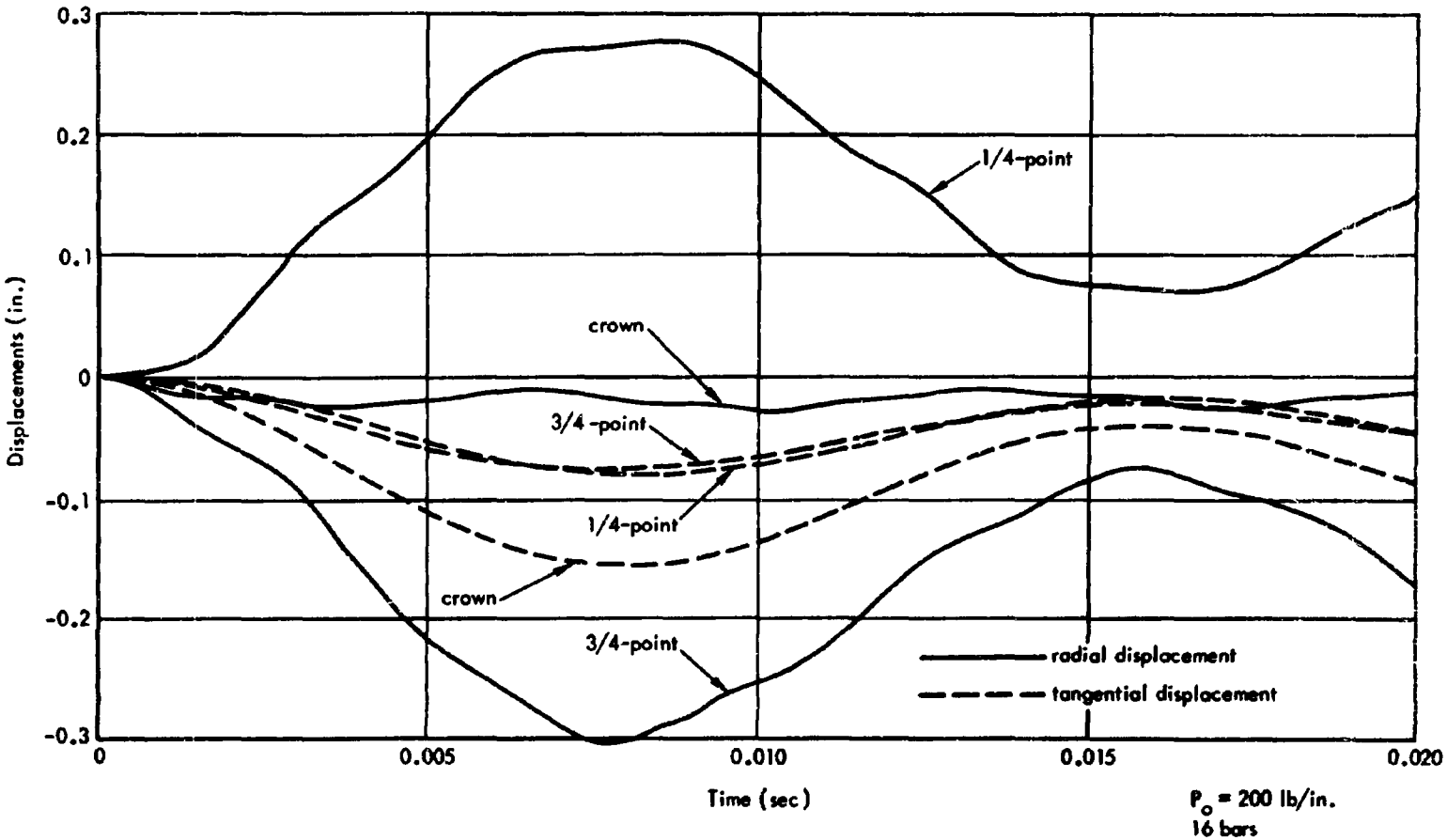

Figure C-14. Displacement versus time.

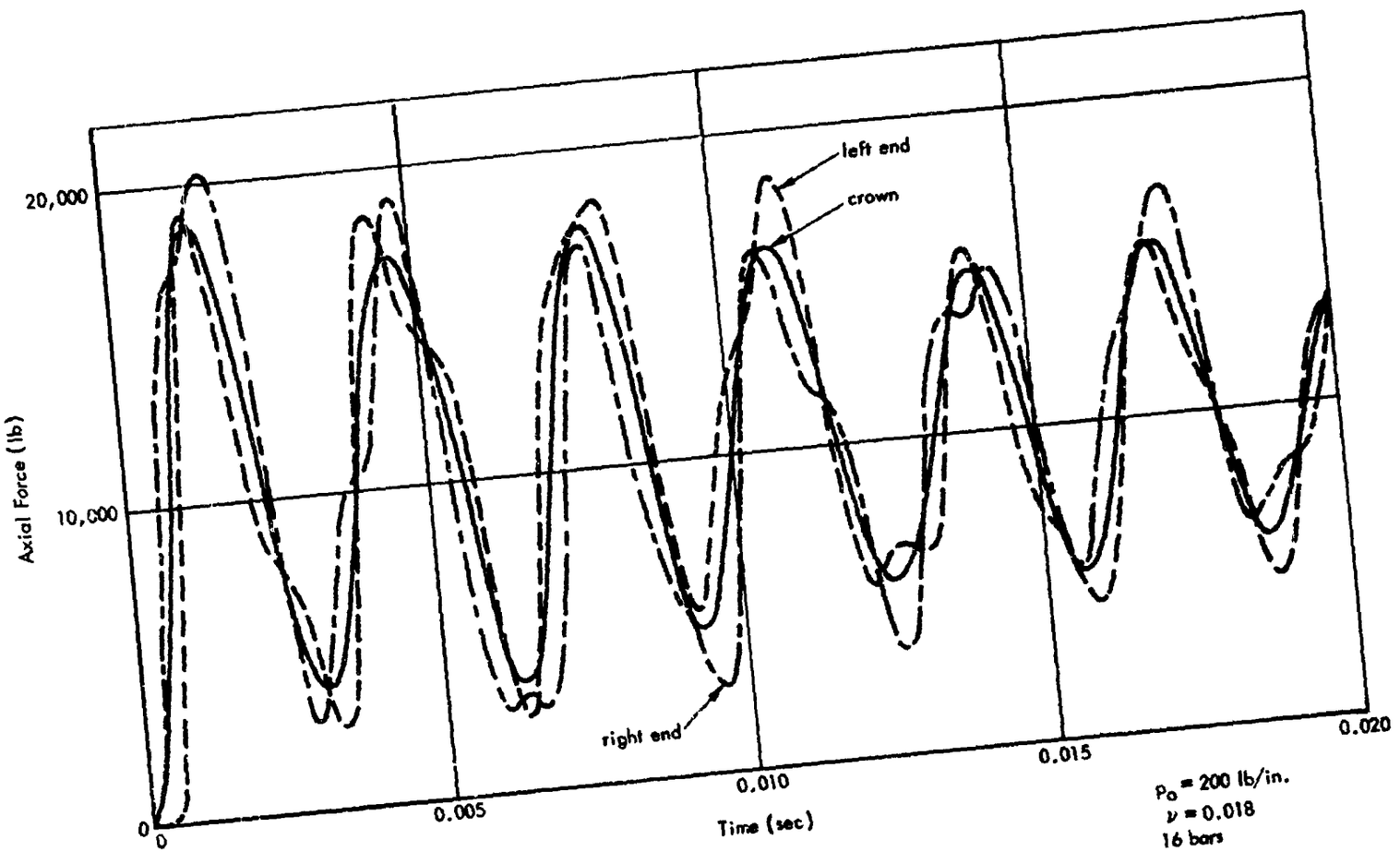

Figure C-15. Axial forces versus time.

Appendix D

ANALYSIS FOR NATURAL FREQUENCIES AND BUCKLING LOADS

In the analysis of the two-hinged circular arch for its natural frequencies and buckling loads, the active continuous structure of Figure B-1 is reduced to a discrete framework consisting of a series of rigid bars and flexible joints as described in Appendix C. The mass may either be considered lumped at the joints or distributed along the bars. A uniform static normal pressure may be introduced in the frequency equations; i.e., the frequencies of the arch can be determined for free vibration or forced vibration. The theoretical development of equations was performed by Eppink (Reference 15). Additional remarks are made primarily for clarity and continuity of this report.

Derivation of Equations

In considering the uniform static pressure acting on the arch, the following additional assumptions are made:

1. The arch maintains its circular shape under the external normal pressure.

2. The arch undergoes only a uniform compression under the external normal pressure.

3. All measurements are taken from the compressed position of the arch.

4. The oscillation of the arch is small.

5. The effect of damping is negligible.

The above assumptions serve to linearize the vibration of the arch under uniform normal pressure. The axial force, P_{jt}, can be expressed in the form

$$P_{jt} = -\frac{1}{2} w L \cot\frac{\phi}{2} + N_j \tag{D-1}$$

where the first term represents the force due to uniform compression and the second term represents the force due to displacements. By substituting Equations C-3 and D-1 into Equations C-1 and C-2 and omitting the product terms of $N\psi$ and $M\psi$, the following expressions for Z_{jr} and Z_{jt} are obtained:

$$Z_{jr} = -\left(N_j + N_k\right)\sin\frac{\phi}{2} - \frac{1}{L}\left(M_i - 2M_j + M_k\right)\cos\frac{\phi}{2}$$

$$+ w L \cos\frac{\phi}{2} + \frac{1}{2} w L \left(\psi_k - \psi_j\right)\cot\frac{\phi}{2}\cos\frac{\phi}{2} \tag{D-2}$$

$$Z_{jt} = -\left(N_j - N_k\right)\cos\frac{\phi}{2} + \frac{1}{L}\left(M_i - M_k\right)\sin\frac{\phi}{2}$$

$$+ \frac{1}{2} w L \left(\psi_k + \psi_j\right)\cos\frac{\phi}{2} \tag{D-3}$$

If the axial deformation is taken into account, the components W_{jr} and W_{jt} of the external forces are established by noting that

$$p_j^{\ell} = -\frac{1}{2}\left(L + \delta_j\right) w$$

$$p_j^{r} = -\frac{1}{2}\left(L + \delta_k\right) w$$

Substituting the above expression into Equations C-4 and C-5, and neglecting the product terms of $\delta\psi$, the following expressions for W_{jr} and W_{jt} are obtained

$$W_{jr} = -wL\cos\frac{\phi}{2} - \frac{1}{2}w\left(\delta_k + \delta_j\right)\cos\frac{\phi}{2} + \frac{1}{2}wL\left(\psi_k - \psi_j\right)\sin\frac{\phi}{2} \tag{D-4}$$

$$W_{jt} = -\frac{1}{2}w\left(\delta_k - \delta_j\right)\sin\frac{\phi}{2} - \frac{1}{2}wL\left(\psi_k + \psi_j\right)\cos\frac{\phi}{2} \tag{D-5}$$

The components of the internal force, Z_{jr} and Z_{jt}, of Equations D-2 and D-3 can be expressed in terms of deformations δ and ψ by using Equations C-16 and C-17. The resulting equations along with Equations D-4 and D-5 are then expressed in terms of displacements by using the first-order approximations of Equations C-8, C-9, and C-12. The resulting expressions for Z_{jr}, Z_{jt}, W_{jr}, and W_{jt} are then expressed in terms of displacements Δ_{jr} and Δ_{jt}.

At a natural mode of vibration the conditions of simple harmonic motion are satisfied for each particle of the system, and the equations of motion, Equations C-6 and C-7, become

$$m_j \ddot{\Delta}_{jr} = -\omega^2 m_j \Delta_{jr} = Z_{jr} + W_{jr} \tag{D-6}$$

$$m_j \ddot{\Delta}_{jt} = -\omega^2 m_j \Delta_{jt} = Z_{jt} + W_{jt} \tag{D-7}$$

where ω is the circular frequency of vibration.

Substituting the expressions for Z_{jr}, Z_{jt}, W_{jr}, and W_{jt} into Equations D-6 and D-7, simplifying by letting μ denote the mass per unit length of the arch and r the radius of gyration of the arch cross section, and introducing the following notations

$$c = \tan\frac{\phi}{2} \tag{D-8}$$

$$\rho = \left(\frac{L}{r}\right)^2 \tag{D-9}$$

$$\lambda = \left(4c \sin \frac{\phi}{2}\right)^2 \frac{\mu R^4}{EI} \omega^2 \tag{D-10}$$

$$k = 4c \sin^3 \left(\frac{\phi}{2}\right) \frac{wR^3}{EI} \tag{D-11}$$

the following expression for the equation of motion in the radial direction is obtained:

$$\left[\Delta_{hr} + \left(-4 + \rho c^2\right)\Delta_{ir} + \left(6 + 2\rho c^2\right)\Delta_{jr} + \left(-4 + \rho c^2\right)\Delta_{kr} + \Delta_{\ell r}\right]$$

$$+ c\left[\Delta_{ht} - (2 + \rho)\Delta_{it} + (2 + \rho)\Delta_{kt} - \Delta_{\ell t}\right]$$

$$= \lambda \Delta_{jr} + k\left[-\left(2 + \frac{1}{c^2}\right)\Delta_{ir} + \frac{2}{c^2}\Delta_{jr} - \left(2 + \frac{1}{c^2}\right)\Delta_{kr} + c\left(-\Delta_{it} + \Delta_{kt}\right)\right] \tag{D-12}$$

The corresponding equation for the tangential direction becomes

$$c\left[-\Delta_{hr} + (2 + \rho)\Delta_{ir} - (2 + \rho)\Delta_{kr} + \Delta_{\ell r}\right]$$

$$+ \left[-c^2 \Delta_{ht} - \rho \Delta_{it} + 2\left(\rho + c^2\right)\Delta_{jt} - \rho \Delta_{kt} - c^2 \Delta_{\ell t}\right]$$

$$= \lambda \Delta_{jt} + k\left[c\left(\Delta_{ir} - \Delta_{kr}\right) + \left(-\Delta_{it} + 2\Delta_{jt} - \Delta_{kt}\right)\right] \tag{D-13}$$

The left sides of Equations D-12 and D-13 are applicable to joints $2 \leq j \leq n-2$. The boundary conditions must be considered in deriving the equations of motion for joints 1 and $n-1$. Figure D-1 is a schematic representation of the equations of motion for the general interior joint j and the joints near the supports.

A system of $2(n-1)$ homogeneous linear algebraic equations can be obtained from Equations D-12 and D-13 with specialized equations for the joints near the supports. The system of equations can be written in abbreviated form as follows:

$$A\Delta - \lambda B\Delta - kC\Delta = 0 \tag{D-14}$$

where A, B, and C are symmetric matrices of order $2(n-1)$, and Δ is a column matrix of the displacement Δ_r and Δ_t. There are $2(n-1)$ characteristic roots and vectors of the above equations corresponding to the natural frequencies and mode shapes of vibration of the system.

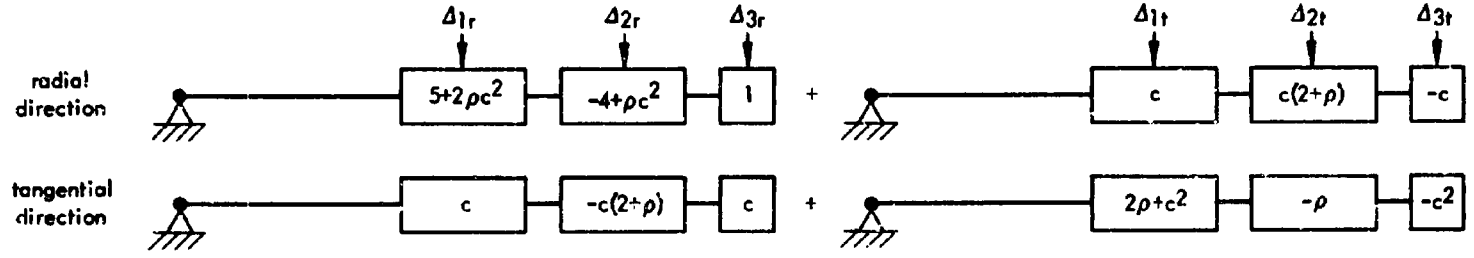

(a) For joint 1 - hinged boundary

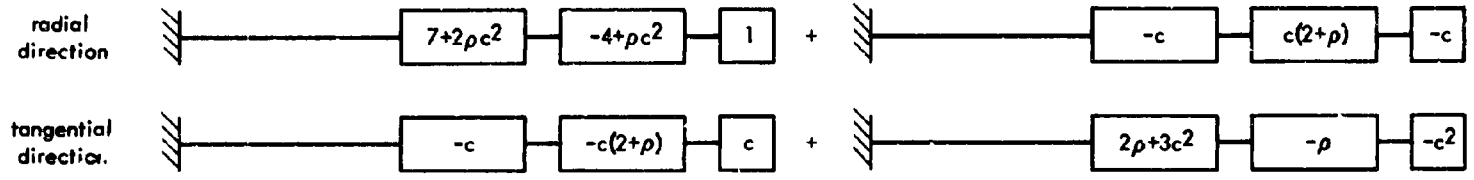

(b) For joint 1 - fixed boundary

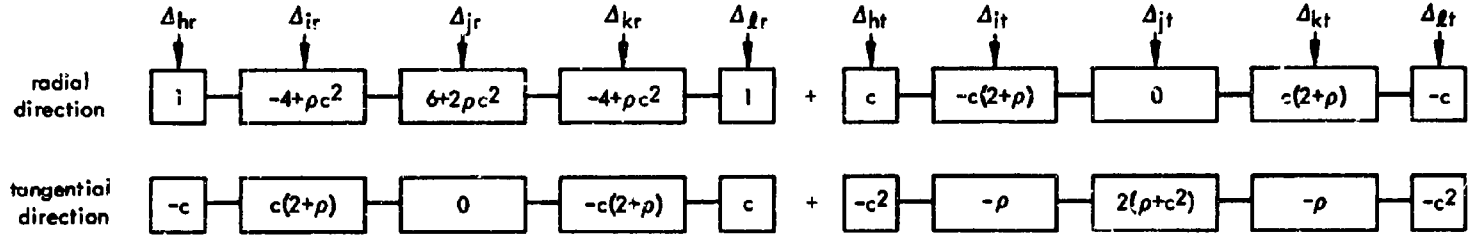

(c) For general interior joint j

Figure D-1. Left side of Equations D-12 and D-13 in block form.

It should be noted that for free vibration the load parameter k is set to zero and Equation D-14 becomes

$$A\Delta - \lambda B\Delta = 0$$

For the buckling loads of the system, the frequency parameter λ is set to zero and the following expression is obtained:

$$A\Delta - kC\Delta = 0$$

The mass of the system can be considered to be distributed along the bars of the discrete framework instead of concentrated at the joints. The equations can be established by using the Lagrange equations of motion. A detailed derivation is presented in Reference 16. The resulting equations can be presented in abbreviated form as follows:

$$A\Delta - \lambda B'\Delta - kC\Delta = 0$$

where B' is a symmetric matrix of order $2(n-1)$. The terms $\lambda B'\Delta$ can be obtained for the equations of motion in the radial direction as follows:

$$\lambda \frac{1}{6}\left(\cos \phi \Delta_{ir} + 4\Delta_{jr} + \cos \phi \Delta_{kr} + \sin \phi \Delta_{it} - \sin \phi \Delta_{kt}\right) \qquad \text{(D-15)}$$

and for equations of motion in the tangential direction as follows:

$$\lambda \frac{1}{6}\left(-\sin \phi \Delta_{ir} + \sin \phi \Delta_{kr} + \cos \phi \Delta_{it} + 4\Delta_{jt} + \cos \phi \Delta_{kt}\right) \qquad \text{(D-16)}$$

For geometrically symmetrical structures, the natural modes of vibration are either symmetrical or antisymmetrical with respect to the line of symmetry of the structure. This can be utilized to determine the complete set of natural modes and the associated frequencies by solving two characteristic value problems, each of order $(n-1)$ instead of one of order $2(n-1)$.

Let joint k be located at the line of symmetry of the discrete framework. For antisymmetrical modes, the radial displacement, Δ_{kr}, at joint k is zero, and

$$\Delta_{\ell r} = -\Delta_{jr} \quad , \quad \Delta_{\ell t} = \Delta_{jt}$$

$$\Delta_{mr} = -\Delta_{ir} \quad , \quad \Delta_{mt} = \Delta_{it}$$

For symmetrical modes, the tangential displacement, Δ_{kt}, at joint j is zero, and

$$\Delta_{\ell r} = \Delta_{jr} \quad , \quad \Delta_{\ell t} = -\Delta_{jt}$$

$$\Delta_{mr} = \Delta_{ir} \quad , \quad \Delta_{mt} = -\Delta_{it}$$

Figure D-2 presents the left side of Equations D-12 and D-13 for joints j and k in block form.

As an example, the frequency equations for a 12-bar system are presented in matrix form in Tables D-1 and D-2 for antisymmetrical modes and for symmetrical modes, respectively. In order that the same matrix equations be applicable to frequency as well as buckling load calculations, three additional parameters, x, y, and z, are introduced.

For free vibration of concentrated mass systems

$$x = \lambda \quad , \quad y = 0 \quad , \quad z = 0$$

For free vibration of distributed mass systems

$$x = \frac{2}{3}\lambda \quad , \quad y = \frac{\lambda}{6}\cos\phi \quad , \quad z = \frac{\lambda}{6}\sin\phi$$

For buckling loads

$$x = \frac{2k}{c^2} \quad , \quad y = -k\left(2 - \frac{1}{c^2}\right) \quad , \quad z = -ck$$

Computer Program

A computer program has been completed which can calculate either the natural frequency or buckling load of an arch of uniform cross section based on the equations given in Tables D-1 and D-2. The source program is written in FORTRAN and can be carried out on an IBM 7094 or IBM 1620II computer. It should be noted that the number of bars considered is limited only by the memory capacity of the computers. However, solutions for more than 40 bars are not recommended considering the computer time involved and the very slight increase in accuracy.

The natural frequency can be determined for either a concentrated mass system or a distributed mass system. For natural frequency calculations, a uniformly distributed load can be acting on the arch. A special case occurs when the natural frequency vanishes: the buckling load for the system is obtained.

The source program can be subdivided into the following:

a. Determination of natural frequencies and buckling load

b. Determination of natural modes

It is possible to divide the program so that a smaller computer can be used for the solutions. To facilitate this operation, complete flow charts are given in Figures D-3, D-4, D-5, and D-6 for general analysis of arches, evaluation of matrices, search for roots, and vector components. The source program in FORTRAN is given in Program D-1.

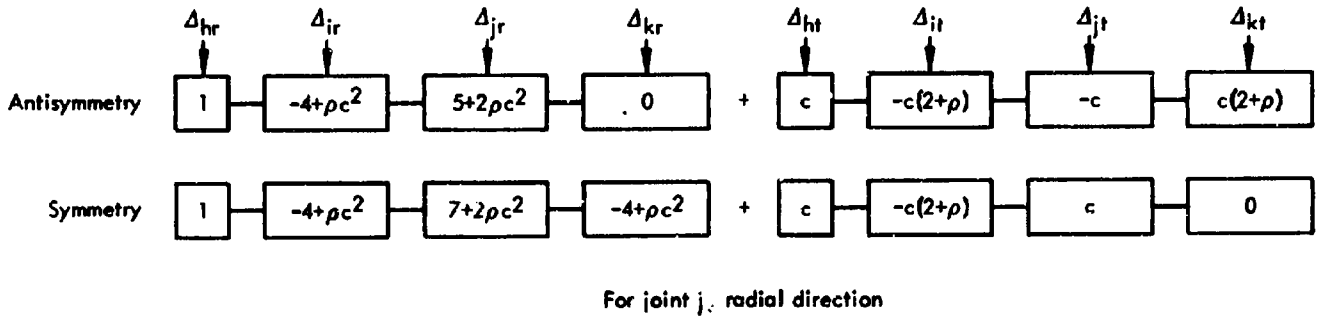

Figure D-2. Left side of Equations D-12 and D-13 in block form.

Table D-1. Frequency Equations of Antisymmetrical Modes for Circular Arches in the Elastic Range

$$
\begin{bmatrix}
5 + 2\rho c^2 - x & -4 + \rho c^2 - y & 1 & 0 & 0 & c & c(2+\rho) - z & -c & 0 & 0 & 0 \\
-4 + \rho c^2 - y & 6 + 2\rho c^2 - x & -4 + \rho c^2 - y & 1 & 0 & -c(2+\rho) - z & 0 & c(2+\rho) - z & -c & 0 & 0 \\
1 & -4 + \rho c^2 - y & 6 + 2\rho c^2 - x & -4 + \rho c^2 - y & 1 & c & -c(2+\rho) - z & 0 & c(2+\rho) - z & -c & 0 \\
0 & 1 & -4 + \rho c^2 - y & 6 + 2\rho c^2 - x & -4 + \rho c^2 - y & 0 & c & -c(2+\rho) - z & 0 & c(2+\rho) - z & -c \\
0 & 0 & 1 & -4 + \rho c^2 - y & 5 + 2\rho c^2 - x & 0 & 0 & c & -c(2+\rho) - z & -c & c(2+\rho) + z \\
c & -c(2+\rho) - z & c & 0 & 0 & 2\rho + c^2 - x & -\rho - y & -c^2 & 0 & 0 & 0 \\
c(2+\rho) + z & 0 & -c(2+\rho) - z & c & 0 & -\rho - y & 2(\rho + c^2) - x & -\rho - y & -c^2 & c & 0 \\
-c & c(2+\rho) + z & 0 & -c(2+\rho) - z & c & -c^2 & -\rho - y & 2(\rho + c^2) - x & -\rho - y & -c^2 & 0 \\
0 & -c & c(2+\rho) + z & 0 & -c(2+\rho) - z & 0 & -c^2 & -\rho - y & 2(\rho + c^2) - x & -\rho - y & -c^2 \\
0 & 0 & -c & c(2+\rho) + z & -c & 0 & 0 & -c^2 & -\rho - y & 2\rho + c^2 - x & -\rho - y \\
0 & 0 & 0 & -2c & 2c(2+\rho) + 2z & 0 & 0 & 0 & -2c^2 & -2(\rho + y) & 2(\rho + c^2) - x
\end{bmatrix}
\begin{bmatrix}
\Delta_{1r} \\ \Delta_{2r} \\ \Delta_{3r} \\ \Delta_{4r} \\ \Delta_{5r} \\ \Delta_{1t} \\ \Delta_{2t} \\ \Delta_{3t} \\ \Delta_{4t} \\ \Delta_{5t} \\ \Delta_{6t}
\end{bmatrix}
=
\begin{bmatrix} 0 \end{bmatrix}
$$

Table D-2. Frequency Equations of Symmetrical Modes for Circular Arches in the Elastic Range

$$
\begin{bmatrix}
5 + 2\rho c^2 - x & -4 + \rho c^2 - y & 1 & 0 & 0 & c & c(2+\rho) + z & -c & 0 & 0 & 0 \\
-4 + \rho c^2 - y & 6 + 2\rho c^2 - x & -4 + \rho c^2 - y & 1 & 0 & -c(2+\rho) - z & 0 & c(2+\rho) + z & -c & 0 & 0 \\
1 & -4 + \rho c^2 - y & 6 + 2\rho c^2 - x & -4 + \rho c^2 - y & 1 & c & -c(2+\rho) - z & 0 & c(2+\rho) + z & -c & 0 \\
0 & 1 & -4 + \rho c^2 - y & 6 + 2\rho c^2 - x & -4 + \rho c^2 - y & 0 & c & -c(2+\rho) - z & 0 & c(2+\rho) + z & 1 \\
0 & 0 & 1 & -4 + \rho c^2 - y & 7 + 2\rho c^2 - x & 0 & 0 & c & -c(2+\rho) - z & c & -4 + \rho c^2 - y \\
c & -c(2+\rho) - z & c & 0 & 0 & 2\rho + c^2 - x & -\rho - y & -c^2 & 0 & 0 & 0 \\
c(2+\rho) + z & 0 & -c(2+\rho) - z & c & 0 & -\rho - y & 2(\rho + c^2) - x & -\rho - y & -c^2 & 0 & 0 \\
-c & c(2+\rho) + z & 0 & -c(2+\rho) - z & c & -c^2 & -\rho - y & 2(\rho + c^2) - x & -\rho - y & -c^2 & 0 \\
0 & -c & c(2+\rho) + z & 0 & -c(2+\rho) - z & 0 & -c^2 & -\rho - y & 2(\rho + c^2) - x & -\rho - y & c \\
0 & 0 & -c & c(2+\rho) + z & c & 0 & 0 & -c^2 & -\rho - y & 2\rho + 2c^2 - x & -c(2+\rho) - z \\
0 & 0 & 0 & 2 & -8 + 2\rho c^2 - 2x & 0 & 0 & 0 & 2z & -2z(2+\rho) + 2z & 6 + 2\rho z^2 - x
\end{bmatrix}
\begin{bmatrix}
\delta_{1r} \\ \delta_{2r} \\ \delta_{3r} \\ \delta_{4r} \\ \delta_{5r} \\ \delta_{1i} \\ \delta_{2i} \\ \delta_{3i} \\ \delta_{4i} \\ \delta_{5i} \\ \omega
\end{bmatrix}
=
\begin{bmatrix} 0 \end{bmatrix}
$$

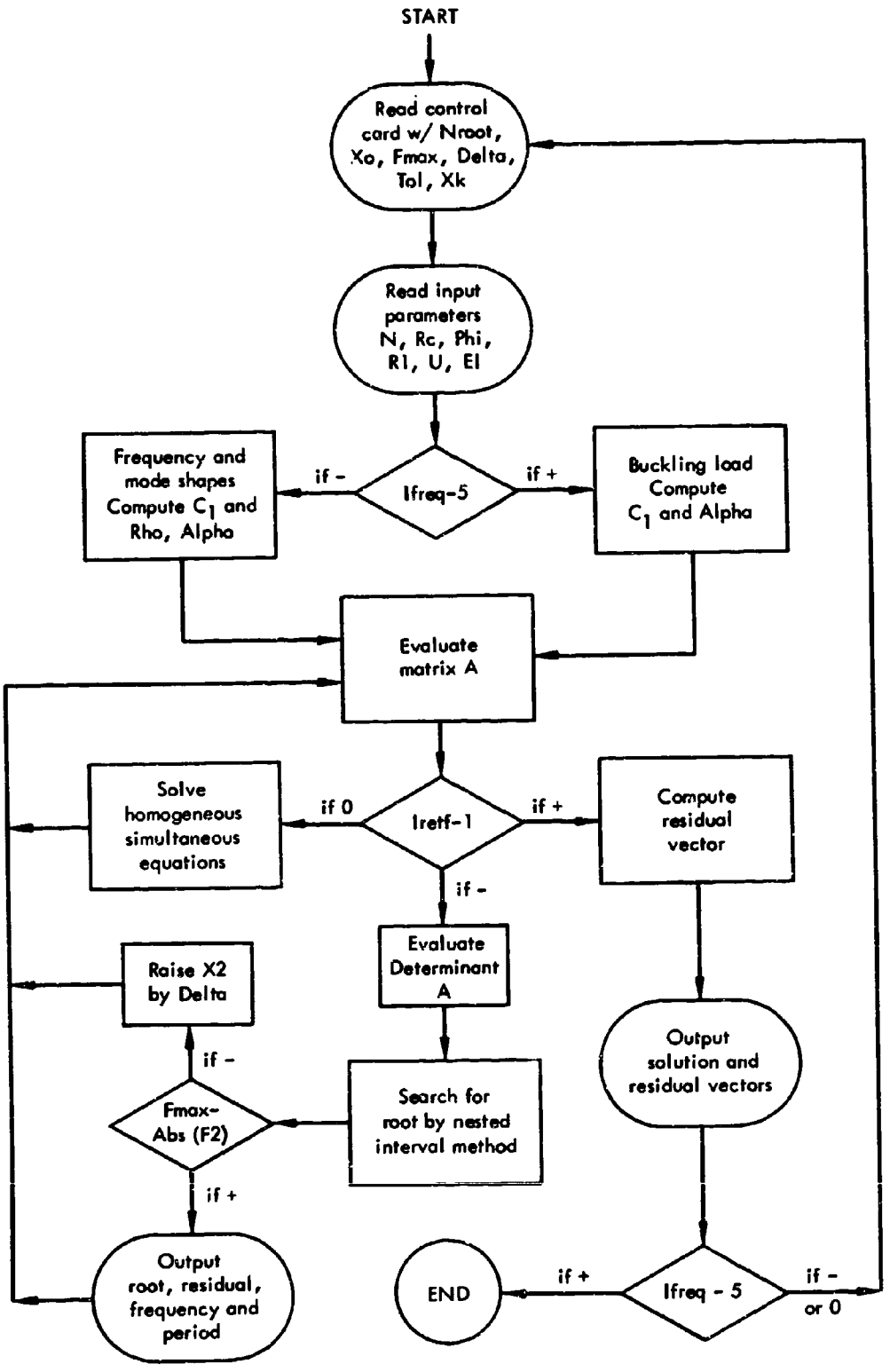

Figure D-3. Flow diagram, analysis of arches.

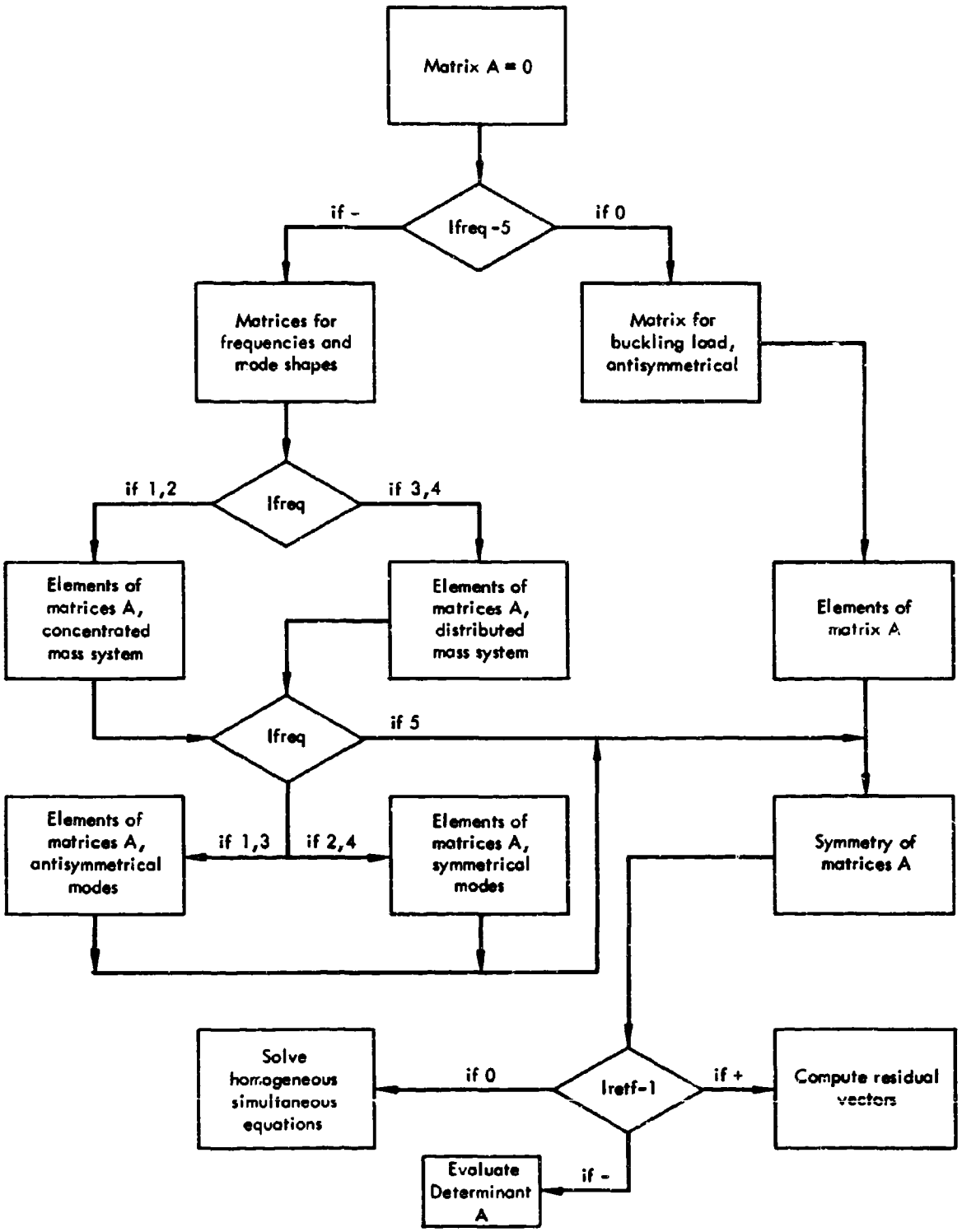

Figure D-4. Flow diagram, evaluation of matrices.

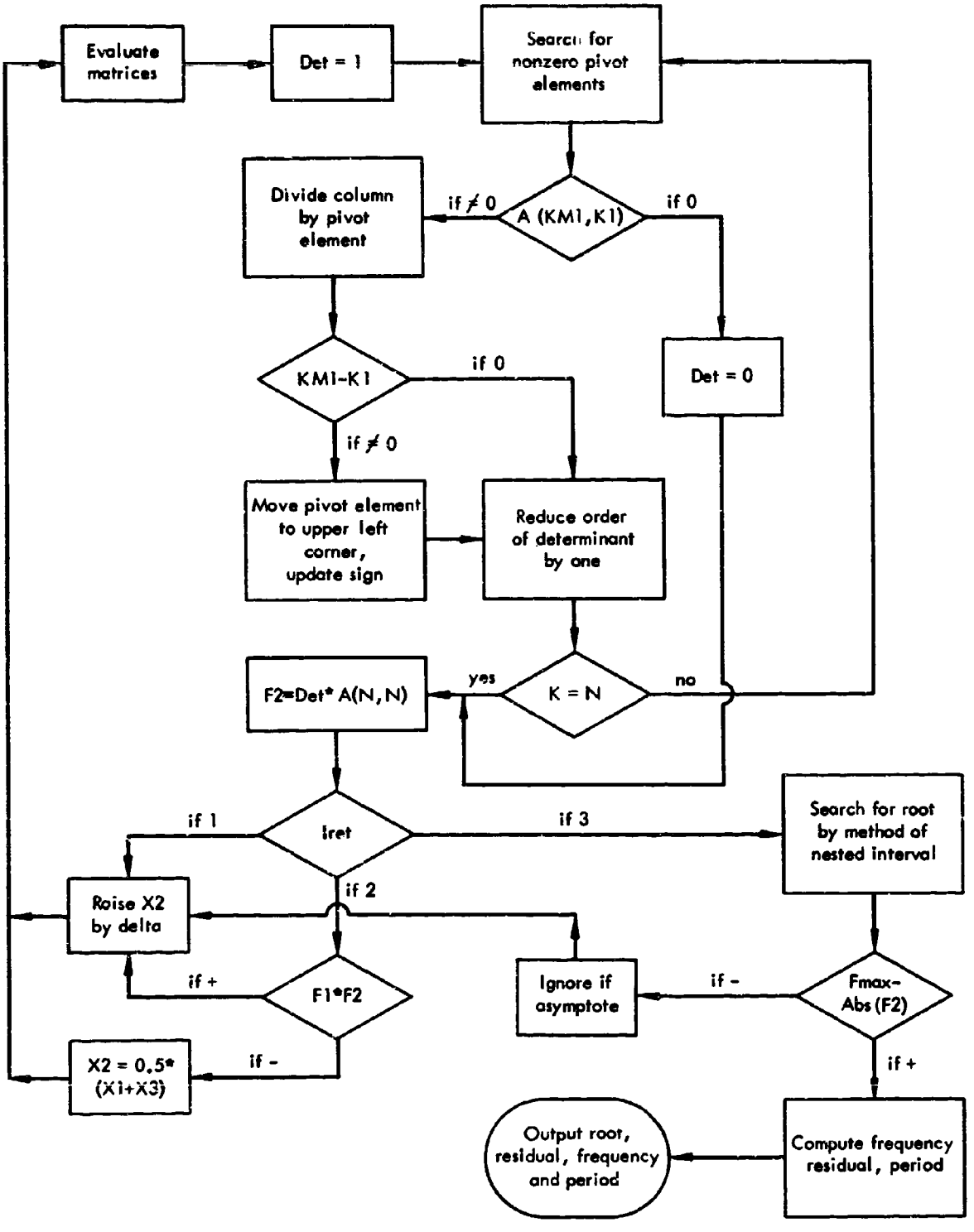

Figure D-5. Flow diagram, search for roots.

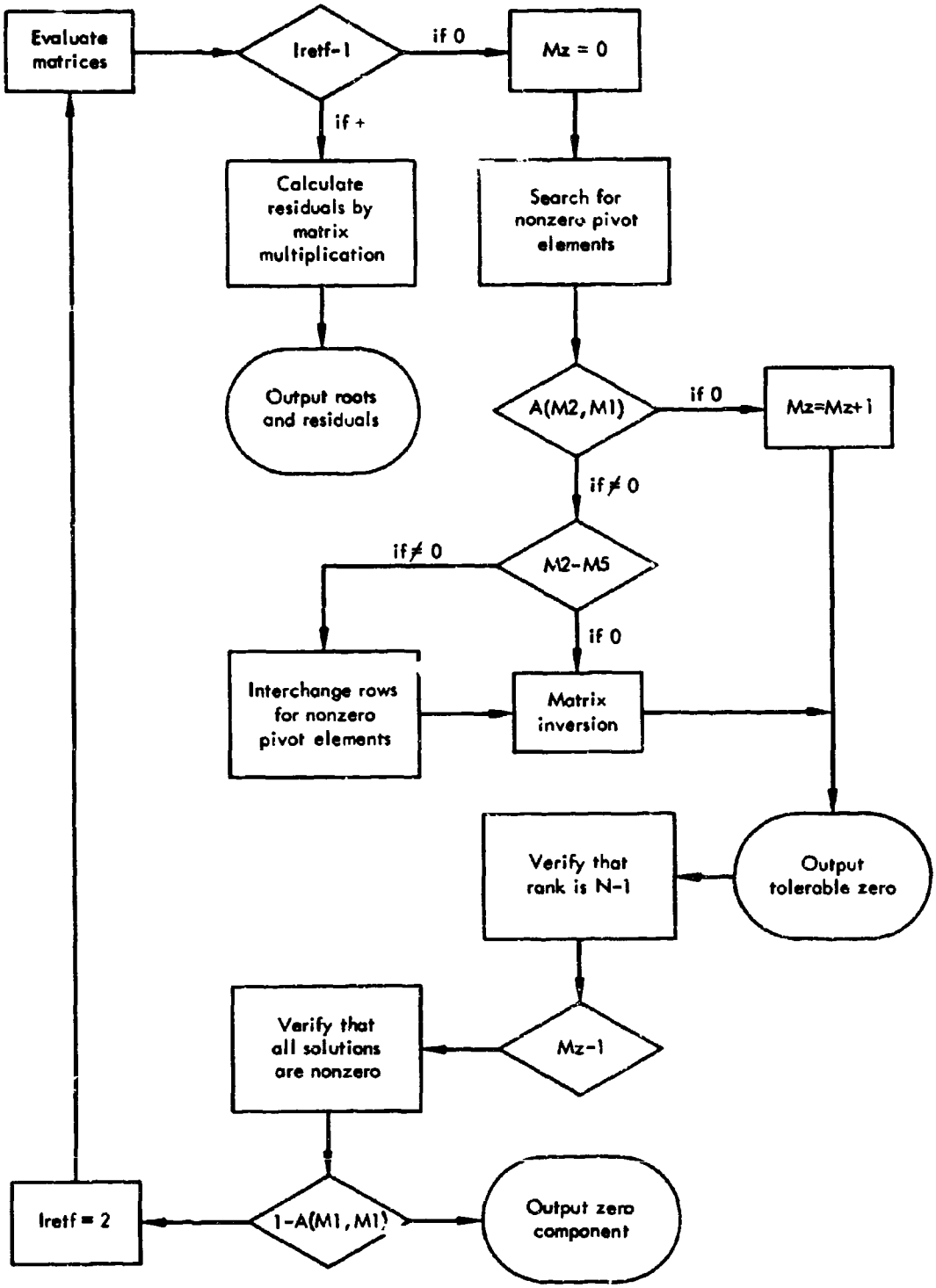

Figure D-6. Flow diagram, vector components X and R.

Program D-1. Natural Frequency and Mode of Circular Arch

```
C       PROGRAM OF CIRCULAR ARCH ANALYSIS
C       PURPOSE OF PROGRAM, TO EVALUATE X2 IN MATRIX OF Ax=0.
C       PROGRAM DETERMINES NATURAL FREQUENCIES OF CIRCULAR ARCH
C       ANTI-SYMMETRICAL AND SYMMETRICAL MODE SHAPES
C       BUCKLING LOAD AND DEFLECTED SHAPE OF THE ARCH
C       PROGRAM CONTROLLED BY VALUES OF IFREQ
C       IFREQ 1, CONCENTRATED MASS SYSTEM ANTI-SYMMETRICAL MODE
C       IFREQ 2, CONCENTRATED MASS SYSTEM SYMMETRICAL MODE
C       IFREQ 3, DISTRIBUTED MASS SYSTEM ANTI-SYMMETRICAL MODE
C       IFREQ 4, DISTRIBUTED MASS SYSTEM SYMMETRICAL MODE
C       IFREQ 5, BUCKLING LOAD OF ANTI-SYMMETRICAL MODE
C       IFREQ 6, BUCKLING LOAD OF SYMMETRICAL MODE
C       MODIFIED 25 JUNE 1965 ( RICHARD H. CHIU )
        DOUBLE PRECISION A,X,R,DUMP,DET,F0,F1,F2,F3
        DIMENSION A(12,12),X(12)
  901   FORMAT (I5,E15.8,D15.8,3E15.8)
  902   FORMAT (/11X,4HROOT,9X,8HRESIDUAL,8X,5HFREQ.,10X,6HPERIOD/)
 1000   DO 1032 IFREQ=1,6
C       READ INPUT TAPE 5, CONTROL CARD
        READ                (5, 1001)NROOT,X0,FMAX,DELTA,TOL,XK
 1001   FORMAT(I5,5E15.8)
C       READ INPUT TAPE 5, INPUT PARAMETERS
C       N=ORDER OF DETERMINANT
C       RC= RADIUS OF ARCH
C       PHI= INCREMENT OF CENTRAL ANGLE
C       RL= RADIUS OF GYRATION OF ARCH SECTION
C       U=MU
C       EI=E*I
        READ                (5, 1001) N,RC,PHI,RL,U,EI
        XL=2.*RC*SIN (PHI/2.)
        C2=SIN (PHI/2.)/COS (PHI/2.)
C       FOR BUCKLING LOAD
        IF (IFREQ-5) 1003,1002,1002
 1002   C1=(C2*XL**3)/(2.*EI)
        GO TO 2000
 1003   C1=XL**4*U/(EI*COS (PHI/2.)**2)
        RHO=(XL/RL)**2
 2000   DO 1032 JROOT=1,NROOT
        WRITE (6, 902)
C       BEGIN SEARCH FOR ROOT
 1004   IRET=1
        IRETF=0
        X1=X0
        X2=X1
        GO TO 1016
 1005   F1=F2
        WRITE               (6,  901) IRET,X2,F2
        IRET=2
 1009   X2=X1+DELTA
        GO TO 1016
 1010   IF(F1*F2)1013,1013,1011
 1011   X1=X2
        F1=F2
        WRITE               (6,  901) IRET,X2,F2
        GO TO 1009
 1013   X3=X2
        F3=F2
        X4=X3
        IRET=3
        X0=X3
        F0=F3
 1015   WRITE               (6,  901) IRET,X2,F2
        X2=X1+(X3-X1)*F1/(F1-F3)
        GO TO 1016
```

Continued

Program D-1. Natural Frequency and Mode of Circular Arch (Contd)

```
C       EVALUATION OF DETERMINANT OF ORDER N
C       A. PLOTKIN AND W. WILCOXSON
C       29 AUGUST 1963
 3005 DET=1.
      DO 3013 K=2,N
      KM1=K-1
C       SEARCH FOR NON-ZERO PIVOT ELEMENT
      DO 3006 K1=KM1,N
      IF(A(KM1,K1))3007,3006,3007
 3006 CONTINUE
C       DETERMINANT IS ZERO
      DET=0.
      GO TO 3014
C       DIVIDE COLUMN BY PIVOTAL ELEMENT
 3007 DO 3008 K2=K,N
 3008 A(K2,K1)=A(K2,K1)/A(KM1,K1)
      IF(KM1-K1)3009,3011,3009
C       MOVE PIVOT ELEM. TO UPPER LEFT HAND CORNER OF REDUCED DETERMINANT
C       UPDATE SIGN FOR INTERCHANGING COLUMNS
 3009 DET=-DET
      DO 3010 K2=KM1,N
      DUMP=A(K2,KM1)
      A(K2,KM1)=A(K2,K1)
 3010 A(K2,K1)=DUMP
C       REDUCE ORDER OF DETERMINANT BY ONE
 3011 DO 3012 I=K,N
      DO 3012 J=K,N
 3012 A(I,J)=A(I,J)-A(I,KM1)*A(KM1,J)
 3013 DET=DET*A(KM1,KM1)
 3014 F2=DET*A(N,N)
      GO TO(1005,1010,1017),IRET
C       SEARCH FOR ROOT BY METHOD OF NESTED INTERVALS
 1017 IF(ABS (X4-X2)-TOL)1029,1029,1018
 1018 IF(X3)1019,1020,1019
 1019 IF(ABS (1.-X2/X4)-TOL)1029,1029,1020
 1020 IF(F1*F3)1021,1021,1029
 1021 IF(F1*F2)1026,1029,1025
 1025 X1=X2
      X4=X1
      F1=F2
      GO TO 1015
 1026 X3=X2
      X4=X3
      F3=F2
      GO TO 1015
C       IGNORE IF ASYMPTOTE
 1029 IF(FMAX-ABS (F2))1004,1004,1030
 1030 XF=X2*X2
      P=1./XF
      WRITE              (6,  901)JROOT,X2,F2,XF,P
C       GO TO 1016 TO EVALUATE ELEMENTS OF COEFFICIENT MATRIX
      IRETF=1
      GO TO 1016
C       SUB-PROGRAM TO SOLVE HOMOGENEOUS SIMULTANEOUS EQUATIONS (RANK=N-1)
C       W. WILCOXSON
C       30 AUGUST 1963
C       OUTPUT MATRIX A
      7000 WRITE              (6, 7500)
```

Continued

Program D-1. Natural Frequency and Mode of Circular Arch (Contd)

```
 7500 FORMAT(14X,8HMATRIX A)
      DO 3 JJ=1,N
      DO 3 II=1,N
 3    WRITE              (6, 2)JJ,II,A(JJ,II)
 2    FORMAT(2HA(,I3,1H,I3,2H)=D14.8)
C     NOTE THAT N-MZ=RANK OF COEFFICIENT MATRIX
      MZ=0
      DO 7028 M1=1,N
      M5=M1-MZ
C     SEARCH FOR NON-ZERO PIVOT ELEMENT
      DO 7001 M2=M5,N
      IF(TOL-ABS (A(M2,M1)))7002,7001,7001
 7001 CONTINUE
      MZ=MZ+1
      GO TO 7028
 7002 IF(M2-M5)7003,7005,7003
C     INTERCHANGE ROWS TO OBTAIN NON-ZERO PIVOT ELEMENT
 7003 DO 7004 M3=M1,N
      DUMP=A(M5,M3)
      A(M5,M3)=A(M2,M3)
 7004 A(M2,M3)=DUMP
 7005 DO 7006 M3=M1,N
      M2=N-M3+M1
 7006 A(M5,M2)=A(M5,M2)/A(M5,M1)
      DO 7018 M4=1,N
      IF(M4-M5)7007,7018,7007
 7007 DO 7008 M3=M1,N
      M2=N-M3+M1
 7008 A(M4,M2)=A(M4,M2)-A(M4,M1)*A(M5,M2)
 7018 CONTINUE
 7028 CONTINUE
C     WRITE OUTPUT TAPE 6, TOLERABLE ZERO
      WRITE              (6, 5)A(N,N)
 5    FORMAT(15HTOLERABLE ZERO=D15.8)
C     VERIFY THAT RANK IS N-1
      IF(MZ-1)7009,7013,7009
 7009 M1=N-MZ
      WRITE              (6, 7010) M1
 7010 FORMAT(11HERR   RANK=,I4)
 7011 WRITE              (6, 7012)
 7012 FORMAT(14HZERO COMPONENT)
C     VERIFY THAT ALL SOLUTIONS ARE NON-ZERO
 7013 NM1=N-1
      DO 7014 M1=1,NM1
      IF(1.-A(M1,M1))7011,7014,7011
 7014 X(M1)=-A(M1,N)
      X(N)=1.
C     CALCULATE RESIDUALS BY MATRIX MULTIPLICATION
C     EVALUATE ELEMENTS OF MATRIX
      IRETF=2
      GO TO 1016
 5004 WRITE              (6, 7501)
 7501 FORMAT(17H  SOLUTION VECTOR,15X,15HRESIDUAL VECTOR)
      DO 5006 I=1,N
      R=0.
      DO 5005 J=1,N
 5005 R=A(I,J)*X(J)+R
C     OUTPUT
 5006 WRITE              (6, 5007)I,X(I),I,R
 5007 FORMAT(2HX(,I2,2H)=,D14.8,10X,2HR(,I2,2H)=,D14.8)
```

Continued

Program D-1. Natural Frequency and Mode of Circular Arch (Contd)

```
 1032 CONTINUE
      GO TO 1000
C     USER MUST INSERT FUNCTION EVALUATION STATEMENTS AFTER 1016
C     AND THEN COMPILE AN OBJECT PROGRAM
C     EVALUATION ROUTINE FOR MATRIX ELEMENTS
 1016 CONTINUE
      DO 2017 I=1,N
      DO 2017 J=I,N
 2017 A(I,J)=0.
      IF ( IFREQ-5) 2019,2018,2018
 2018 ALPHA=C1*X2
      GO TO 2020
 2019 ALPHA=C1*39.478417*X2**4
 2020 N1=N-1
      NW=N1/2
      A(1,1)=5.+2.*RHO*C2*C2
      J1=NW+1
      A(1,J1)=C2
      A(J1,J1)=2.*RHO+C2*C2
      GO TO (121,122,121,122,121,122),IFREQ
C     ANTI-SYMMETRICAL MODES
  121 A(NW,NW)=A(1,1)
      A(NW,N1)=-C2
      A(N1,N1)=A(J1,J1)
      A(NW-1,N)=-C2
      A(NW,N)=C2*(2.+RHO)
      A(N-2,N)=-C2*C2
      A(N1,N)=-RHO
      A(N,N)=A(J1,J1)+C2*C2
      GO TO 123
C     SYMMETRICAL MODES
  122 A(NW,NW)=A(1,1)+2.
      A(NW,N1)= C2
      A(N1,N1)=A(J1,J1)+2.*C2*C2
      A(NW-1,N)=1.
      A(NW,N)=RHO*C2*C2-4.
      A(N-2,N)= C2
      A(N1,N)=-C2*(2.+RHO)
      A(N,N)=A(1,1)+1.
  123 I=1
      DO 101 J=2,NW
      A(I,J)=RHO*C2*C2-4.
  101 I=I+1
      I=1
      DO 102 J=3,NW
      A(I,J)=1.
  102 I=I+1
      J2=NW-1
      DO 105 J=2,J2
  105 A(J,J)=A(1,1)+1.
      I=1
      J1=NW+2
      DO 103 J=J1,N1
      A(I,J)=C2*(2.+RHO)
  103 I=I+1
      I=1
      J1=NW+3
      DO 104 J=J1,N1
      A(I,J)=-C2
```

Continued

Program D-1. Natural Frequency and Mode of Circular Arch (Contd)

```
  104 I=I+1
      I=2
      J1=NW+1
      J2=N-2
      DO 106 J=J1,J2
      A(I,J)=-C2*(2.+RHO)
  106 I=I+1
      I=3
      J2=N-3
      DO 107 J=J1,J2
      A(I,J)=C2
  107 I=I+1
      I=NW+1
      J1=NW+3
      DO 108 J=J1,N1
      A(I,J)=-C2*C2
  108 I=I+1
      I=NW+1
      J1=NW+2
      DO 109 J=J1,N1
      A(I,J1=-RHO
  109 I=I+1
      J1=NW+2
      J2=N-2
      DO 110 J=J1,J2
  110 A(J,J)=2.*(RHO+C2*C2)
      NW=NW+1
      GO TO (125,125,131,131,140,140),IFREQ
C     BUCKLING LOAD
  140 ASN=-ALPHA*C2
      DO 143 J=NW,N
  143 A(J,J)=A(J,J)-2.*ALPHA
      J1=NW+1
      DO 144 J=J1,N
  144 A(J-1,J)=A(J-1,J)+ALPHA
      ACS=-ALPHA*(2.+1./(C2*C2))
      ALPHA=ALPHA*2./(C2*C2)
      J2=Nw-1
      DO 141 J=2,J2
  141 A(J-1,J)=A(J-1,J)-ACS
      DO 142 J=1,J2
  142 A(J,J)=A(J,J)-ALPHA
      GO TO 139
C     CONCENTRATED MASS SYSTEM
  125 DO 126 J=1,N
  126 A(J,J)=A(J,J)-ALPHA
      GO TO 127
C     DISTRIBUTED MASS SYSTEM
  131 ASN=ALPHA*SIN (PHI)/6.
      ACS=ALPHA*COS (PHI)/6.
      ALPHA=ALPHA*2./3.
      DO 132 J=1,N
  132 A(J,J)=A(J,J)-ALPHA
      J2=NW-1
      DO 133 J=2,J2
  133 A(J-1,J)=A(J-1,J)-ACS
      J1=NW+1
      DO 134 J=J1,N
  134 A(J-1,J)=A(J-1,J)-ACS
```

Continued

Program D-1. Natural Frequency and Mode of Circular Arch (Contd)

```
139 J2=N-2
    I=2
    DO 135 J=NW,J2
    A(I,J)=A(I,J)-ASN
135 I=I+1
    J1=NW+1
    I=1
    DO 136 J=J1,N
    A(I,J)=A(I,J)+ASN
136 I=I+1
127 DO 111 I=2,N1
    NC=I-1
    DO111J=1,NC
111 A(I,J)=A(J,I)
    DO 112 J=1,N1
112 A(N,J)=2.*A(J,N)
    IF (IRETF-1) 3005,7000,5C04
    END
```

Presentation of Numerical Results

The input parameters used in the numerical analysis of the natural modes and the associated frequencies of the two-hinged circular arch are the same as those used in the elastic program of Appendix C. In the solutions presented in this section, the effects of the number of bars and the assumptions regarding the mass distribution of the discrete framework are studied.

Solutions for increasing the number of bars from 8 to 40 in the discrete framework, considering the mass to be concentrated at the joints, are tabulated in Table D-3. The corresponding results for the distributed mass system are given in Table D-4. The first six natural frequencies of the antisymmetrical and symmetrical modes are presented in both tables.

A comparison of the antisymmetrical modal frequencies for the concentrated mass and distributed mass systems is presented in Figure D-7. The frequencies were plotted against the number of bars used in the discrete framework. A corresponding comparison of the symmetrical modal frequencies is presented in Figure D-8. It should be noted that both assumptions regarding the mass distribution of the framework lead to the same asymptotic frequency. However, the asymptotic frequency can be obtained much more rapidly by the distributed mass assumption.

As shown in Figures D-7 and D-8, nearly all the asymptotic frequencies are obtained for fewer than 40 bars. For practical purposes, the solutions of the 40-bar distributed mass system may be regarded as "exact" solutions for the arch considered in this report.

The normalized natural modes of vibration of a 40-bar distributed mass system are given in Figures D-9 and D-10 for antisymmetrical and symmetrical modes, respectively. It is observed that the normalized modes are predominantly flexural. However, the axial deformation of the second antisymmetrical mode is significant and is closely related to the "breathing" mode of a complete ring having the same cross-sectional properties. A comparison can readily be made by considering the frequency of vibration of a complete ring of uniform cross section as given by the following expression:

$$\omega = \frac{1}{2\pi} \sqrt{\frac{EA}{\mu R^2}}$$

which is calculated to be 317.3 cps for the cross-sectional properties of the arch. This value is comparable to the frequency of 301.1 cps for the second symmetrical mode of the arch.

Table D-3. Natural Frequencies and Periods of a Two-Hinged Arch

Concentrated Mass

Mode	Number of Bars							Period T*
	8	12	16	20	24	32	40	
	Frequencies for Antisymmetrical Modes (cps)							
1	57.66	58.89	59.30	59.51	59.63	59.72	59.79	16.73
2	224.5	250.3	259.8	264.2	266.7	269.3	270.4	3.70
3	392.1	510.8	555.6	575.9	586.6	596.7	601.1	1.66
4	644.3	655.4	664.2	669.5	673.2	677.5	679.9	1.47
5	---	780.3	922.3	994.6	1,036	1,078	1,098	0.911
6	---	970.4	1,276	1,441	1,536	1,635	1,682	0.595
Mode	Frequencies for Symmetrical Modes (cps)							
1	128.5	135.2	137.5	138.6	139.2	139.8	140.1	7.14
2	286.1	295.8	298.1	299.3	299.7	300.2	300.4	3.33
3	329.2	388.0	411.5	422.8	429.3	435.5	438.8	2.28
4	414.3	651.9	739.2	782.6	806.9	831.6	843.1	1.19
5	---	886.5	1,099	1,191	1,206	1,211	1,213	0.824
6	1,172	1,197	1,208	1,233	1,286	1,350	1,382	0.724

*Natural period (msec) based on 40-bar solutions.

Table D-4. Natural Frequencies and Periods of a Two-Hinged Arch

Distributed Mass

Mode	Number of Bars							Period T*
	8	12	16	20	24	32	40	
	Frequencies for Antisymmetrical Modes (cps)							
1	59.83	59.86	59.86	59.86	59.86	59.86	59.86	16.71
2	270.2	272.0	272.3	272.5	272.5	272.5	272.5	3.63
3	583.1	607.1	608.5	608.7	608.7	608.7	608.7	1.64
4	677.5	685.4	685.6	685.4	685.2	684.7	684.7	1.46
5	---	1,095	1,125	1,131	1,132	1,133	1,134	0.882
6	---	1,569	1,728	1,752	1,757	1,759	1,759	0.569
Mode	Frequencies for Symmetrical Modes (cps)							
1	140.3	140.5	140.5	140.5	140.5	140.6	140.6	7.11
2	302.3	301.6	301.4	301.1	301.1	301.1	301.1	3.32
3	432.1	442.2	443.4	443.6	443.8	443.8	443.8	2.25
4	733.0	849.6	860.4	862.8	863.4	863.9	864.1	1.16
5	---	1,233	1,226	1,222	1,220	1,218	1,217	0.822
6	1,257	1,347	1,420	1,433	1,436	1,438	1,439	0.695

*Natural period (msec) based on 40-bar solutions.

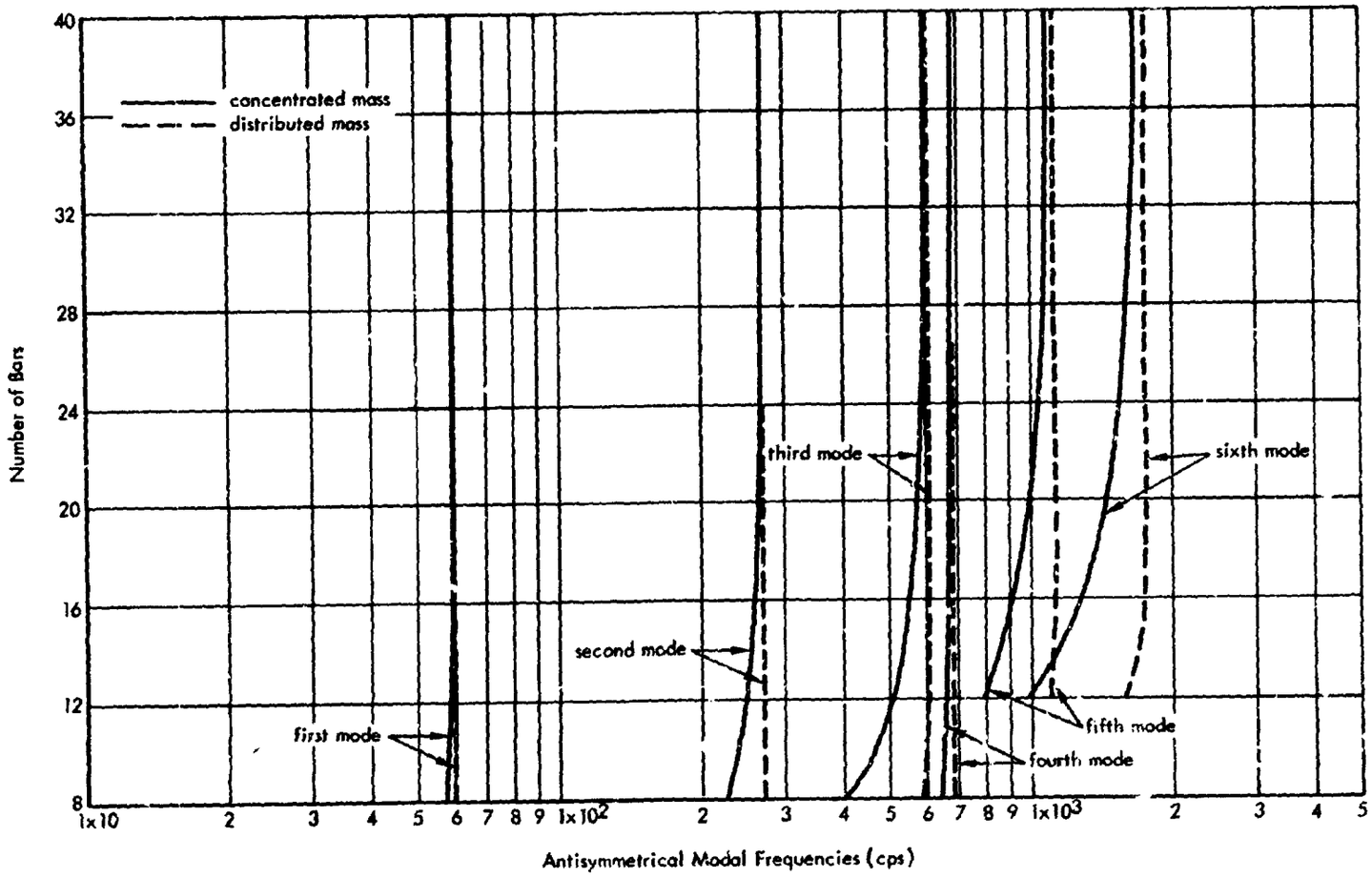

Figure D-7. Effect of number of bars on natural frequencies.

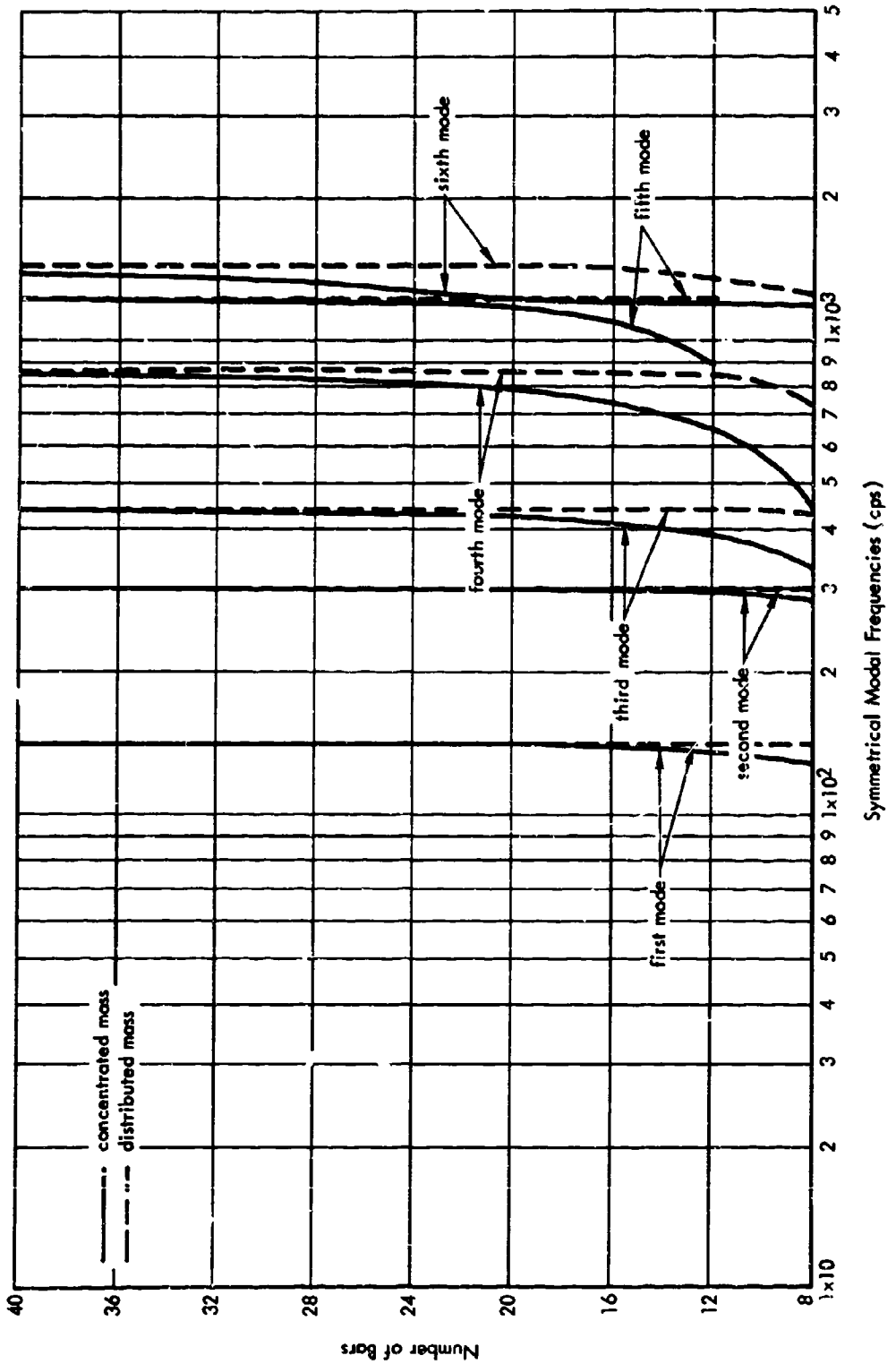

Figure D-8. Effect of number of bars on natural frequencies.

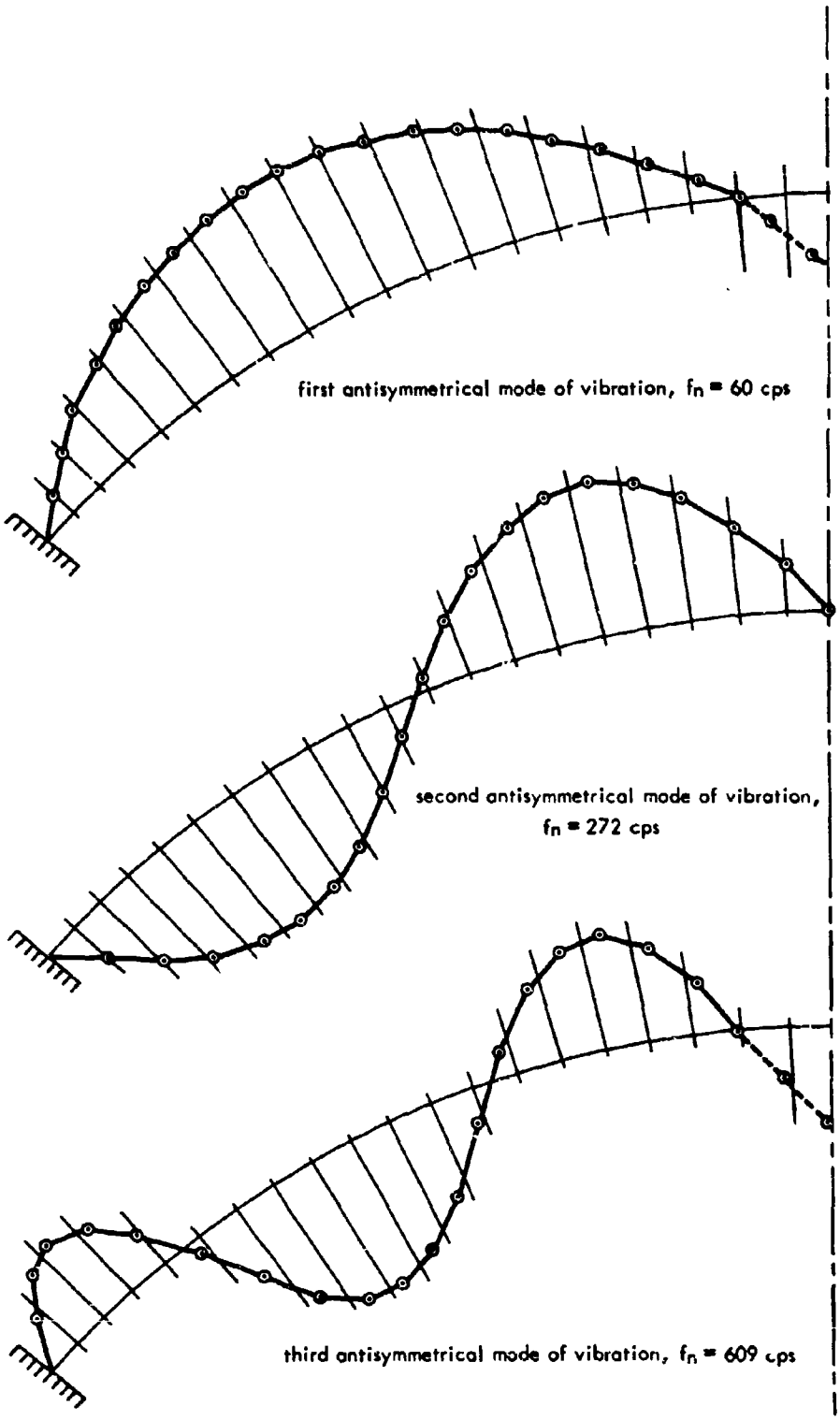

Figure D-9. Antisymmetrical modes of two-hinged arch.

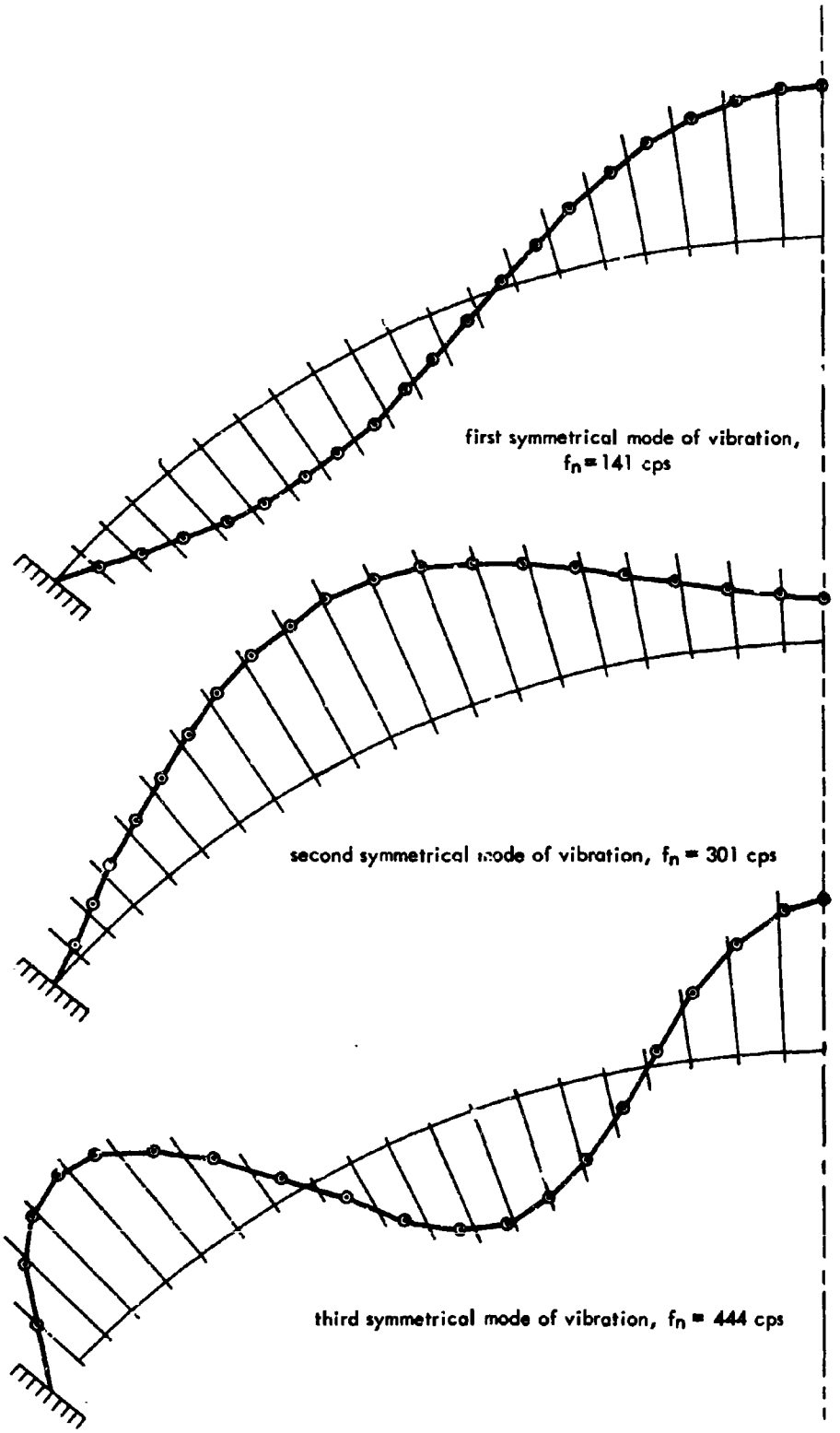

Figure D-10. Symmetrical modes of two-hinged arch.

Appendix E

SIMPLIFIED ANALYSIS OF A CIRCULAR ARCH

In the static analysis (Appendix B) of the two-hinged arch of Figure B-1, the distributions of moments and stresses are basically antisymmetrical and the axial force along the arch does not vary appreciably. In the dynamic analysis of Appendix C, the response of the arch is largely contributed by the first antisymmetric mode of vibration; the axial force also remains essentially uniform along the arch. The findings suggest that a simplified analysis and design procedure similar to those proposed by Newmark[18,19] can be used. All notations in this appendix conform to the previous definitions unless otherwise noted.

Static Analysis

Assuming that the principle of superposition holds true in the elastic range of the arch response, the uniform load distributed over one-half the arch length can be obtained by two components as follows:

1. Symmetrical loading uniformly distributed over the entire arch span with a magnitude equal to one-half the original load.

2. Antisymmetrical loading consisting of an inward uniform loading distributed over one-half the arch length and an outward uniform loading over the other half of the arch length. The magnitude of the antisymmetrical loading is also one-half the original load.

The sum of the two components is equivalent to the original loading condition.

For a circular arch with uniform cross section along its length, the critical section is at the quarter point of the loaded half of the arch. The static axial force at the critical section due either to symmetrical or antisymmetrical loading is given by the approximate expression as follows:

$$P_t = wR \tag{E-1}$$

For the symmetrical loading, the maximum bending moments at the quarter points are given by the approximate expression

$$M_1 = \frac{1}{216}\left[\frac{\phi_o^2}{1 - \left(\frac{\phi_o}{3\pi}\right)^2}\right] wR^2 \tag{E-2}$$

For the antisymmetrical loading, the maximum bending moment at the quarter point under the inward loading is given by the approximate expression

$$M_2 = \frac{1}{32}\left[\frac{\phi_o^2}{1 - \left(\frac{\phi_o}{2\pi}\right)^2}\right] wR^2 \tag{E-3}$$

and the corresponding buckling load, w_{cr}, can be obtained from

$$w_{cr} = \left(\frac{4\pi^2}{\phi_o^2} - 1\right)\frac{EI}{R^3} \qquad \text{(E-4)}$$

Stress amplification as a result of the tendency of the arch to buckle under the axial force can be expressed by the amplification factor

$$A_m = \frac{1}{1 - \frac{w}{w_{cr}}} \qquad \text{(E-5)}$$

The amplification factor will be used as a multiplier for the moment terms of Equations E-2 and E-3. The total static moment is the sum of M_1 and M_2; the stresses and strains caused by the bending moment and the axial force can be obtained by applying Equations B-30 through B-33. The static yield condition may be established with the aid of stress-strain curves such as shown in Figure B-8.

Dynamic Analysis

The above static expressions of Equations E-1 through E-3 are used for the simplified dynamic analysis by introducing a dynamic amplification factor, D, for a step function load, as follows:

$$D = 1 - \cos\frac{2\pi t}{T}$$

where T is the appropriate response period of each of the three functions considered. The amplification factor, D, reflects the time-variant characteristics and the frequency of each function. The above expression can be expressed in terms of the functions of a variable, x, as follows:

$$D(x) = 1 - \cos\frac{2\pi t}{T(x)} \qquad \text{(E-6)}$$

where x is the particular variable of Equations E-1 through E-3.

As shown in Appendix C, the frequency of the axial force corresponds to the "breathing" mode of a complete ring. The simplified dynamic response of the axial force is given by the expression

$$P_t(t) = \left[1 - \cos\frac{2\pi t}{T(P_t)}\right] P_t \qquad \text{(E-7)}$$

where the period, $T(P_t)$, is given by

$$T(P_t) = 2\pi \sqrt{\frac{\mu R^2}{EA}}$$

The moment due to the symmetrical loading varies at the frequency of the first symmetrical mode of vibration. The time variant response of moment at the quarter points can be expressed as

$$M_1(t) = \left[1 - \cos \frac{2\pi t}{T(M_1)}\right] M_1 \qquad \text{(E-8)}$$

where the corresponding period is given approximately by

$$T(M_1) = \frac{2\left(R\phi_o\right)^2}{9\pi} A_m \sqrt{\frac{\mu}{EI}}$$

where A_m is given in Equation E-5.

The moment due to the antisymmetrical loading varies at the frequency of the first antisymmetrical mode of vibration. The time-variant response of moment at the quarter point under the inward loading can be expressed as

$$M_2(t) = \left[1 - \cos \frac{2\pi t}{T(M_2)}\right] M_2 \qquad \text{(E-9)}$$

and the corresponding period is given approximately by

$$T(M_2) = \frac{C\left(R\phi_o\right)^2}{2\pi} A_m \sqrt{\frac{\mu}{EI}}$$

where

$$C = \frac{n^2 + 1.5}{n^2 - 1}$$

and

$$n = \frac{2\pi}{\phi_o}$$

The total time-variant moment is obtained by summing the results of Equations E-8 and E-9 at each time. The stresses and strains at the quarter point under the inward loading can be obtained by the same procedure used in the static analysis.

It should be noted that the maximum dynamic amplification factor, D(x), of Equation E-6 is two for a step function load.

Presentation of Numerical Results

A computer program (Program E-1) based on the procedure described in the previous sections was used to obtain the numerical solution of the simplified analyses. Comparisons of the natural periods of vibration for the first antisymmetrical mode, the first symmetrical mode, and the second symmetrical mode are made between the simplified analysis and the corresponding values of Appendix D, and are presented in Table E-1. Close agreement is obtained in all cases.

Comparisons between the simplified analysis and the more rigorous analysis of the dynamic response of bending moment and axial force as given in Appendix C are presented in Table E-2. Similar comparisons for static values are presented in Table E-3. Comparisons of the dynamic response of axial forces show excellent agreement. The difference in the static values of axial forces is a result of the elastic support conditions introduced in Appendix B. The static bending moments of the simplified analysis are slightly higher than the corresponding results of Appendix B. The large difference (about 20 percent) in the dynamic moments is due to the damping effects of the system considered in Appendix C; the simplified analysis did not consider damping.

Table E-1. Comparison of Natural Periods of the Simplified Analysis to the Results of Appendix D

Load (lb/in.)	Antisymmetrical (msec)		Symmetrical (msec)			
	First Mode		First Mode		Second Mode	
	1	2	1	2	1	2
200	17.0	16.7	6.3	7.1	3.0	3.3
400	17.3	16.7	6.4	7.1	3.0	3.3
600	17.6	16.7	6.5	7.1	3.0	3.3

1 - Results of the simplified analysis

2 - Results of Appendix D

Table E-2. Comparison of Maximum Dynamic Moments and Axial Forces of the Simplified Analysis to the Results of Appendix C (at 3/4-point of the arch)

Load (lb/in.)	Simplified Analysis				Appendix C			
	Moment (in. -lb)	Time (msec)	Axial Force (lb)	Time (msec)	Moment (in. -lb)	Time (msec)	Axial Force (lb)	Time (msec)
200	204,000	9.0	19,100	1.6	161,000	7.2	19,000	1.7
400	415,000	9.2	38,100	1.6	327,000	7.2	38,100	1.7
600	634,000	9.4	57,200	1.6	442,000	8.0	57,100	1.8

Table E-3. Comparison of Static Moments and Axial Forces of the Simplified Analysis to the Results of Appendix B

Load (lb/in.)	Moments (in. -lb)		Axial Forces (lb)	
	1	2	1	2
200	103,500	95,300	9,600	8,500
400	210,700	194,200	19,200	17,000
500	266,300	245,200	24,000	21,300

1 - Results of the simplified analysis

2 - Results of Appendix B

Program E-1. Simplified Analysis of Circular Arches

```
C       SIMPLIFIED ANALYSIS OF CIRCULAR ARCHES
        DIMENSION T(3),X(3),FT(3),E(4)
      1 FORMAT (I4,6E12.6,I4)
      2 FORMAT (/I4,23H    HALF LOADED ARCH AT,F8.2,6H LB/IN/)
      3 FORMAT(/6H  TIME6X4HAX F7X6HM(MAX)7X5HST(T)7X5HST(B)8X4HS(T)8X
     1 4HS(B)/)
      4 FORMAT (F8.4,6E12.6)
      5 FORMAT (/9X2HEA10X2HMU10X3HEAY9X3HSUM9X2HEI/)
      6 FORMAT(/5H   R=,E12.6,5HPHIO=,E12.6,5H PCR=,E12.6,5H FAX=,E12.6)
      7 FORMAT (5H   N=,E12.6,5H  MS=,E12.6,5H  MA=,E12.6)
      8 FORMAT (5H  TN=,E12.6,5H TMS=,E12.6,5H TMA=,E12.6)
C       READ CONTROL CARD
        READ 1, NI,R,PHIO,PO,DP,TO,DT,NJ
        EI=0.
        EA=0.
        EAY=0.
        UM=0.
        PUNCH 5
        DO 11 L=1,4
        READ 1, J,H,B,Y,E(L),D
        A=H*B
        UM=UM+A*490./(1728.*386.4)
        AY=A*Y*E(L)
        EI=EI+AY*Y+A*H*H*E(L)/12.
        EA=EA+A*E(L)
        EAY=EAY+AY
     11 PUNCH 1, L,EA,UM,AY,EAY,EI
        C1=EAY/EA
        C2=D-C1
        EI=EI-EA*C1*C1
        PUNCH 1, L,EA,UM,C1,C2,EI
        PI=3.1415927
        DO 32 I=1,NI
        P=PO+DP
        X(1)=P*R
        C=2.*PI/PHIO
        PCR=EI*(C*C-1.)/R**3
        FAX=1./(1.-P/PCR)
        S=FAX*(R*PHIO)**2
        X(2)=S*P/((1.-(2./(3.*C))**2)*216.)
        X(3)=S*P/((1.-1./(C*C))*32.)
        T(1)=2.*PI*R*SQRT(UM/EA)
        S=S*SQRT(UM/EI)
        T(2)=2.*S/(9.*PI)
        C1=(C*C+1.5)/(C*C-1.)
        T(3)=C1*S/(2.*PI)
        PUNCH 6, R,PHIO,PCR,FAX
        PUNCH 7, X(1),X(2),X(3)
        PUNCH 8, T(1),T(2),T(3)
```

Continued

Program E-1. Simplified Analysis of Circular Arches (Contd)

```
      PO=P
      P=2.*P
      PUNCH 2, 1,P
      PUNCH 3
      TO=0.
      DO 31 J=1,NJ
      XT=TO+DT
      DO 21 K=1,3
      AF=1.-COS(2.*PI*XT/T(K))
   21 FT(K)=X(K)*AF
      XM=FT(2)+FT(3)
      ST=FT(1)/FA+XM*C1/FI
      SB=FT(1)/FA-XM*C2/FI
      STT=ST*E(2)
      STB=SB*E(4)
      PUNCH 4, XT,FT(1),XM,ST,SB,STT,STB
   31 TO=XT
   32 CONTINUE
      PAUSE
      END
```

Appendix F

PHOTOGRAPHS OF TESTED ARCHES

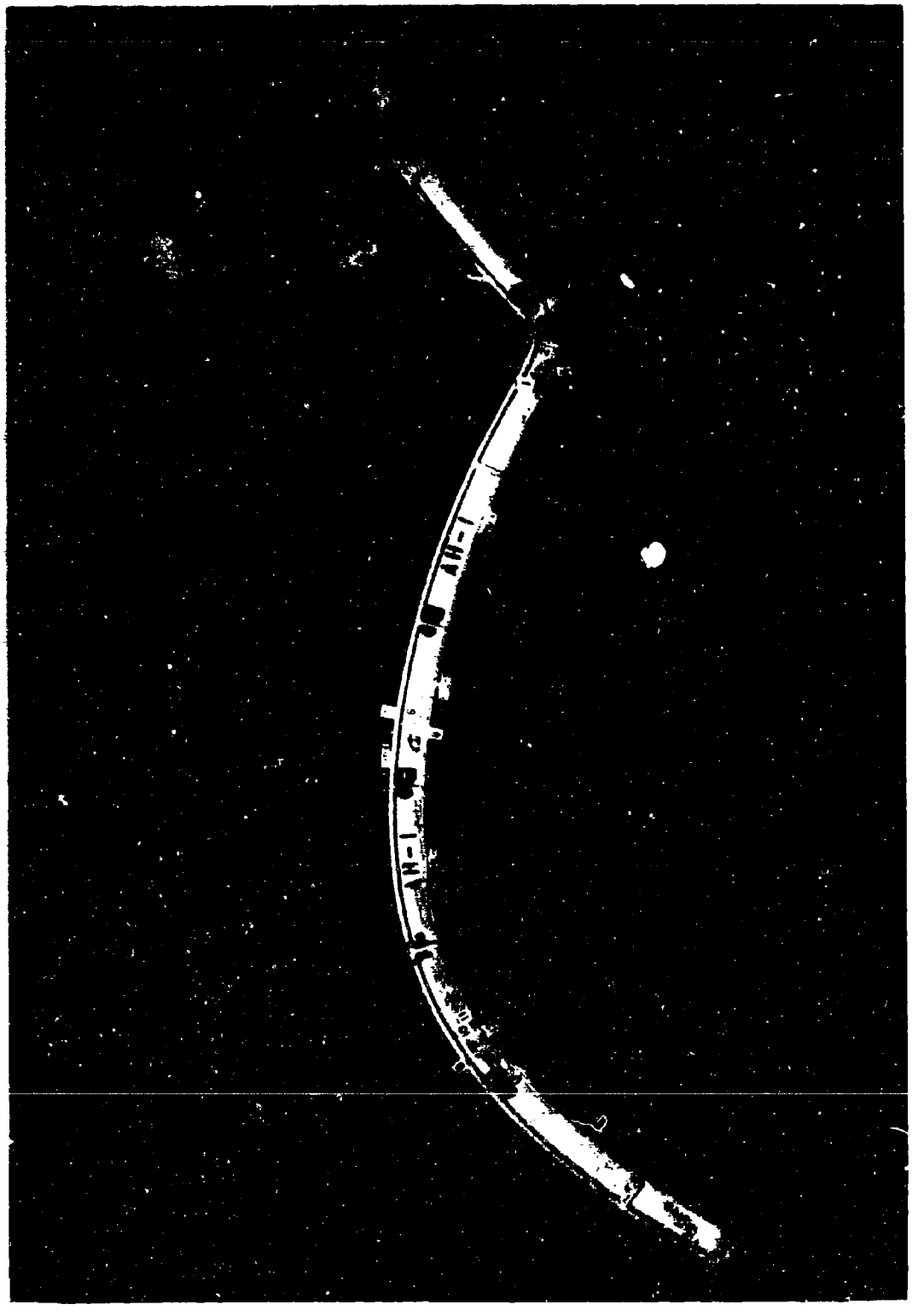

Figure F-1. Antisymmetrically loaded arch AH-1 after a static load of 876 lb/in.

Figure F-2. Top view of loaded portion of arch AH-1 after test.

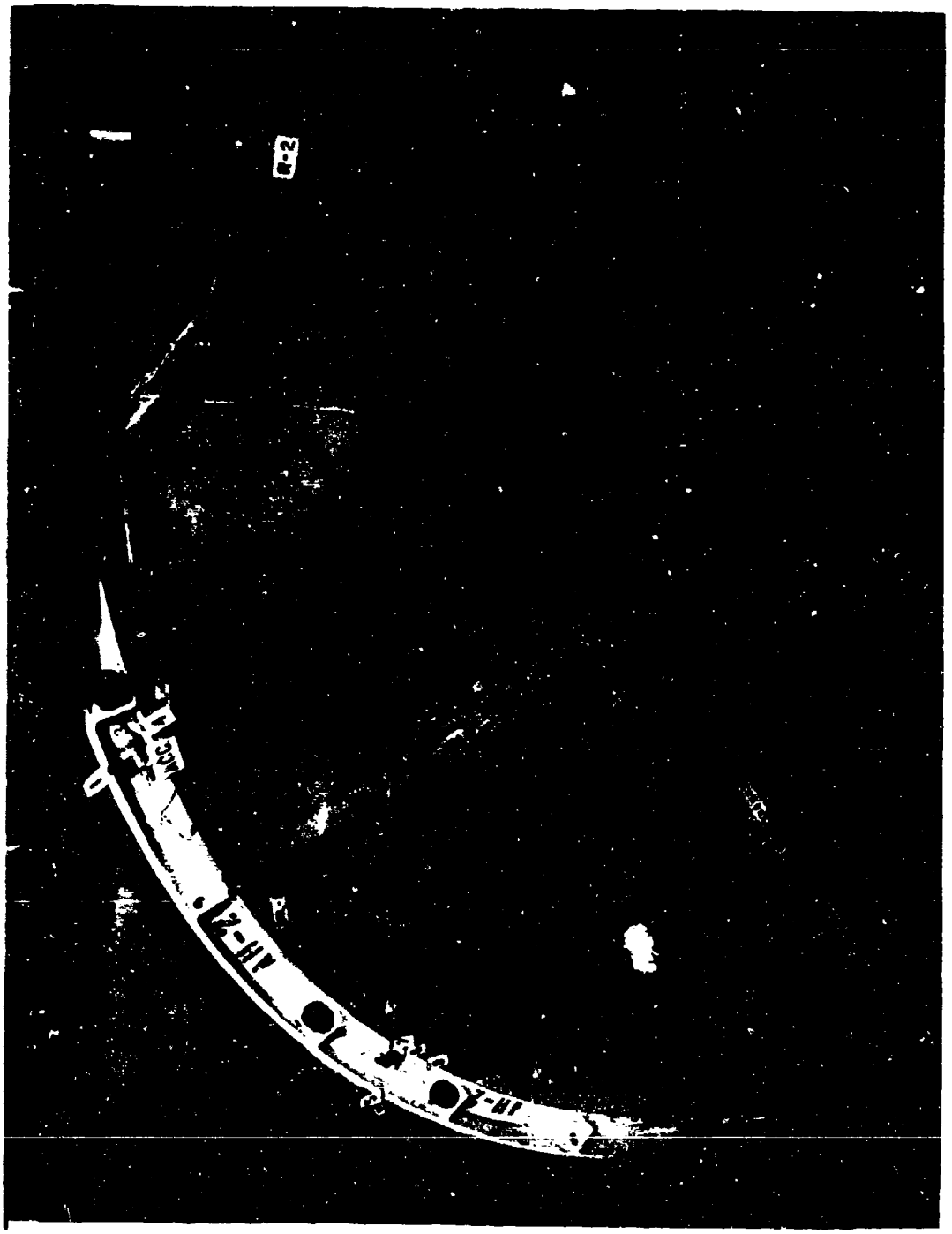

Figure F-3. View of arch AH-2 before test.

Figure F-4. View of arch AH-2 after a dynamic load of 618 lb/in. on the right half.

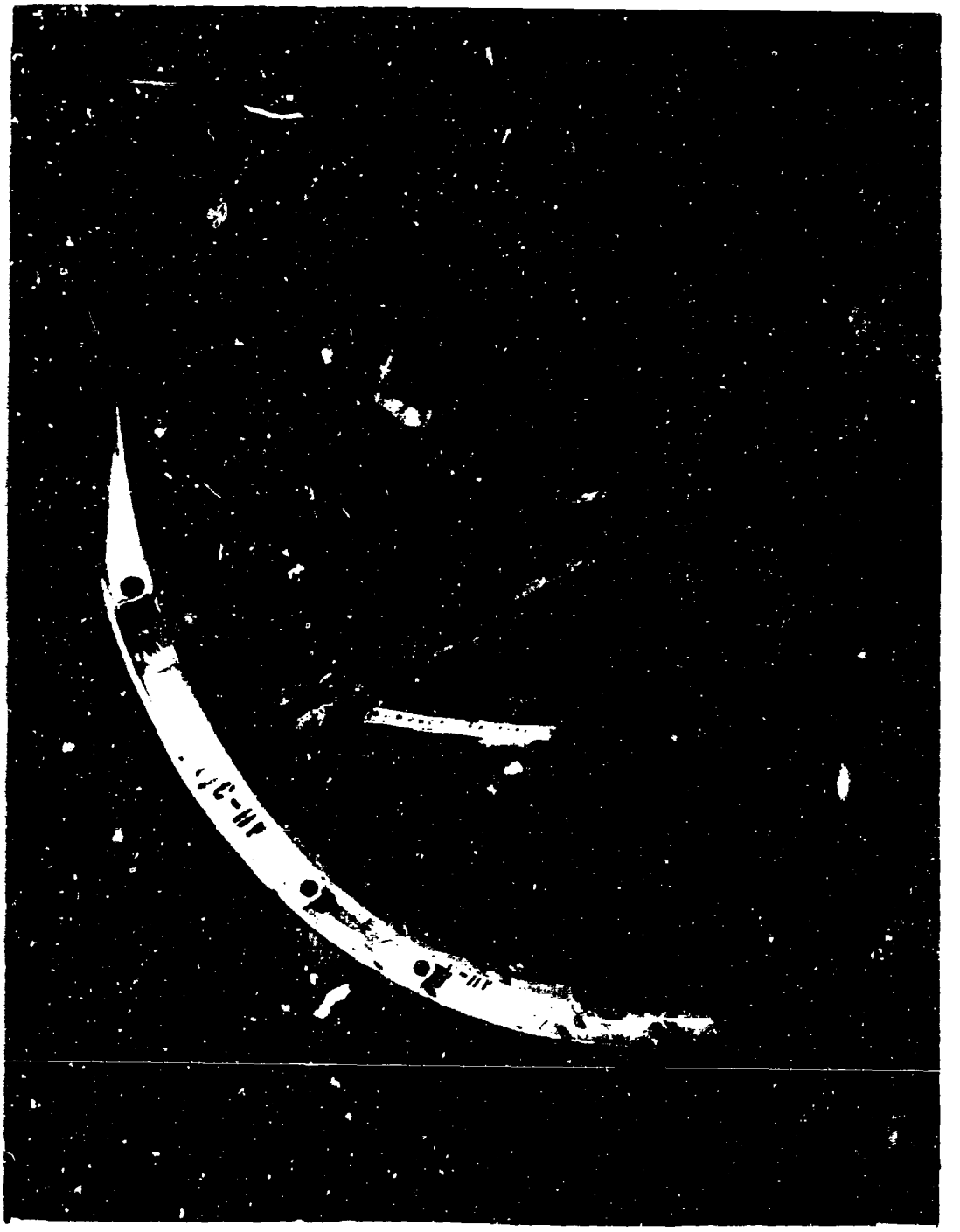

Figure F-5. View of arch AH-3 before test.

REFERENCES

1. U.S. Naval Civil Engineering Laboratory. Technical Report R-183: Static and dynamic behavior of portal frame knee connections, by W. A. Shaw. Port Hueneme, Calif., May 1962.

2. U.S. Naval Civil Engineering Laboratory. Technical Report R-336: Static and dynamic behavior of pinned-based portal frames, by S. K. Takahashi and R. H. Chiu. Port Hueneme, Calif., Feb. 1965.

3. U.S. Naval Civil Engineering Laboratory. Technical Report R-337: Static and dynamic behavior of fixed-based portal frames, by S. K. Takahashi and R. H. Chiu. Port Hueneme, Calif., June 1965.

4. U.S. Navy Department, Bureau of Yards and Docks. Navy Contract NBy-3186: Program on the dynamic testing of structural frames and arches, by B. G. Johnston. Final Report to the U.S. Naval Civil Engineering Laboratory, Port Hueneme, Calif., May 1960.

5. L.S. Beedle. Plastic design of steel frames. New York, John Wiley & Sons, Inc., 1958.

6. W. A. Shaw and J. R. Allgood. "An atomic blast simulator," SESA Proceedings, vol. 17, no. 1, 1959.

7. U.S. Naval Civil Engineering Laboratory. Technical Report R-331: NCEL dynamic testing machine, by W. L. Cowell. Port Hueneme, Calif., Oct. 1964.

8. G. Murphy. Properties of engineering materials, International Textbook Co., 1947.

9. D. McLean. Mechanical properties of metals. New York, John Wiley & Sons, Inc., 1962, p. 204.

10. L.S. Jacobsen and R.S. Ayre. Engineering vibration. New York, McGraw-Hill, 1958.

11. U.S. Naval Civil Engineering Laboratory. Technical Note N-598: Determination of damping constants for a dry friction-viscous damped oscillator, by D. A. DaDeppo. Port Hueneme, Calif., Nov. 1964.

12. N.M. Newmark. "A method of computation for structural dynamics," Transactions, American Society of Civil Engineers, vol. 127, 1962.

13. L.E. Grinter. Theory of modern steel structures, vol. II. New York, Macmillan, 1949.

14. C.D. Williams. Analysis of statically indeterminate structures. International Textbook Company, 1951.

15. U.S. Navy Department, Bureau of Yards and Docks. Navy Contract NBy-32271: Calculation of static and dynamic response of circular arches, by R. T. Eppink. Final Report to U.S. Naval Civil Engineering Laboratory, Port Hueneme, Calif., Aug. 1965.

16. Air Force Special Weapons Center. Report No. AFSWC-TR-59-9: Analysis and design of shells, arches, and domes, vol. II: Analysis of circular arches, by R. T. Eppink and A.S. Veletsos. Kirtland Air Force Base, New Mexico, July 1959.

17. Air Force Special Weapons Center. Report No. AFSWC-TR-60-53: Response of arches under dynamic loads, by R. T. Eppink and A.S. Veletsos. Kirtland Air Force Base, New Mexico, Aug. 1960.

18. N.M. Newmark. "Vulnerability of arches -- preliminary notes," prepared for the Physical Vulnerability Division of the Directorate of Intelligence, U.S. Air Force, Department of Civil Engineering, University of Illinois, May 1956 (unpublished manuscript).

19. Air Force Special Weapons Center. Report No. AFSWC-TR-61-90: Studies of response of arches and domes under dynamic loads, by T. Huang, S. Iyengar, and R. L. Jennings. Kirtland Air Force Base, New Mexico, Oct. 1961.

Unclassified
Security Classification

DOCUMENT CONTROL DATA - R&D

(Security classification of title, body of abstract and indexing annotation must be entered when the overall report is classified)

1. ORIGINATING ACTIVITY (Corporate author) U. S. Naval Civil Engineering Laboratory Port Hueneme, California 93041	2c. REPORT SECURITY CLASSIFICATION Unclassified 2b. GROUP

3. REPORT TITLE

Static and Dynamic Behavior of Antisymmetrically Loaded Arches

4. DESCRIPTIVE NOTES (Type of report and inclusive dates)
Not final; 6 Feb. 1961 to 1 Sept. 1965

5. AUTHOR(S) (Last name, first name, initial)
Chiu, R. H.
Takahashi, S. K.

6. REPORT DATE	7a. TOTAL NO. OF PAGES	7b. NO. OF REFS
September 1966	152	19

8a. CONTRACT OR GRANT NO. DASA-13.018 b. PROJECT NO. Y-F008-08-02-102 c. d.	9a. ORIGINATOR'S REPORT NUMBER(S) TR-474 9b. OTHER REPORT NO(S) (Any other numbers that may be assigned this report)

10. AVAILABILITY/LIMITATION NOTICES

Distribution of this document is unlimited.

11. SUPPLEMENTARY NOTES	12. SPONSORING MILITARY ACTIVITY
	Naval Facilities Engineering Command — DASA

13. ABSTRACT

Four pinned-base steel arches wit. a 96-inch radius, 143.8-inch span, and uniform cross section were cold-rolled from 4M13 sections and tested under various static and dynamic loads uniformly distributed over one-half the arc length. A maximum static load of 72,000 pounds was applied by the NCEL blast simulator using compressed air. A dynamic peak load of 64,000 pounds was attained by detonating Primacord in the blast simulator. The blast loading had a rise time of about 3 milliseconds and a decay time of about 1.6 seconds. An equivalent triangular load-time function was used for the dynamic analysis. The applied loads and the resulting deflections, strains, and reactions were measured. The reduced data are presented in graphical and tabular form.

The theoretical analyses for statically and dynamically loaded arches were based on the discrete framework which represented the continuous arches tested. A 16-bar system was used for both static and dynamic response calculations, and a 40-bar system was used for natural mode and frequency calculations.

In the static analysis, the effects of stress amplification, misalignment, and elastic supports on the response of the arch were considered. Due to the strain-hardening characteristics of the arch material, the idealized stress-strain curve was represented by a trilinear curve rather than by the usual bilinear stress-strain curve.

DD FORM 1 JAN 64 1473 0101-807-6800

Unclassified
Security Classification

14. KEY WORDS	LINK A		LINK B		LINK C	
	ROLE	WT	ROLE	WT	ROLE	WT
Blast simulation Arches, loaded Dynamic loads Static loads Antisymmetrical loads Strain hardening Trilinear curve						

INSTRUCTIONS

1. **ORIGINATING ACTIVITY:** Enter the name and address of the contractor, subcontractor, grantee, Department of Defense activity or other organization *(corporate author)* issuing the report.

2a. **REPORT SECURITY CLASSIFICATION:** Enter the overall security classification of the report. Indicate whether "Restricted Data" is included. Marking is to be in accordance with appropriate security regulations.

2b. **GROUP:** Automatic downgrading is specified in DoD Directive 5200.10 and Armed Forces Industrial Manual. Enter the group number. Also, when applicable, show that optional markings have been used for Group 3 and Group 4 as authorized.

3. **REPORT TITLE:** Enter the complete report title in all capital letters. Titles in all cases should be unclassified. If a meaningful title cannot be selected without classification, show title classification in all capitals in parenthesis immediately following the title.

4. **DESCRIPTIVE NOTES:** If appropriate, enter the type of report, e.g., interim, progress, summary, annual, or final. Give the inclusive dates when a specific reporting period is covered.

5. **AUTHOR(S):** Enter the name(s) of author(s) as shown on or in the report. Enter last name, first name, middle initial. If military, show rank and branch of service. The name of the principal author is an absolute minimum requirement.

6. **REPORT DATE:** Enter the date of the report as day, month, year; or month, year. If more than one date appears on the report, use date of publication.

7a. **TOTAL NUMBER OF PAGES:** The total page count should follow normal pagination procedures, i.e., enter the number of pages containing information.

7b. **NUMBER OF REFERENCES:** Enter the total number of references cited in the report.

8a. **CONTRACT OR GRANT NUMBER:** If appropriate, enter the applicable number of the contract or grant under which the report was written.

8b, 8c, & 8d. **PROJECT NUMBER:** Enter the appropriate military department identification, such as project number, subproject number, system numbers, task number, etc.

9a. **ORIGINATOR'S REPORT NUMBER(S):** Enter the official report number by which the document will be identified and controlled by the originating activity. This number must be unique to this report.

9b. **OTHER REPORT NUMBER(S):** If the report has been assigned any other report numbers *(either by the originator or by the sponsor)*, also enter this number(s).

10. **AVAILABILITY/LIMITATION NOTICES:** Enter any limitations on further dissemination of the report, other than those imposed by security classification, using standard statements such as:

(1) "Qualified requesters may obtain copies of this report from DDC."

(2) "Foreign announcement and dissemination of this report by DDC is not authorized."

(3) "U. S. Government agencies may obtain copies of this report directly from DDC. Other qualified DDC users shall request through _____."

(4) "U. S. military agencies may obtain copies of this report directly from DDC. Other qualified users shall request through _____."

(5) "All distribution of this report is controlled. Qualified DDC users shall request through _____."

If the report has been furnished to the Office of Technical Services, Department of Commerce, for sale to the public, indicate this fact and enter the price, if known.

11. **SUPPLEMENTARY NOTES:** Use for additional explanatory notes.

12. **SPONSORING MILITARY ACTIVITY:** Enter the name of the departmental project office or laboratory sponsoring *(paying for)* the research and development. Include address.

13. **ABSTRACT:** Enter an abstract giving a brief and factual summary of the document indicative of the report, even though it may also appear elsewhere in the body of the technical report. If additional space is required, a continuation sheet shall be attached.

It is highly desirable that the abstract of classified reports be unclassified. Each paragraph of the abstract shall end with an indication of the military security classification of the information in the paragraph, represented as *(TS), (S), (C), or (U)*

There is no limitation on the length of the abstract. However, the suggested length is from 150 to 225 words.

14. **KEY WORDS:** Key words are technically meaningful terms or short phrases that characterize a report and may be used as index entries for cataloging the report. Key words must be selected so that no security classification is required. Identifiers, such as equipment model designation, trade name, military project code name, geographic location, may be used as key words but will be followed by an indication of technical context. The assignment of links, roles, and weights is optional.